School of Electrical Engineering and Computing
Department of Electrical and Computer Engineering

Pulse Shaping Approach to PAPR Reduction for OFDM Communication Systems

Regina Reine Hendranata

This thesis is presented for the degree of
Doctor of Philosophy
of
Curtin University

November 2015

Declaration

To the best of my knowledge and belief this thesis contains no material previously published by any other person except where due acknowledgment has been made.

This thesis contains no material which has been accepted for the award of any other degree or diploma in any university.

Signature: *Regina Reine* .....

Date: 31/10/2015

To my parents, my husband Peter Watson, my daughter Jessica and my son Robert

for their love and support

Acknowledgement

First and foremost, my deepest gratitude goes to my supervisor, Associate Prof. Zhuquan Zang. I am grateful for the tremendous amount of time he devoted to me and this research. His invaluable advice, constant encouragement, and constructive criticism during the entire period of my PhD study. He guided me to learn and enjoy the world of research.

I also would like to thank the Chairperson of my thesis committee, Associate Prof. Chua Han Bing, for his necessary administrative guidance.

My appreciation also extends to Dr. Lenin Gopal and Mohd Amaluddin Yusoff for their generosity in sharing and discussing technical knowledge with me. Their advice and feedback are much appreciated.

I am deeply indebted to my family who has supported me throughout the years. I would like to express my deepest gratitude to my lovely husband, Peter Watson. Without his patience, support and encouragement, this research work had been abandoned a long time ago. For my beloved parents and sister, thank you for all of your abundance love and encouragement. For Filbert Juwono, thank you for sharing the technical discussion and advice along the way.

I would like to thank those who have helped me in various ways throughout my study period, especially Imelda Idao.

Last but not least, I thank my Creator for making everything possible. I am very humbled and grateful for this great opportunity.

Abstract

Orthogonal frequency division multiplexing (OFDM) modulation technique has been used for high data rate transmission in wireless communications due to its spectral efficiency and its resilience against fading channels. One of the major drawbacks of the OFDM system is the high peak-to-average power ratio (PAPR) of the transmitted signal. A high PAPR will introduce nonlinearity when the OFDM signal is passed through a high power amplifier (HPA) at the transmitter. The HPA is often peak-power limited, either because of telecommunication regulations or application constraints. Nonlinearity creates inter-modulation between carriers and introduces signal distortion which lead to an increase of the bit error ratio (BER). In order to prevent nonlinearity, the power backoff can be increased to ensure the HPA operates in its linear region. However, increasing the power backoff will reduce the power efficiency of the HPA. Power efficiency is one of the essential factors in wireless applications. Therefore, reducing the PAPR of the OFDM signal is necessary to maintain the efficiency of the HPA.

Shaping the OFDM subcarriers with a properly selected pulse will reduce the PAPR of the OFDM signal. Ideal filters are often used as the shaping pulses. However, ideal filters are often non-causal and have to be truncated and shifted properly before being put into implementation. Instead of using non-causal ideal filters, a computationally efficient optimisation approach is proposed to design causal pulse shaping filters. Numerical results illustrate the effectiveness of the designed pulse shaping filters in reducing the PAPR of the OFDM signals.

The complementary cumulative distribution function (CCDF) is a meaningful tool to analyse and quantify the PAPR of the OFDM signal. Theoretical analyses and quantification of the CCDF have been thoroughly investigated in the existing literature. However, those theoretical analyses were carried out on the assumption that the OFDM signal is a stationary signal. When the OFDM signal is subjected to pulse shaping, the resulting signal is not stationary anymore, it becomes a cyclostationary signal. By introducing a random phase, the cyclostationary signal can be stationarised. After the stationarisation process, the level crossing rate (LCR)

theorem is used to derive an upper bound for the CCDF of PAPR. The proposed theoretical upper bound is validated by numerical simulations.

OFDM modulation technique has been incorporated into multiuser communication systems. To reduce the high PAPR in multiuser OFDM systems, a pulse shaping approach can be used. However, the pulse shaping approach cannot be implemented directly. It is necessary to establish users' independence in multiuser OFDM systems. An optimisation approach is proposed to design a set of orthogonal filters to generate a set of pulse shaping waveforms for different users. Numerical examples illustrate the effectiveness of the designed set of pulse shaping filters in reducing the PAPR of the multiuser OFDM signal.

Contents

List of Figures

List of Tables

List of Acronyms

3G	third generation
4G	fourth generation
5G	fifth generation
AWGN	additive white Gaussian noise
BPSK	binary phase shift keying
BER	bit-error-rate
BTRC	better than raised cosine
CCDF	complementary cumulative distribution function
CCI	co-channel interference
CDF	cumulative distribution function
CP	cyclic prefix
CSI	channel state information
DAB	digital audio broadcasting
DFT	discrete Fourier transform
DSL	digital subscriber lines
DVB	digital video broadcasting
FBMC	filter bank multi-carrier

FFT	fast Fourier transform
FIR	finite impulse response
GI	guard interval
HIPERLAN	high performance radio local area network
HPA	high power amplifier
ICI	inter-carrier interference
IDFT	inverse discrete Fourier transform
IFFT	inverse fast Fourier transform
i.i.d.	independent and identically distributed
ISI	inter-symbol interference
LCR	level crossing rate
LOS	line-of-sight
MIMO	multiple-input multiple-output
MPSK	multiple phase shift keying
MMSE	minimal mean squared error
OFDM	orthogonal frequency division multiplexing
OQAM	offset quadrature amplitude modulation
PAPR	peak-to-average power ratio
pdf	probability density function
PLC	power line communication
PTS	partial transmit sequence
QAM	quadratic amplitude modulation
QP	quadratic programming

QPSK	quadrature phase-shift keying
RAT	radio access technology
RC	raised cosine
RF	radio frequency
SIP	semi-infinite programming
SNR	signal-to-noise ratio
SLM	selected mapping
SRRC	squared root raised cosine
TR	tone reservation
UWA	underwater acoustic
UWB	ultra-wideband
WLAN	wireless local area networks
WSCS	wide sense cyclostationary
WSS	wide sense stationary

Chapter 1

Introduction

1.1 Overview of Orthogonal Frequency Division Multiplexing

Multicarrier modulation schemes have been developed to provide reliable high speed data transmission over wired and wireless channels. Multicarrier modulation schemes use the principle of frequency division multiplexing (FDM). At the transmitter, data are assigned to non-overlapping frequency carriers and at the receiver, a filter bank is used to demodulate the received data. Orthogonal frequency division multiplexing (OFDM) was proposed as a special multicarrier modulation scheme. OFDM has emerged as one of the key technologies for supporting high data rate transmissions because of its high spectral efficiency and its robustnesss against multipath fading channels.

OFDM has been incorporated in wireline applications, such as power line communication (PLC), digital subscriber lines (DSL) [2], wireless broadcast applications, such as digital audio broadcasting (DAB) and digital video broadcasting (DVB). In addition, it has been widely implemented in wireless local area networks (WLANs), the IEEE 802.11 standard, 3G wireless systems [4]; the IEEE 802.16 (WiMax) standard [5] and the ETSI HIPERLAN/2 standards [6]. OFDM has recently been adopted for 4G wireless systems and ultra-wideband (UWB) systems [3]. At present, it is highly considered as a candidate to support the future fifth generation (5G) communication systems [8].

The fundamental principle of OFDM is to divide a stream of high-rate data into many of parallel low-rate data streams which are mapped to a number of orthogonal subcarriers. The spectrums of the OFDM subcarriers overlap with each other without introducing interference, as illustrated in Fig. 1.1. Due to the orthogonality between the OFDM subcarriers, the receiver can demodulate the transmitted data without introducing inter-carrier interference (ICI). Consequently, OFDM has a higher spectrum efficiency compared to the conventional FDM multicarrier transmission schemes.

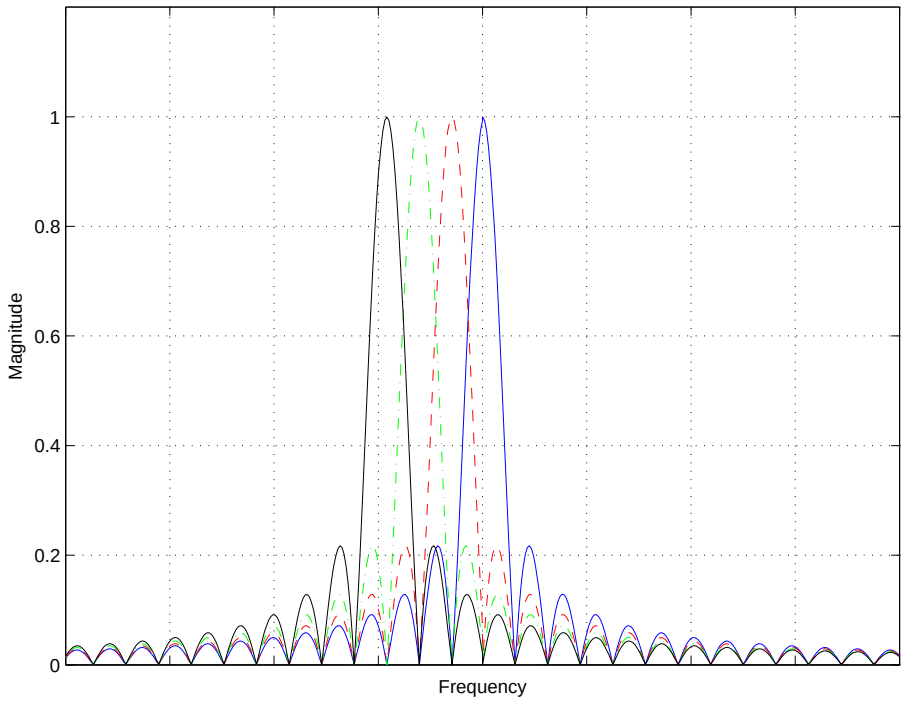

Figure 1.1: Spectrum of an OFDM signal.

One of the significant advantages of OFDM systems is its robustness against multipath fading channels. A lower complexity equalizers can be used to demodulate the received data [7]. In single carrier systems, on the other hand, complex equilizers are required to recover the distorted signal caused by frequency selective fading.

OFDM can be efficiently implemented using Inverse Fast Fourier Transform (IFFT)/ Fast Fourier Transform (FFT) . At the transmitter, the IFFT is used

for data modulation and the FFT is used to demodulate the data at the receiver. OFDM can eliminate inter-symbol interference (ISI) by employing cyclic prefix (CP) with a duration longer than the impulse response of the multipath fading channels.

The OFDM transmission block diagram is illustrated in Fig. 1.2. Consider that the data symbols are divided into N parallel orthogonal subcarriers with each of time duration T_s at the transmitter. Each N data symbols are grouped as an OFDM block $\mathbf{Z}$ where $\mathbf{Z}$=$[Z_0, Z_1, ..., Z_{N-1}]$. The data symbols in $\mathbf{Z}$ are modulated to N subcarriers and passed to IFFT before transmission.

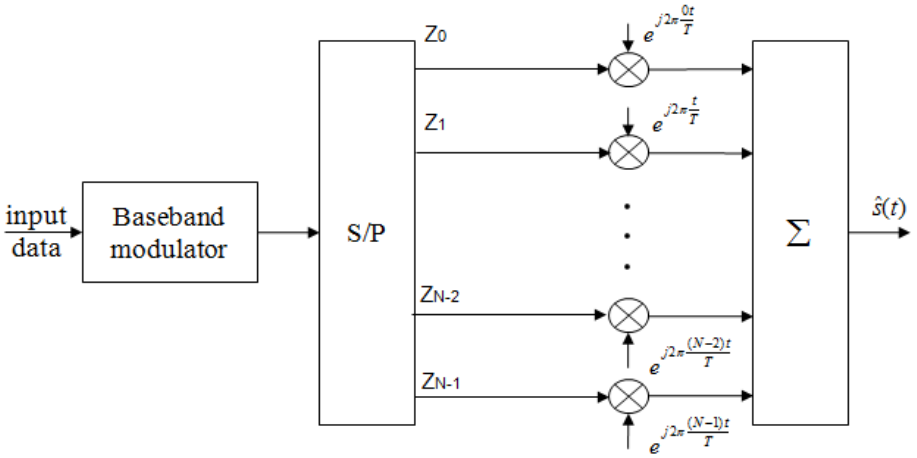

Figure 1.2: Block diagram of OFDM system model.

The OFDM bandpass transmitted signal can be defined by

$$s_c(t) = \Re\{\hat{s}(t)e^{j2\pi f_c t}\} \tag{1.1}$$

where f_c denotes the carrier frequency and $\Re\{s\}$ the real part of s. The baseband equivalent of the OFDM transmitted signal, $\hat{s}(t)$, can be expressed as

$$\hat{s}(t) = \sum_{k=0}^{N-1} Z_k e^{j2\pi kt/T}, \quad 0 \leq t < T \tag{1.2}$$

where $T = NT_s$ represents the time duration of the OFDM symbol. It is assumed that Z_k are independent and identically distributed (i.i.d) random variables where

it has zero mean and variance as

$$E[Z_k Z_n^*] = \begin{cases} \sigma^2, & k = n \\ 0, & k \neq n \end{cases} \tag{1.3}$$

where $(*)$ represents the complex conjugate operator.

1.2 Peak-to-Average Power Ratio

Despite having been implemented in many communication systems due to the multidimensional benefits, OFDM has several drawbacks. One of the drawbacks is that the OFDM transmitted signal often exhibits high peak-to-average power ratio (PAPR) [1].

Theoretically, increasing the number of subcarriers should be able to give better performance in a sense that the OFDM systems will able to handle larger delay spreads. However, in the time domain, the subcarriers sum up coherently and this results in a large dynamic signal range and may produce a very high PAPR. The high PAPR is a challenge for high power amplifier (HPA) at the transmitter. In order to avoid nonlinearity, the peak power must be within the HPA linear region. Nonlinearity will create inter-modulation between the carriers and introduces signal distortion. The in-band and out-of-band distortions will degrade the bit error rate (BER) performance. Distortion can be reduced and generally avoided by increasing the power backoff to keep the HPA operating in the linear range. However, additional power backoff means a larger dynamic range for the HPA. This type of HPA reduces the power efficiency which then reduces the battery life in portable systems. Due to the fact that the efficiency of battery life is a critical issue to the success of portable products, the high PAPR should be reduced before transmitting the OFDM signal to end user.

The PAPR of the OFDM signal in (1.2) can be defined by

$$PAPR = \frac{\max\limits_{0 \leq t < T} |\hat{s}(t)|^2}{E\left\{|\hat{s}(t)|^2\right\}} \tag{1.4}$$

where $\max|\hat{s}(t)|^2$ represents the peak power and the $E\left\{|\hat{s}(t)|^2\right\}$ denotes the average power of the OFDM signal. When the envelope of the OFDM signal is normalised, it can be expressed as

$$\hat{r}(t) \triangleq \frac{|\hat{s}(t)|}{\sqrt{P_{av}}} \tag{1.5}$$

where P_{av} denotes the average power of the OFDM signals. Using (1.5), the PAPR can be written as

$$PAPR = \max_{0\leq t<T} |\hat{r}(t)|^2 \tag{1.6}$$

For a large number of subcarriers, the probability of the PAPR reaching the maximum value is very low [1]. A more meaningful way to analyse the PAPR of the OFDM signal is to use the complementary cumulative distribution function (CCDF). The CCDF calculates the probability of the OFDM signal exceeding a specified PAPR threshold, γ. The CCDF of the PAPR can be defined by

$$C_{PAPR}(\gamma) = Pr\left\{\frac{\max\limits_{0\leq t<T}|\hat{s}(t)|^2}{P_{av}} \geq \gamma\right\} \tag{1.7}$$

If (1.5) is used, the CCDF can also be written as

$$C_{PAPR}(\gamma) = Pr\left\{\max_{0\leq t<T} \hat{r}(t) \geq \sqrt{\gamma}\right\} \tag{1.8}$$

1.3 Thesis Objectives

The objectives of this thesis are as follows:

1. Design pulse shaping filters using a computationally efficient optimisation approach to reduce the PAPR of the OFDM signal and evaluate the effectiveness of the proposed design with numerical simulations.

2. Investigate the PAPR distribution of the OFDM signal with pulse shaping.

3. Design a set of pulse shaping waveforms using an optimisation approach to reduce the PAPR of the OFDM signal in multiuser communication systems.

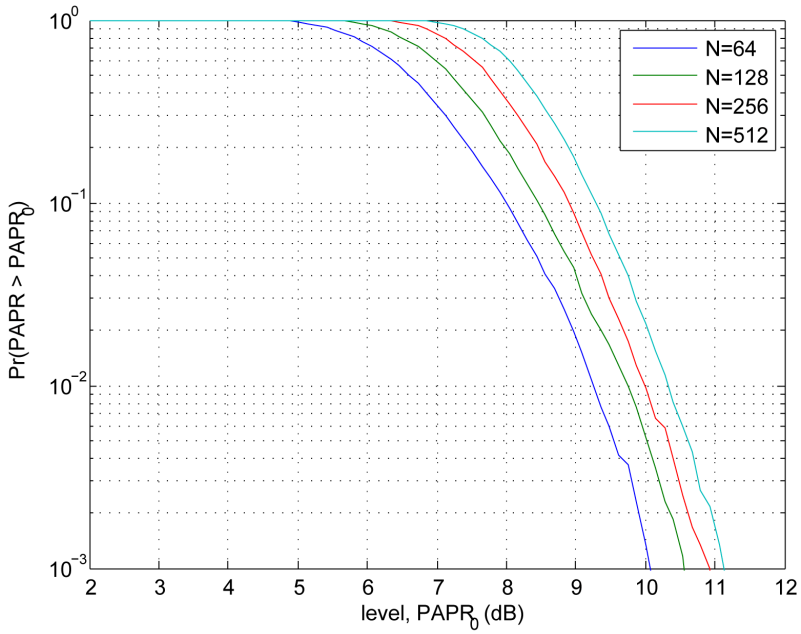

Figure 1.3: PAPR of the OFDM signal for different number of subcarriers

1.4 Thesis Overview and Contributions

The PAPR can be mitigated by using PAPR reduction techniques such as clipping and filtering [26] [27], coding [19], phase manipulation techniques (e.g selected mapping, Partial Transmit Sequences) [16] [17] [18] and pulse shaping [9]. However, some of these PAPR reduction techniques cause signal distortion that increases the BER or increases the implementation complexity of the OFDM systems.

Pulse shaping technique reduces the PAPR of the OFDM signal without destroying the orthogonality of the OFDM subcarriers. Pulse shaping can be implemented in OFDM system with only minimal increase of implementation complexity.

Chapter 2 presents some of the currently existing PAPR reduction techniques and introduces the pulse shaping approach. Chapter 3 introduces causal pulse shaping filter designs using a computationally efficient optimisation algorithm for reducing the PAPR of the OFDM transmitted signal. Chapter 4 investigates the BER performance of OFDM signal with the designed pulse shaping filters in multipath fading channels. Chapter 5 investigates the PAPR distribution of the OFDM signal after pulse shaping is applied. Chapter 6 presents the design of a set of pulse

shaping waveforms to reduce the PAPR of the OFDM signal in multiuser communication systems. Chapter 7 summarises this thesis and highlights the potential further research.

Chapter 2: PAPR Reduction Using Pulse Shaping

In this chapter, after a brief overview of the currently existing PAPR reduction techniques reported in the literature, the pulse shaping technique is investigated. By shaping the OFDM subcarriers properly, the PAPR of the OFDM signals can be reduced. The properly selected shaping pulse should be within the bandwidth of the OFDM signal and the orthogonality of the OFDM subcarriers should be maintained. Simulation results illustrate that by selecting the shaping pulse properly, the PAPR of the OFDM signal can be reduced.

Chapter 3: Optimal Pulse Shaping Filter Design for PAPR Reduction

In the current literature, ideal filters are used as shaping pulses to reduce the PAPR of the OFDM signal. However, an ideal filter is often non-causal and truncation is required for implementation. Truncation may introduce undesired ISI and lead to unnecessary additional bandwidth. Instead of using non-causal ideal filters, this chapter introduces the direct design of causal filters using computationally efficient optimisation approach to reduce the PAPR of the OFDM transmitted signal. The filter design problem is formulated as non-linear constrained optimisation problem. The non-linear constraints are linearised in order to solve the optimisation problem efficiently. Numerical results illustrate that the designed pulse shaping filters have better performance than the ideal filters in terms of PAPR reduction.

Chapter 4: BER Performance of the OFDM System with Pulse Shaping over Multipath Fading Channels

Reducing the PAPR can be at the expense of an increase of BER at the receiver. In this chapter, BER performance of the OFDM signal with pulse shaping is investigated. It is assumed that a matched filter is used and the full CSI is known at the receiver. HIPERLAN/2 channel models are used to simulate the multipath fading channels and low complexity detector is employed at the receiver. Numer-

ical results illustrate that the designed pulse shaping filters improves the BER performance of OFDM system over multipath fading channels.

Chapter 5: PAPR Distribution Analysis of OFDM Signal with Pulse Shaping

In this chapter, the PAPR distribution of the OFDM signal with pulse shaping is mathematically derived. Various theoretical analysis of PAPR distributions in the current literature were carried out based on the OFDM signal as a stationary signal. When pulse shaping is applied, the OFDM signal can be categorised as a wide sense cyclostationary (WSCS) signal. By introducing a random phase, a WSCS signal can be stationarised. After the proper stationarisation process, the CCDF of the PAPR is analysed using level crossing rate (LCR) theorem and an upper bound for the CCDF of the PAPR is derived. Numerical results show the proposed upper bound is tight.

Chapter 6: Pulse Shaping Approach to PAPR Reduction for Multiuser OFDM Systems

Multiuser OFDM (MU-OFDM) communication systems have higher system efficiency compared to single user OFDM systems. However, the high PAPR of the MU-OFDM signal is considered as one of the major drawbacks of the MU-OFDM systems. To reduce the high PAPR, pulse shaping approach can be used. However, direct implementation is not possible because in multiuser communication systems, users' independence should be established to ensure that users do not interfere with each other. In this chapter, computationally efficient optimisation approach is proposed to design a set of orthogonal pulse shaping waveforms to reduce the PAPR of the MU-OFDM signal. Autocorrelation and cross-correlation of the pulse shaping waveforms are specified in the constraints in order to minimise ISI and co-channel interference (CCI). Designing a set of pulse shaping waveforms with the autocorrelation and cross-correlation constraints is fundamentally different than designing a single pulse shaping waveform. A computationally efficient method to solve the optimisation design problem is presented. Numerical results illustrate that the designed set of pulse shaping waveforms is efficient in reducing

the PAPR of the OFDM signal in multiuser communication systems.

1.5 Publications

Parts of the contents in this thesis have been presented in the following conferences:

1. R. Reine and Z. Zang, "Analysis and comparison of a set of ISI waveforms for PAPR reduction in OFDM systems." *IEEE TENCON Conf.*, pp. 246-250, Nov. 2011.

2. R. Reine and Z. Zang, "A quadratic programming approach in pulse shaping filter design to reducing PAPR in OFDM systems." *IEEE Conference on Asia Pacific Commun. (APCC)*, pp. 572-576, Aug. 2013.

3. R. Reine and Z. Zang, "Semi-infinite quadratic programming approach to design FIR filter for PAPR reduction in OFDM system." *IEEE Statistical Signal Processing (SSP) Workshop*, Gold Coast, July 2014.

4. R. Reine and Z. Zang, "Waveform Set Design Using Non-Convex Optimisation Technique for PAPR reduction in Multiuser OFDM Signal." *IEEE Conf. on Industrial Electronics and Applications (ICIEA)*, submitted .

Chapter 2

PAPR Reduction Using Pulse Shaping

In this chapter, some of the existing PAPR reduction techniques are briefly analysed. The main discussion in this chapter is the pulse shaping technique. The rest of this chapter is organised as follows: Section 2.1 presents the overview of the PAPR reduction techniques. Pulse shaping technique is introduced in Section 2.2. The PAPR of the OFDM signals with pulse shaping is defined in Section 2.3. Section 2.4 investigates the type of the shaping pulse that reduces the PAPR of the OFDM signal. Section 2.5 introduces the existing Nyquist pulses. Numerical simulations are presented in Section 2.6 to show that shaping the OFDM subcarriers with a properly selected pulse reduces the PAPR of the OFDM signal. Finally, the conclusion of the chapter is drawn in Section 2.7.

2.1 Overview of PAPR Reduction Techniques

Various approaches have been proposed in the literature to mitigate the high PAPR of OFDM signals. Clipping [26] causes nonlinearity to the transmitted data and introduces out-of-band noise. Filtering is used to minimise the distortion caused by clipping but the peaks of the signal often return. Coding based PAPR reduction technique sacrifices data rate as well as increases the complexity of the transceiver design when the number of subcarriers is increasingly large[19]. Phase manipulation techniques (e.g selected mapping, Partial Transmit Sequences) require addi-

tional information to be sent to the receiver which increases the complexity to the OFDM systems[16][17][18].

2.1.1 Clipping

In clipping technique, the peak values above a specified threshold in the time domain is removed. Clipping process introduces nonlinearity. Clipping may cause significant in-band distortion that leads to the increase of the BER and out-of-band distortion which degrades the spectral efficiency of the OFDM signal. To reduce the effect of distortion, filtering can be used after the clipping process, however, filtering often causes significant peak-regrowth.

The clipped OFDM signal is generally represented as [26]

$$s_{clip}(t) = \begin{cases} \hat{s}(t), & \text{if } |\hat{s}(t)| \leq A \\ A, & \text{if } |\hat{s}(t)| > A \end{cases} \tag{2.1}$$

where $\hat{s}(t)$ is the baseband equivalent OFDM signal defined by

$$\hat{s}(t) = \sum_{k=0}^{N-1} Z_k e^{j2\pi kt/T}, \quad 0 \leq t < T \tag{2.2}$$

and $A = CR * \sqrt{\sigma_s}$, CR is the clipping ratio and σ_s is the average power of $\hat{s}(t)$.

Fig. 2.1 shows the CCDF of the PAPR of OFDM signal with different clipping ratios. Iterative clipping and filtering without an increase in the out-of-band power has been suggested [14] to minimise the distortion caused by clipping. Deep clipping method can be used as in [15] in order to reduce the peak regrowth problem due to out-of-band filtering. However these techniques have high complexity and are difficult to be implemented in OFDM systems.

2.1.2 Selected Mapping (SLM)

In SLM technique, different sets of signals which represent the same data are generated from the original data signal. The set of signals with the lowest value of PAPR will be selected for transmission. The transmitter needs to send side information regarding the selected set of signals to the receiver. The side information

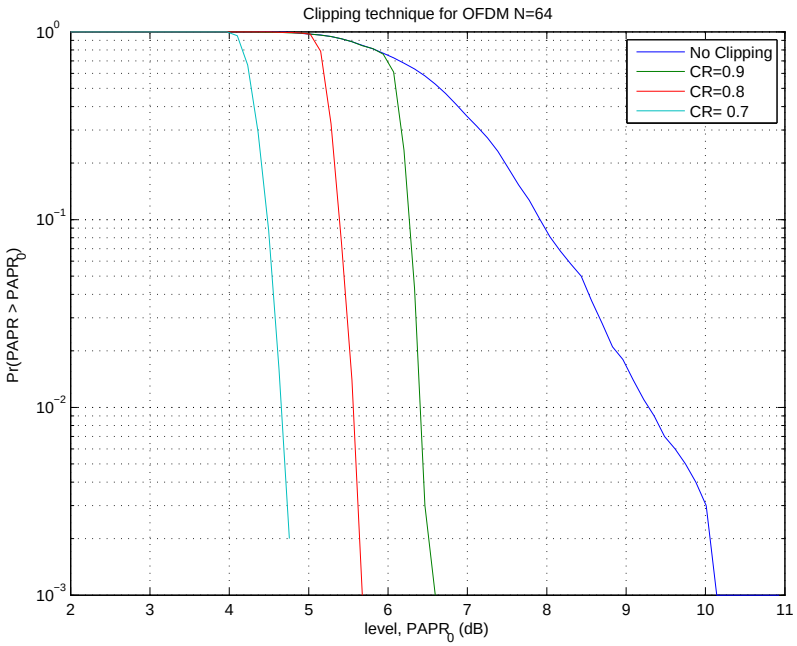

Figure 2.1: PAPR of OFDM with clipping (N=64).

is used to decode the received data at the transmitter.

The block diagram of OFDM signal with SLM is illustrated in Fig. 2.2. Consider that the data symbol $Z = [Z_0, Z_1, ..., Z_{N-1}]$ is the input to U number of statistically independendent phase sequences $B^{(u)} = [b_0^{(u)}, b_1^{(u)}, ..., b_{N-1}^{(u)}]^T$ where $1 \leq u \leq U$. If the u^{th} phase sequence is given by $Z^{(u)} = [Z_0 b_0^{(u)}, Z_1 b_1^{(u)}, ..., Z_{N-1} b_{N-1}^{(u)}]^T$ where $u = 1, 2, ..., U$, every $Z_k^{(u)}$ can be defined as

$$Z_k^{(u)} = Z_k b_k^{(u)} \qquad 1 \leq u \leq U \tag{2.3}$$

Then, the baseband equivalent of the OFDM signal is expressed as

$$s_l(t)^{(u)} = \sum_{k=0}^{N-1} Z_k^{(u)} e^{j2\pi kt/t} \tag{2.4}$$

The PAPR of the SLM-OFDM signal is defined as follows

$$PAPR_{slm} = \arg \min_{0 \leq u \leq U} \frac{\max_{0 \leq t < T} |s_l(t)^{(u)}|^2}{E\{|s_l(t)^{(u)}|^2\}} \tag{2.5}$$

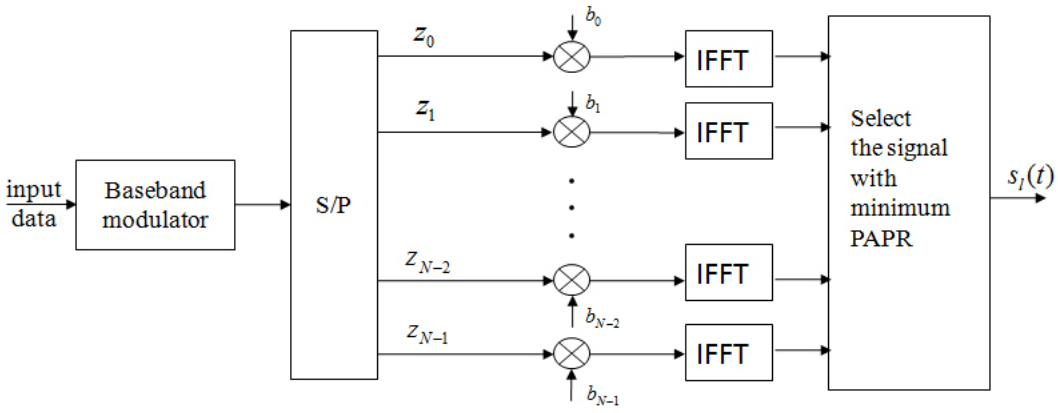

Figure 2.2: Block diagram of OFDM with SLM

Fig. 2.3 shows the CCDF of the PAPR of the OFDM signal using SLM where different sets of phase sequence are generated by Riemann, Hadamard, and a uniform random sequences [16][17][18]. A side information contains the information of the $B^{(u)}$ for the OFDM signal with the lowest PAPR. A lower PAPR value can be achieved by increasing U. However, it means that U of IFFT sets will be required at the OFDM transmitter. Hence, the implementation complexity of SLM in OFDM systems is increased when U is increased.

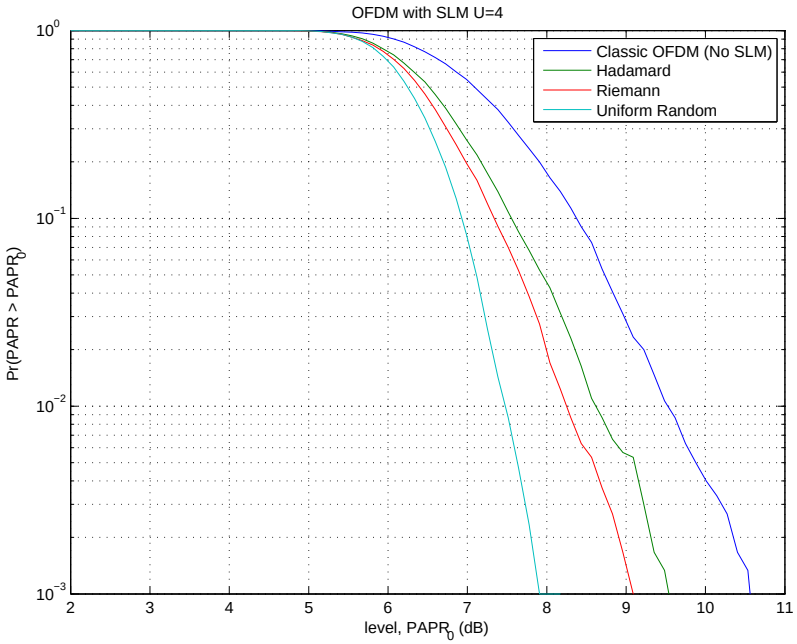

Figure 2.3: PAPR of the OFDM signal with SLM (N=64).

2.1.3 Tone Reservation

Tone reservation (TR) is categorised as a distortionless PAPR reduction technique. TR uses reserved tones to reduce the high PAPR of the OFDM signal. TR often requires extra information in the receiver to locate the position of the reserved tones. This results in an increase of the OFDM system implementation complexity.

The TR technique [30] reserves N_t tones for peak reduction and uses the rest of the tones $(N - N_t)$ for data transmission. The ratio of TR, N_t/N, is typically small and the peak-cancelling signal vector is $C_r = [C_{r(0)}, C_{r(1)}, ..., C_{r(N-1)}]$. The OFDM signal is given by

$$s(t) = IFFT(X + C_r) = x(t) + c_r(t) \tag{2.6}$$

where $X = [X_0, X_1, ..., X_{N-1}]$ is the data symbol. The PAPR of the OFDM signal is given by

$$PAPR_{TR} = \frac{\max |x(t) + c_r(t)|^2}{E\{|x(t)|^2\}} \tag{2.7}$$

By using more tones, the PAPR can be further reduced. However, this sacrifices the efficiency of the bandwidth as more subcarriers are used to carry the tones instead of the data information.

2.2 OFDM System Model with Pulse Shaping

The block diagram of the OFDM signal with pulse shaping is illustrated in Fig. 2.4. Consider that the OFDM system consists of N subcarriers. The modulated symbol $Z_k = [Z_0, Z_1, ..., Z_{N-1}]^T$ is mapped to the k^{th} subcarrier and has symbol interval of T_s. The baseband equivalent of the OFDM transmitted signal with pulse shaping can be expressed as:

$$s(t) = \sum_{k=0}^{N-1} Z_k p_k(t) e^{j2\pi kt/T}, 0 \leq t \leq T \tag{2.8}$$

where $p_k(t)$ is a pulse shaping waveform at the k^{th} subcarrier with duration of T.

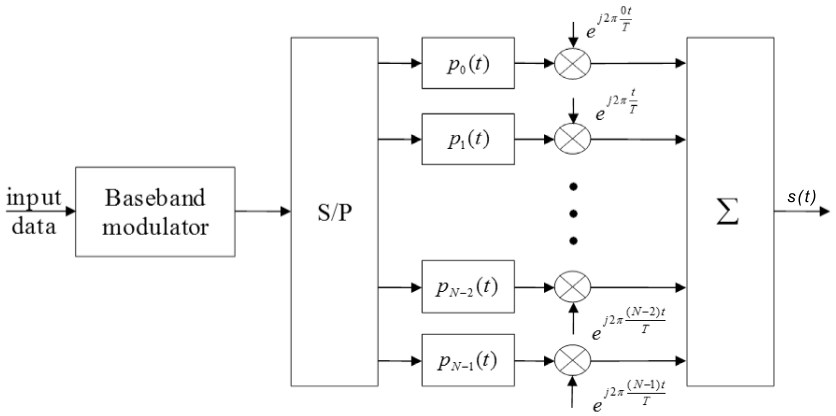

Figure 2.4: Block diagram of OFDM transmitter with pulse shaping.

2.3 PAPR of the OFDM Signals with Pulse Shaping

The PAPR of the OFDM signal with pulse shaping (2.8) is given by:

$$PAPR = \frac{\max\limits_{0\leq t<T} |s(t)|^2}{E\{|s(t)|^2\}} \tag{2.9}$$

If it is assumed that MPSK modulation is used, then $E\{|Z_k|^2\} = 1$ where the OFDM symbols are uncorrelated to each other. The upper bound of the PAPR is given by

$$PAPR \leq PAPR_{max} = \frac{1}{N} \max_{0\leq t\leq T} \left(\sum_{k=0}^{N-1} |p_k(t)| \right)^2 \tag{2.10}$$

It can be seen from (2.10) that the pulse shaping waveform and the number of subcarriers influence the PAPR.

2.4 Characterisation of Shaping Pulses That Reduces the PAPR

PAPR can be mitigated by creating a proper correlation between OFDM subcarriers [25]. One method is to use coding to find the pulse shape that reduces the PAPR. However, searching for the optimal pulse by coding-search can be exhaustive and complex for a large number of subcarriers. Another method is to shape different subcarriers in such a way that the peak amplitudes in the time domain do not appear at the same time. However, designing different pulse for different

subcarrier can be very complex. A simpler and effective way to achieve this is to cyclic shift the pulse for every subcarrier [9].

Assume that $p(t)$ is a time limited pulse of duration T and can be extended periodically as follows

$$q(t) = \sum_{i=-\infty}^{\infty} p(t - iT) \tag{2.11}$$

where its Fourier series representation can be written as

$$q(t) = \sum_{i=-\infty}^{\infty} C_i e^{j2\pi f_i t} \tag{2.12}$$

where its Fourier coefficient can be expressed as

$$C_i = \frac{1}{T} \int_0^T q(t) e^{-j2\pi f_i t} dt \tag{2.13}$$

The pulse $p_k(t)$ at the k^{th} subcarrier can be obtained by truncating equation(2.12) within the duration of T, which can be written as

$$p_k(t) = \begin{cases} q(t - kT_s), & 0 \leq t \leq T \\ 0, & \text{, otherwise} \end{cases} \tag{2.14}$$

From (2.14), the upper bound of the PAPR can be expressed as

$$PAPR_{max} = \frac{1}{N} \max_{0 \leq t \leq T} \left(\sum_{k=0}^{N-1} |q(t - kT_s)| \right)^2 \tag{2.15}$$

$$= \frac{1}{N} \left(\sum_{k=0}^{N-1} |q(kT_s)| \right)^2 \tag{2.16}$$

For a large number of subcarriers, (2.15) can be expressed as

$$\sum_{k=0}^{N-1} |q(t - kT_s)| \approx \frac{N}{T} \int_0^T |q(t)| dt \tag{2.17}$$

where the upper bound of the PAPR will be

$$PAPR_{max} = \frac{N}{T^2} \left(\int_0^T |q(t)| dt \right)^2 \leq N \tag{2.18}$$

2.5 Nyquist Pulses

In order to prevent ISI, the shaping pulse should satisfy the following [22]:

$$P(f) \approx 0 \quad \left| f - \frac{1}{2T_s} \right| > \frac{1}{2T_s} + \frac{\beta}{2T_s} \tag{2.19}$$

where $P(f)$ represents the Fourier transform of $p(t)$, β denotes the excess bandwidth ($0 < \beta < 1$) and $T_s = \frac{T}{N}$.

In the following example, four different sets of Nyquist pulses are investigated. The Raised Cosine (RC), Squared Root Raised Cosine (SRRC), Better than Raised Cosine (BTRC) and Orthogonal Better than Raised Cosine (OBTRC).

Raised Cosine. The Fourier transform of the RC, denoted as $P_{rc}(f)$, is given by [35]

$$P_{rc}(f) = \begin{cases} T_s \sin\left(\frac{\pi f T_s}{2\beta} + \frac{\pi}{4}\right), & |f| \leq \frac{\beta}{2T_s} \\ T_s & \frac{\beta}{2T_s} \leq f \leq \frac{2-\beta}{2T_s} \\ T_s \sin\left[\frac{\pi(fT_s - 1)}{2\beta} + \frac{3\pi}{4}\right], & \left| f - \frac{1}{T_s} \right| \leq \frac{2+\beta}{2T_s} \\ 0, & \text{otherwise} \end{cases} \tag{2.20}$$

SRRC. This SRRC is obtained by using RC as the base function. The Fourier transform of SRRC, denoted as $P_{srrc}(f)$, is given by [35]

$$P_{srrc}(f) = \begin{cases} \sqrt{T_s} \sin\left(\frac{\pi f T_s}{2\beta} + \frac{\pi}{4}\right), & |f| \leq \frac{\beta}{2T_s} \\ \sqrt{T_s} & \frac{\beta}{2T_s} \leq f \leq \frac{2-\beta}{2T_s} \\ \sqrt{T_s} \sin\left[\frac{\pi(fT_s - 1)}{2\beta} + \frac{3\pi}{4}\right], & \left| f - \frac{1}{T_s} \right| \leq \frac{2+\beta}{2T_s} \\ 0, & \text{otherwise} \end{cases} \tag{2.21}$$

BTRC. The BTRC pulse was designed to improve the robustness in the RC pulse in reducing the ISI in the OFDM systems. The Fourier transform of the

BTRC pulse is given as follows [32]

$$P_{btrc}(f)=\begin{cases} T_s, & 0 \le |f| \le \frac{1-\beta}{2T_s} \\ T_s e^{\frac{-2ln2T_s}{\beta}\left[|f|-\frac{1-\beta}{2T_s}\right]}, & \frac{1-\beta}{2T_s} \le |f| \le \frac{1}{2T_s} \\ T_s\left\{1-e^{\frac{-2ln2T_s}{\beta}\left[\frac{1+\beta}{2T_s}-|f|\right]}\right\}, & \frac{1}{2T_s} \le |f| \le \frac{1+\beta}{2T_s} \end{cases}$$

OBTRC. The *Optimized Better Than Raised Cosine* (OBTRC) pulse was designed to improve the robustness in reducing the ICI. The Fourier transform of the OBTRC pulse is given as follows [67]

$$P_{obtrc}(f)=\begin{cases} T_s, & 0 \le |f| \le \frac{1-\beta}{2T_s} \\ T_s e^{\frac{-2^n ln2T_s^n}{\beta^n}\left[|f|-\frac{1-\beta}{2T_s}\right]}, & \frac{1-\beta}{2T_s} \le |f| \le \frac{1}{2T_s} \\ T_s\left\{1-e^{\frac{-2^n ln2T_s^n}{\beta^n}\left[\frac{1+\beta}{2T_s}-|f|\right]}\right\}, & \frac{1}{2T_s} \le |f| \le \frac{1+\beta}{2T_s} \end{cases}$$

where $n > 1$.

2.6 Numerical Simulations

Computer simulations are carried out to investigate the effectiveness of pulse shaping technique in reducing the PAPR of the OFDM transmitted signal. The 10^4 QPSK data symbols are generated and $T = 1$. The shaping pulse in different subcarriers are originated from the main shaping pulse $p(t)$. Consider that a shaping pulse $p(t)$ is time limited where

$$p(t) = \sum_{i=0}^{L-1} C_i e^{j2\pi i \frac{t}{T}}, 0 \le t \le T \tag{2.22}$$

where $L = (1+\beta)N$ and its Fourier coefficient can be expressed as

$$C_i = \frac{1}{T}\int_0^T p(t)e^{-j2\pi i\frac{t}{T}}dt \tag{2.23}$$

$$= \frac{1}{T}P(\frac{i}{NT_s}) \tag{2.24}$$

From $p(t)$, the shaping pulse at the k^{th} subcarrier can be obtained by

$$p_k(t) = \sum_{k=0}^{N-1} \sum_{i=0}^{L-1} C_i e^{-j2\pi \frac{ki}{N}} e^{j2\pi \frac{k-i}{N}}, \quad 0 \leq t \leq T \tag{2.25}$$

Fig. 2.5 illustrates when the SRRC pulse is used to shape the OFDM subcarriers. Fig. 2.5 illustrates the $p_0(t)$ as the main pulse and $p_1(t)$, $p_2(t)$ and $p_3(t)$ are obtained from (2.25). Even though it is not shown in Fig. 2.5, there are total of $N = 64$ subcarriers.

Fig. 2.6 illustrates the frequency spectrum of RC, SRRC, BTRC and OBTRC.

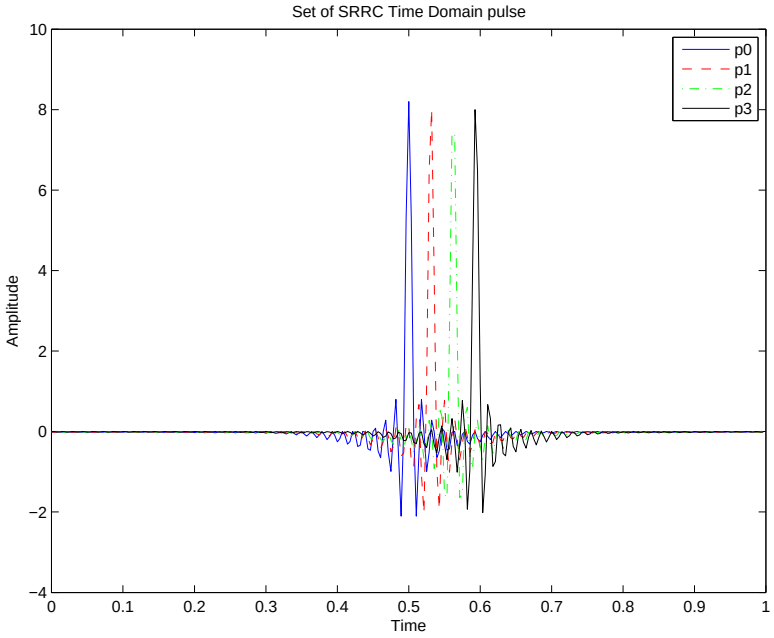

Figure 2.5: The first four sets of pulse with SRRC as the main pulse for N=64 subcarriers.

the decay rate can be analysed from Fig. 2.6 and it can be seen that SRRC has the fastest decay rate.

Fig. 2.7 depicts that by using a proper selection of pulse shape, the maximum of the PAPR of the OFDM signals can be reduced. Without pulse shaping, the maximum PAPR is around 12 dB for $N = 128$ and 11 dB for $N = 64$. It is observed that the maximum value of the PAPR of the OFDM signal with pulse shaping is near to the PAPR of the single carrier modulated signals. In the case of a single carrier signal with $\beta = 35\%$, the maximum PAPR is about 4 dB [74]. The

PAPR result of single carrier is close to the result of the PAPR of the OFDM signal shaped by the SRRC pulse as illustrated in Fig. 2.7. The PAPR maximum of the OFDM signal shaped by the SRRC pulse is approximately 4.2 dB. It can be seen from Fig.2.7 that when the roll-off parameter is increased, the PAPR decreases rapidly.

Fig. 2.8 depicts the CCDF of the PAPR of the OFDM signal with pulse shaping for $N = 64$. It is shown that when RC and SRRC pulses are used, a lower PAPR can be obtained compared to using a rectangular pulse. For the case of using RC and SRRC pulses with $\beta = 20\%$, the PAPR is reduced by approximately 4.5 dB and 5.5 dB respectively.

Fig. 2.10 illustrates that for $N = 512$, the CCDF of the PAPR is only slightly increased as compared to $N = 64$. This shows that when the pulse shaping is used, the PAPR is less sensitive to the increase of the number of subcarriers.

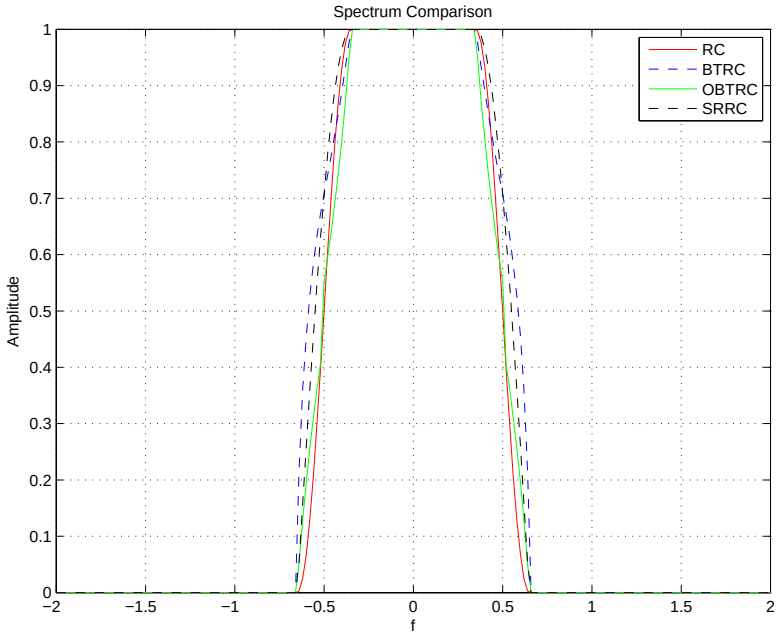

Figure 2.6: Spectrum frequency comparison.

To assess the effects of the number of subcarriers on the OFDM signal with pulse shaping, Fig. 2.9 presents the CCDF of the PAPR for $N = 128$ subcarriers. The PAPR reduction using pulse shaping is consistent for $N = 64$. The maximum PAPR ratio of both $N = 64$ and $N = 128$ is illustrated in Fig.2.11.

PAPR reduction performance using BTRC pulse and OBTRC pulse is demon-

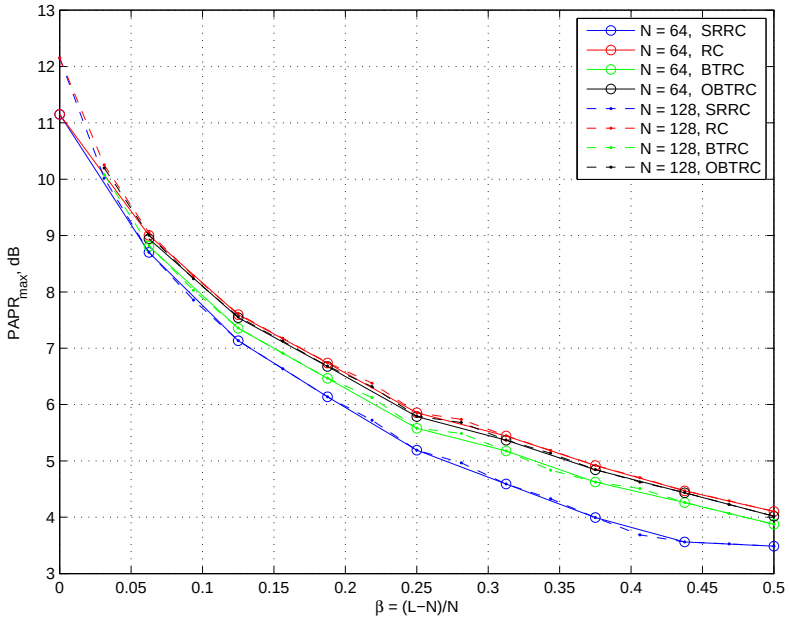

Figure 2.7: Maximum PAPR ratio for different number of OFDM subcarriers.

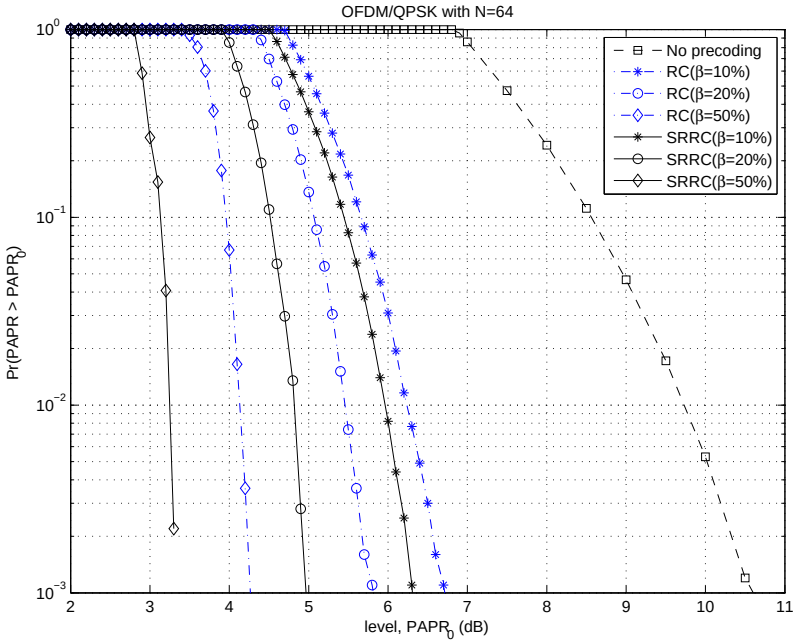

Figure 2.8: CCDF of PAPR for RC and SRRC pulses for N=64.

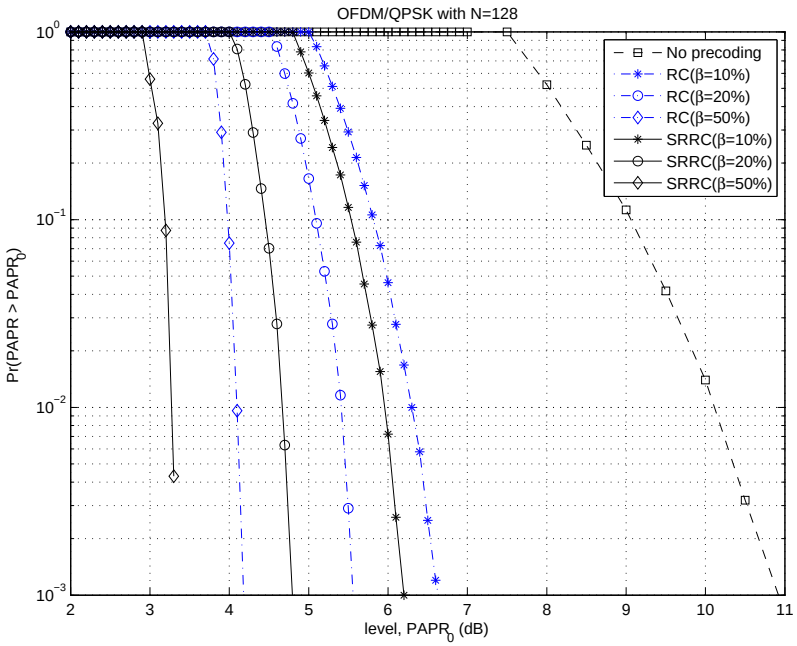

Figure 2.9: CCDF of PAPR of RC and SRRC pulses for N=128.

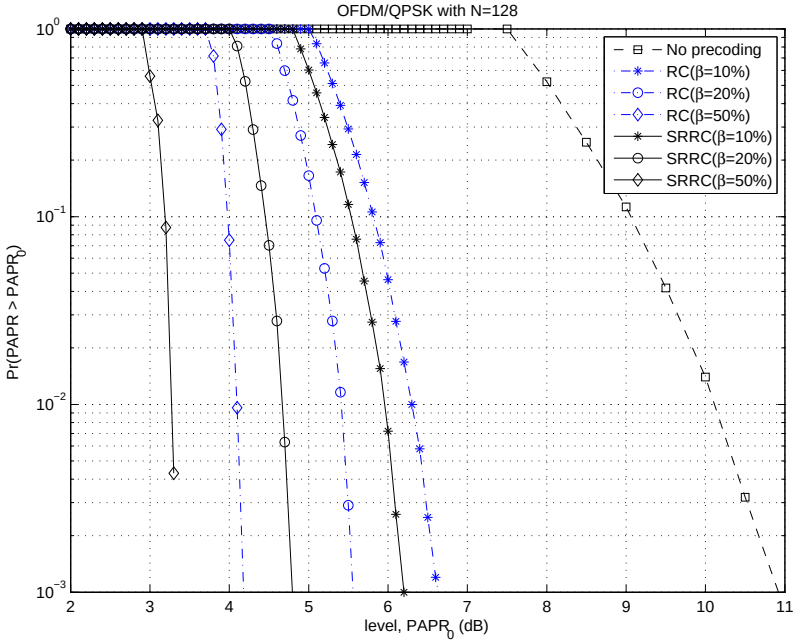

Figure 2.10: CCDF of PAPR of RC and SRRC pulses for N=512.

strated in Fig. 2.12. It is observed that for the case of $N = 64$ and $\beta = 20\%$, the PAPR can be reduced approximately 4.7 dB and 5.4 dB when OFDM signal uses OBTRC pulse and BTRC pulse, respectively.

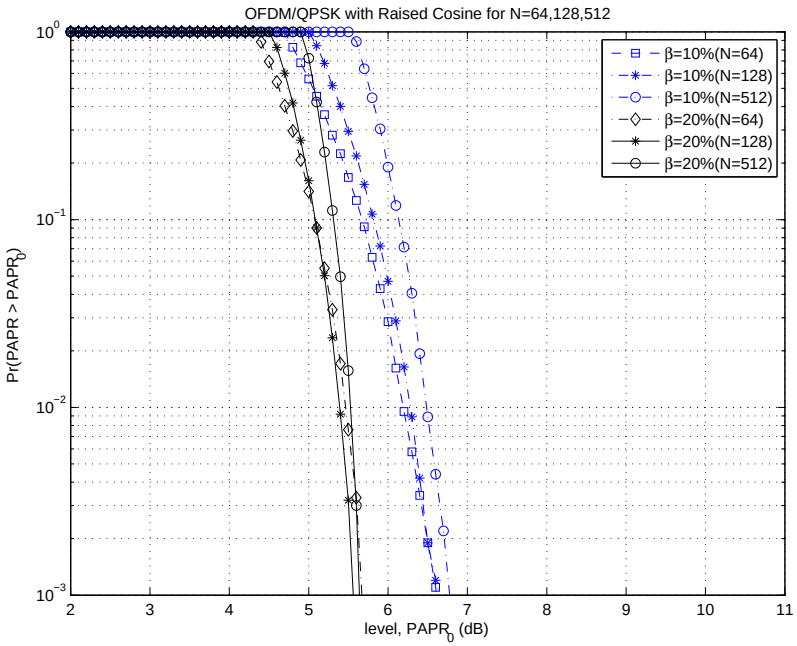

Figure 2.11: CCDF of PAPR using RC for N=64,128 and 512.

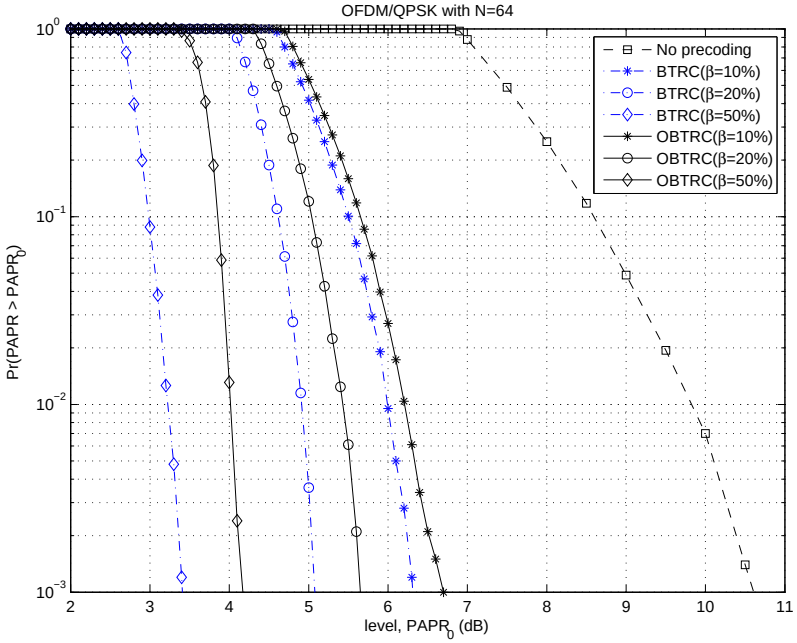

Figure 2.12: CCDF of PAPR for BTRC and OBTRC pulses.

2.7 Concluding Remarks

In this chapter, the effectiveness of selected Nyquist pulses as shaping pulses to reduce the PAPR of the OFDM signal is investigated. The impact of different

value of roll-off parameter and different number of subcarriers on the PAPR of the OFDM signal with pulse shaping are also analysed. The simulation results demonstrate that the selected Nyquist pulses outperforms the rectangular pulse in terms of PAPR reduction of the OFDM signal.

Chapter 3

Optimal Pulse Shaping Filter Design for PAPR Reduction

Chapter 2 shows that shaping the OFDM subcarriers using Nyquist pulses can reduce the PAPR of the OFDM signal. Nyquist pulses are ideal pulses. Ideal pulses or ideal filters are often non-causal where truncation and shifting are required in practical implementation. Direct truncation may introduce undesired ISI.

In this chapter, instead of using the existing non-causal ideal pulses, computationally efficient optimisation approach is proposed to design pulse shaping waveforms to reduce the PAPR of the OFDM signal.

The rest of this chapter is organised as follows: Section 3.1 introduces the system model of the OFDM signal with pulse shaping. In Section 3.2, the causal filter design problem is formulated using an optimisation approach and a method to solve the design problem is presented. The PAPR reduction performances are presented in Section 3.3. Finally, the chapter is concluded in Section 3.4.

3.1 Overview of OFDM System Model with Pulse Shaping

At the transmitter part of an OFDM system, the incoming data stream is divided into parallel low rate data streams over a number of subcarriers. The modulated symbol for the k^{th} subcarrier is represented as Z_k, with symbol interval T_s.

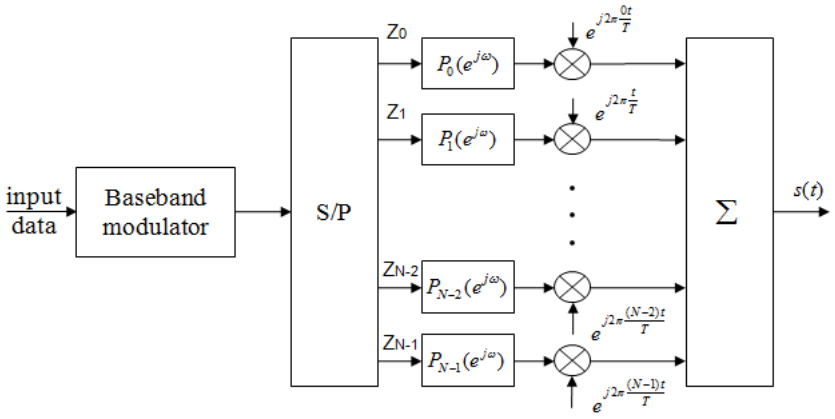

Figure 3.1: OFDM with pulse shaping system model.

Fig. 3.1 illustrates the transmitter part of an OFDM system with pulse shaping. It can be seen that the modulated data symbol Z_k is multiplied with the shaping pulse $P_k(e^{j\omega})$ at the k^{th} subcarrier. This process can be written as:

$$d_k = P_k(e^{j\omega})Z_k \tag{3.1}$$

where Z_k are often assumed to be i.i.d random variables with zero mean and variance $\sigma^2 = E[|Z_k|^2]$ and N denotes the number of subcarriers. Then, the N-points IFFT is applied to d_k. The baseband equivalent of the OFDM signal with pulse shaping can be expressed as

$$s(t) = \sum_{k=0}^{N-1} d_k e^{j2\pi kt/T}, \quad 0 \leq t < T \tag{3.2}$$

It is worth to mention that (3.2) is different from single-carrier signals in [23]. Pulse shaping technique in frequency domain can also be regarded as precoding technique.

It is considered that MPSK OFDM system with $E\{|Z_k|^2\} = 1$ and the symbols are uncorrelated within every OFDM block. The maximum PAPR of OFDM signal with pulse shaping is given as follows:

$$PAPR = \frac{1}{N} \max_{0 \leq t \leq T} \left(\sum_{k=0}^{N-1} \left| P_k(e^{j\omega}) e^{j2\pi kt/T} \right| \right)^2 \tag{3.3}$$

In order to preserve orthogonality of the OFDM subcarriers and to avoid ISI, it was suggested in [25] that the shaping pulse should satisfy the following:

$$\begin{cases} p_k(t) = 0 & \left|t - \frac{T}{2}\right| > \frac{T}{2} \\ P_k(f - \frac{k}{T}) \approx 0 & \left|f - \frac{1}{2T_s}\right| > \frac{1}{2T_s} + \frac{\beta}{2T_s} \end{cases}$$

The minimum bandwidth of the shaping pulse should be comparable to the bandwidth of OFDM signal which is $\frac{1}{T_s}$ where T_s is the symbol duration of the baseband modulated signal Z_k with $T_s = \frac{T}{N}$. Also, β is a design parameter that represents the roll-off parameter.

To reduce the PAPR of the OFDM transmitted signal, the shaping pulse should be designed in such a way so that the peaks should not appear at the same time instant. One way is to select different shaping pulse for every subcarrier and this way can be significantly complex. A simpler yet efficient approach is to design one principle pulse and the rest of the pulse are generated by cyclic shifts the principle pulse within the time interval $0 \leq t < T$. The frequency response of the principle pulse is denoted by $P_0(e^{j\omega})$, then

$$P_k(e^{j\omega}) = P_0(e^{j\omega})e^{-j\omega k}, k = 1, ..., N-1 \tag{3.4}$$

where in the existing literature $P_0(e^{j\omega})$ is usually a frequency response of an ideal pulse (e.g. a rectangular pulse, raised cosine pulse or square root raised cosine pulse) or an ideal filter. In practical implementations, (3.4) is often discretised and the discretised form of (3.4) can be written as:

$$P_{i,k} = P_{i,0}e^{-j2\pi\frac{ik}{N}} \tag{3.5}$$

where $i = 0, 1, ..., L-1$, $L = (1+\beta)N$ and $k = 0, 1, ..., N-1$.

Thus, instead of choosing ideal filters to construct the shaping pulse via truncation followed by discretisation, in the next section, an optimisation approach is used to directly design a FIR filter to generate the shaping pulse without the need of truncation.

3.2 Pulse Shaping Filter Design

3.2.1 Problem Formulation

The frequency response of an M coefficients filter is given by

$$P(e^{j\omega}) = \sum_{k=0}^{M-1} h_k \phi_k(e^{j\omega}) = \boldsymbol{h}^T \boldsymbol{\phi}(e^{j\omega}) \tag{3.6}$$

where

$$\boldsymbol{h} = [h_0, h_1, \dots h_{(M-1)}]^T$$
$$\boldsymbol{\phi} = [\phi_0, \phi_1, \dots, \phi_{(M-1)}]^T$$

and $\phi_k(e^{j\omega})$ is a set of orthogonal basis functions.

Here, the main focus is to design an M-tap FIR filter where

$$\phi_k(e^{j\omega}) = e^{-j\omega k} \quad , k = 0, 1, 2, \dots \tag{3.7}$$

The passband-to-stopband ratio of energies is a crucial performance measurement for many applications, it is effectively a signal-to-noise ratio. The signal corresponds to the passband energy and the noise corresponds to the stopband energy.

The stopband energy is defined by E_s, where

$$E_s = \frac{1}{\pi} \int_{\omega_s}^{\pi} |P(e^{j\omega})|^2 d\omega \tag{3.8}$$

and the passband energy is defined as E_p, which can be written as

$$E_p = \frac{1}{\pi} \int_{0}^{\omega_p} |P(e^{j\omega})|^2 d\omega \tag{3.9}$$

It is desireable to minimise the stopband to passband energy ratio. However, adjusting the energy in the passband can be difficult [36]. Therefore, it is more meaningful to minimise the stopband energy.

Mathematically the FIR filter design problem can be stated as:

Problem (P). Design an FIR filter $P(e^{j\omega})$ which solves the following constrained

optimisation problem

$$\min_{\mathbf{h}} \ \frac{1}{\pi}\int_{\Omega_s} |P(e^{j\omega})|^2 d\omega \tag{3.10}$$

subject to

$$|P(e^{j\omega}) - D(\omega)| \leq \sigma_p, \ \omega \in \Omega_p \tag{3.11}$$

$$|P(e^{j\omega}) - D(\omega)| \leq \sigma_s, \ \omega \in \Omega_s \tag{3.12}$$

where $D(\omega)$ is the desired (often non-causal) frequency response, Ω_p the set of passband frequencies, Ω_s the set of stopband frequencies, σ_p a small strictly positive amplitude error upper bound for the passband, σ_s a small strictly positive amplitude error upper bound for the stopband.

Remarks: (a) The magnitude constraints in (3.11) and (3.12) are non-linear due to the fact that $P(e^{j\omega})$ is complex. Therefore, problem (P) is a general nonlinear optimisation problem. Solving this nonlinear optimisation problem will only result in local minimum solutions. (b) While the objective function is chosen to minimise stopband energy, the magnitude constraints (3.11) and (3.12) are chosen to shape the digital filter to a desired spectral shape.

To effectively solve the nonlinear optimisation problem (P), in the following, both the objective function and the constraints will be simplified. In particular, the two sets of nonlinear constraints (3.11) and (3.12) will be linearised by introducing an additional constraint parameter.

3.2.2 Problem Conversion

By simple algebraic manipulation, the objective function (3.10) can be simplified to

$$\min_{\mathbf{h}} \ \left\{\frac{1}{2}\mathbf{h}^T Q\mathbf{h} + g^T\mathbf{h}\right\} \tag{3.13}$$

where

$$\begin{aligned} Q &= \frac{2}{\pi}\int_{\Omega_s} \boldsymbol{\phi}(e^{j\omega})\boldsymbol{\phi}^T(e^{j\omega})d\omega \\ g &= -\frac{2}{\pi}\int_{\Omega_s} \boldsymbol{\phi}(e^{j\omega})D(\omega)d\omega \end{aligned}$$

and

$$\mathbf{e}(\omega) = [1, e^{-j\omega}, \ldots, e^{-j\omega(M-1)}]^T$$

Then, the nonlinear magnitude constraints (3.11) and (3.12) need to be simplified. Non-linear constraints can be linearised by using the *real rotation* theorem [22]. The *real rotation* theorem states that minimising $|f|$ is equivalent to minimising $\Re(e^{j\Theta})$, $\Theta \in [0\ 2\pi]$. According to the *real rotation* theorem [22], a magnitude of inequality in complex number z=a+jb can be written in the equivalent form as:

$$|z| \leq \sigma \ \Leftrightarrow \ \max_{0\leq\theta<2\pi} \Re\left\{ze^{j\theta}\right\} \leq \sigma \tag{3.14}$$

where $\Re\{\cdot\}$ denotes the real part of a complex value number.

After the linearisation process (see Appendix 3.A), it is clear that the constraints are now linear with respect to the design variable $\mathbf{h}$.

From (3.13), (3.23) and (3.24), the optimisation problem ($\mathbf{P}$) can be written as :

$$\min_{\mathbf{h}} \left\{ \frac{1}{2}\mathbf{h}^T Q\mathbf{h} + g^T\mathbf{h} \right\} \tag{3.15}$$

subject to

$$a_p^T(\omega,\theta)\mathbf{h} \leq b_p(\omega,\theta) \ \ \omega \in \Omega_p, \theta \in [0, 2\pi) \tag{3.16}$$

$$a_s^T(\omega,\theta)\mathbf{h} \leq b_s(\omega,\theta) \ \ \omega \in \Omega_s, \theta \in [0, 2\pi) \tag{3.17}$$

It can be seen that the optimisation problem (3.15)-(3.17) is a semi-infinite quadratic programming problem. The number of variables $\mathbf{h}$ to be optimised is finite but the number of constraints, which depends on both ω and θ is infinite. This problem can be solved via discretisation of ω and θ or using the approach in [20].

From solving the semi-infinite quadratic programming problem (see Appendix 3.B), it suggests that the following version of the optimisation problem should be considered:

Problem ($\mathbf{P_b}$): *Given discrete sets of* $\{\theta_i\}_{i=1}^{2p}$ *and* $\{\omega_l\}_{l=1}^{L}$, *find* $\boldsymbol{h}$ *which solves*

the following quadratic programming problem.

$$\min_{\mathbf{h}} \left\{ \frac{1}{2}\mathbf{h}^T Q\mathbf{h} + g^T\mathbf{h} \right\} \tag{3.18}$$

subject to

$$A_{lp}\mathbf{h} \leq b_{lp} \tag{3.19}$$

$$A_{ls}\mathbf{h} \leq b_{ls} \tag{3.20}$$

where, in passband, for each l, A_{lp} is a 2p × M matrix with $a_p^T(\omega_l, \theta_i) = cos(\omega_l k - \theta_i)$ as its i^{th} row and b_{lp} is a 2p-dimensional column vector with all its entries $b_{lp} = \frac{\sigma_p}{sec(\frac{\pi}{2p})} + D(\omega_l)cos(\theta_i)$. In stopband, for each l, A_{ls} is a 2p × M matrix with $a_s^T(\omega_l, \theta_i) = cos(\omega_l k - \theta_i)$ as its i^{th} row and b_{ls} is a 2p-dimensional column vector with all its entries $b_{ls} = \frac{\sigma_s}{sec(\frac{\pi}{2p})}$.

Existing computationally efficient optimisation subroutines, such as *quadprog*, in MATLAB Optimisation Toolbox can be used to solve the problem (P_b) to obtain the global solution.

Note that (3.6) is the frequency response of nonlinear phase FIR filter. Linear phase FIR filter can be used and the optimisation problem can be formulated and converted as derived in Apendix 3.C.

3.3 Numerical Results

In this section, numerical results are carried out to show the effectiveness of the designed pulse shaping filter to reduce the PAPR of the OFDM signal.

There are various ways to generate the pulse shaping matrix. One way is to use a coding based technique such as *Walsh Hadamard Transform* (WHT). Another way is to use filters to generate the pulse shaping matrix using (3.5). It can be seen in Fig. 3.8 that the PAPR reduction using WHT coding is insignificant as compared to the proposed method as in (3.5). The parameters for the FIR filter design are $\sigma_p = 10^{-5}$, $\sigma_s = 10^{-4}$, $M = 30$ and $N = 64$. Raised cosine is chosen to be the desired ideal filter. The comparison of time domain response of the proposed FIR to non-causal RC is illustrated in Fig. 3.2. The frequency

reponse of the proposed FIR filter is illustrated in Fig.3.3 and it can be seen that its shape is very closed to the ideal RC filter ($\beta = 20$ %). It is observed that when parameter σ_p is set to smaller value, it reduces the ripple in the passband which results in the increased in the stopband energy and this leads to higher PAPR of the OFDM signals. Fig. 3.4 illustrates that the proposed FIR filter design approach can improve the PAPR reduction of the OFDM signals. The OFDM symbols are QPSK modulated.

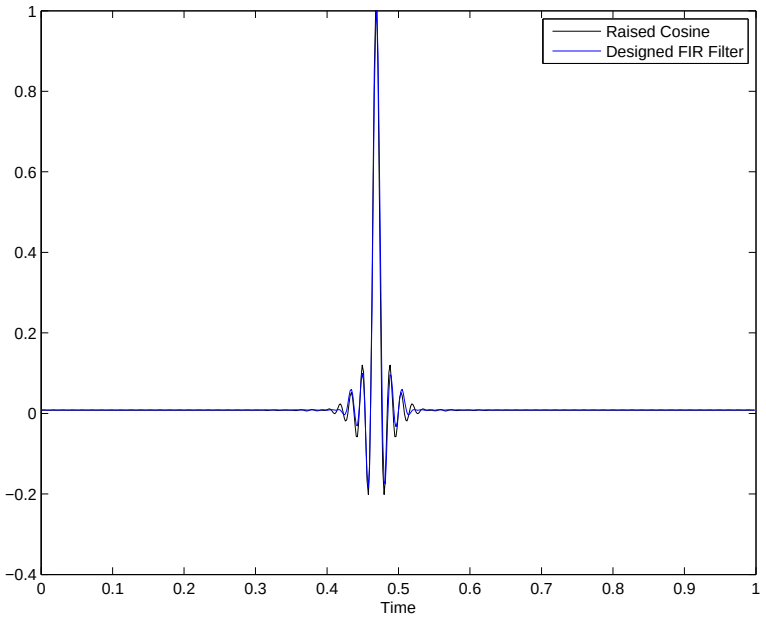

Figure 3.2: Time domain response of designed FIR filter M=30.

Fig.3.5 illustrates the CCDF of PAPR of the OFDM signal for $N = 64$, $\sigma_p = 10^{-5}$, $\sigma_s = 10^{-4}$ and $M = 26$ ($\beta = 10$ % and $\beta = 20$ %). Fig.3.6 illustrates the CCDF of PAPR of the OFDM signal for the case of $N = 64$, $\sigma_p = 10^{-5}$ and $\sigma_s = 10^{-4}$ with $M = 20$ ($\beta = 10$ % and $\beta = 20$ %). Fig. 3.6 and Fig. 3.5 show the effectiveness of the proposed filter design in reducing the PAPR of the OFDM signal.

To assess the effect of different subcarriers, Fig. 3.7 illustrates for $N = 128$ subcarriers. The parameters for the FIR filter design are $\sigma_p = 10^{-5}$, $\sigma_s = 10^{-4}$ and $M = 26$ ($\beta = 10$ % and $\beta = 20$ %). It shows that the CCDF of the PAPR of the precoded OFDM using the proposed designed FIR filter outperforms the one

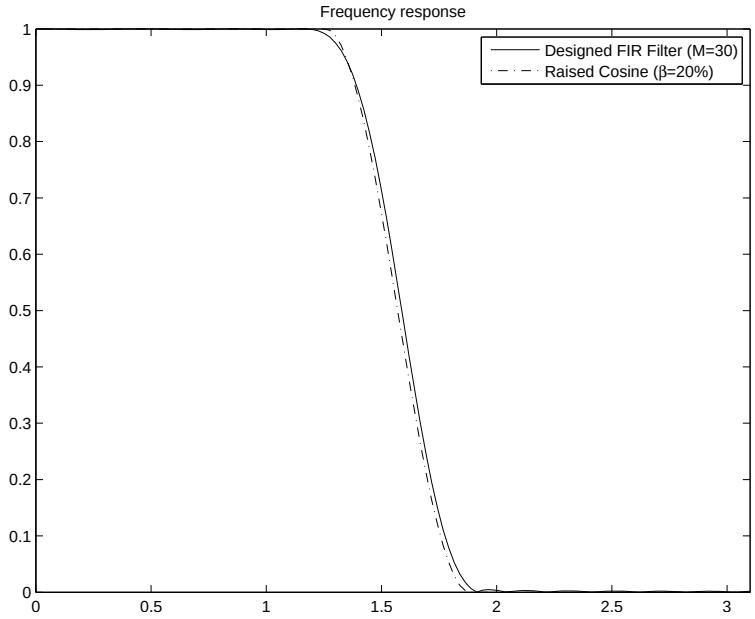

Figure 3.3: Frequency response of designed FIR filter M=30.

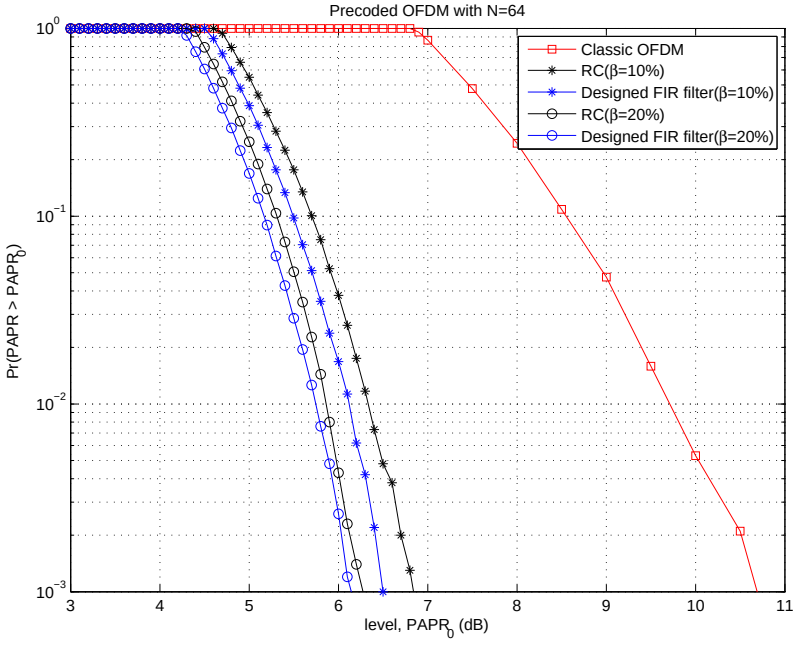

Figure 3.4: CCDF of PAPR of OFDM signal with the designed FIR filter.

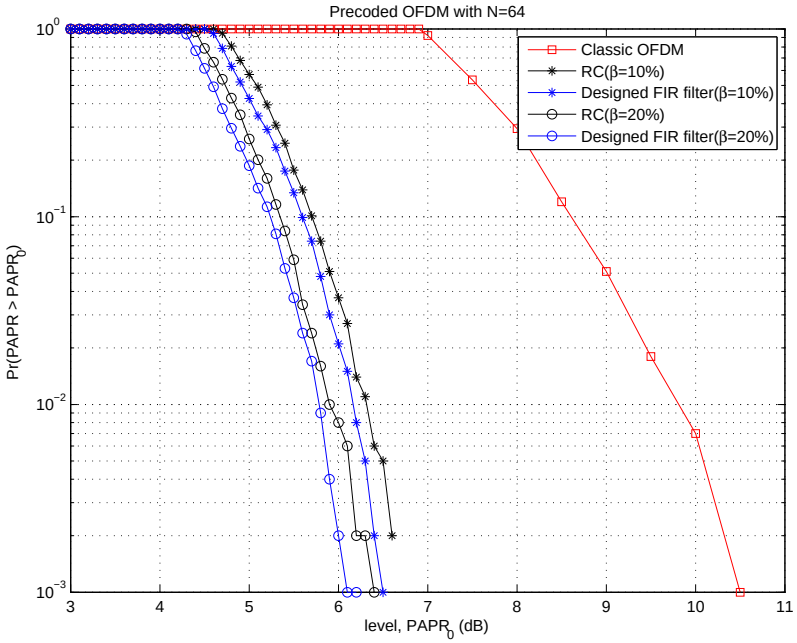

Figure 3.5: CCDF of the PAPR with the designed FIR filter (M=26).

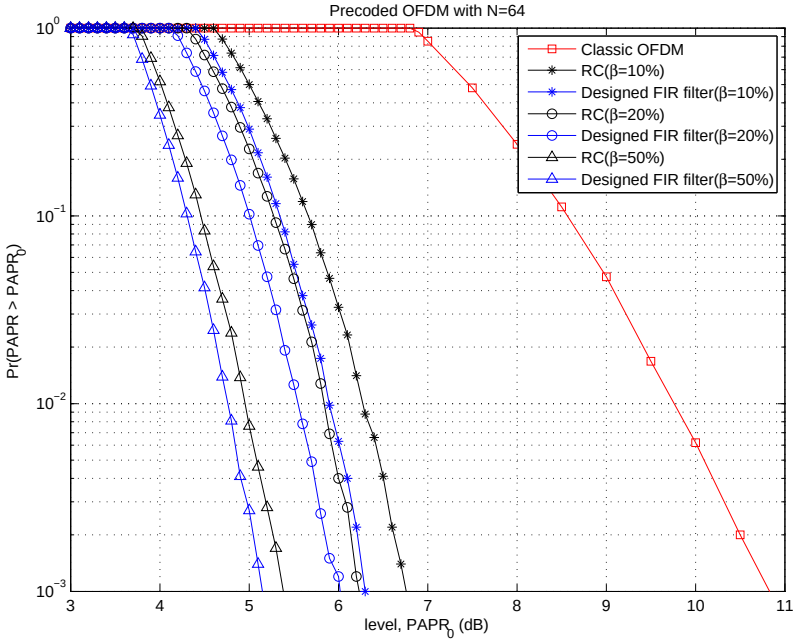

Figure 3.6: CCDF of PAPR of OFDM signal with the designed FIR filter (M=20).

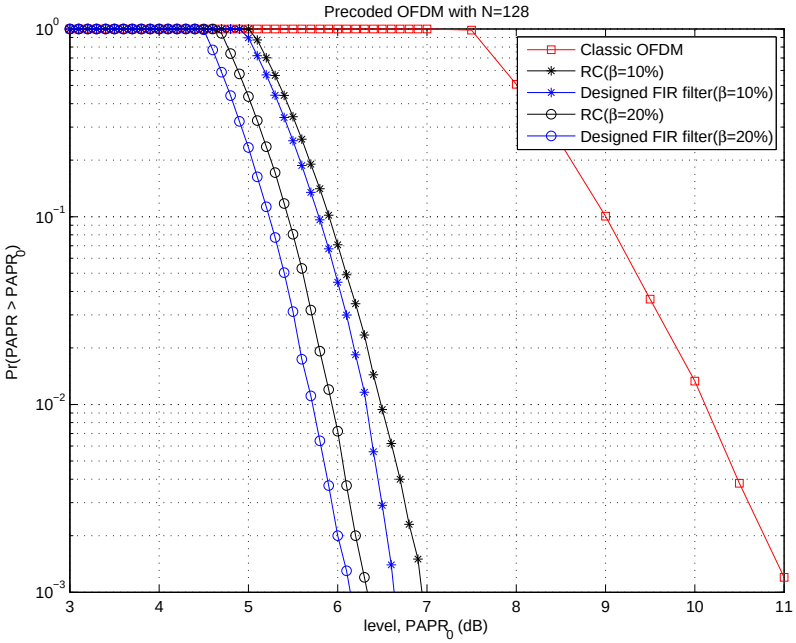

Figure 3.7: CCDF of PAPR of OFDM signal with the designed FIR filter for N=128.

using the ideal RC filter.

3.4 Concluding Remarks

In this chapter, instead of using ideal filters, causal filters designed using an optimisation approach to generate the shaping pulse in order to reduce the PAPR of the OFDM signal. The causal filter design was formulated to minimise the stopband energy subjected to nonlinear magnitude constraints in both stopband and passband. In order to solve this filter design problem efficiently, the nonlinear constraint is linearised using the *real rotation* theorem. Finally, the filter design problem is simplified and solved as a quadratic programming problem. The numerical results demonstrate that shaping the OFDM subcarriers with the proposed filter design has better performance in terms of the PAPR reduction as compared to using ideal filters (e.g. rectangular pulse and raised cosine pulse) as the shaping pulse.

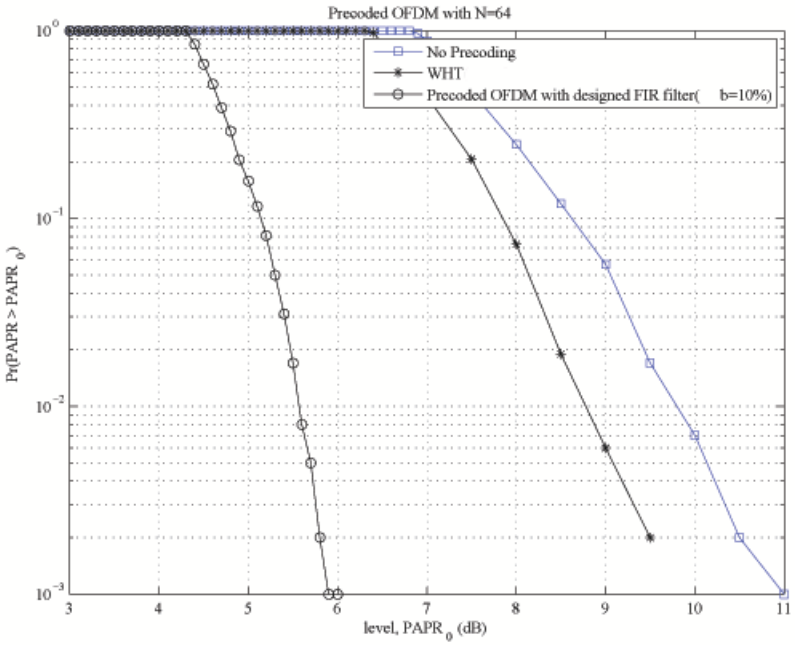

Figure 3.8: Comparison of the PAPR of the designed precoded OFDM signal vs WHT OFDM signal.

3.A Appendix: Constraint Linearisation

In this section, the nonlinear magnitude constraints (3.11) and (3.12) are linearised using the *real rotation* theorem in (3.14). By using (3.14), the inequality constraint (3.11) can be written as:

$$\max_{0\leq\theta<2\pi} \Re\left\{(P(e^{j\omega}) - D(\omega))e^{j\theta}\right\} \leq \sigma_p,\ \omega \in \Omega_p \tag{3.21}$$

Note that by substituting (3.6) in (3.21), the (3.21) can be rewritten as

$$\Re\left\{(\mathbf{h}^T\boldsymbol{\phi}(e^{j\omega}) - D(\omega))e^{j\theta}\right\} \leq \sigma_p\ \omega \in \Omega_p \tag{3.22}$$

for $\theta \in [0, 2\pi)$, which can be expressed as

$$a_p^T(\omega,\theta)\mathbf{h} \leq b_p(\omega,\theta), \quad \omega \in \Omega_p, \theta \in [0, 2\pi) \tag{3.23}$$

where

$$\begin{aligned} a_p(\omega,\theta) &= \Re\left\{\boldsymbol{\phi}(e^{j\omega})e^{j\theta}\right\} \\ b_p(\omega,\theta) &= \sigma_p + \Re\left\{D(\omega)e^{j\theta}\right\} \end{aligned}$$

In the stopband, it is often considered that $D(\omega) = 0$. By using the *real rotation* theorem, the constraint in stopband (3.12) can be simplified as

$$a_s^T(\omega,\theta)\mathbf{h} \leq b_s(\omega,\theta), \quad \omega \in \Omega_s, \theta \in [0, 2\pi) \tag{3.24}$$

where

$$\begin{aligned} a_s(\omega,\theta) &= \Re\left\{\boldsymbol{\phi}(e^{j\omega})e^{j\theta}\right\} \\ b_s(\omega,\theta) &= \sigma_s \end{aligned}$$

3.B Appendix: Solving Semi-Infinite Quadratic Programming Problem

In this section, the semi-infinite quadratic programming problem (3.15)-(3.17) is solved via discretisation of ω and θ.

For simplicity, parameter θ is discretised as $\{\theta_i\}_{i=1}^{2p}$ with $\theta_i = \frac{\pi(i-1)}{p},\ p \geq 2$. Consider the following definition for the magnitude constraint in (3.23)

$$Y_n^p(\omega) = \max_{1\leq i<2p} \Re\left\{(\mathbf{h}^T\boldsymbol{\phi}(e^{j\omega}) - D(\omega))e^{j\theta_i}\right\} \tag{3.25}$$

which can be expressed as [21]

$$Y_n^p(\omega) \leq \max_{0\leq\theta<2\pi} \Re\left\{(\mathbf{h}^T\boldsymbol{\phi}(e^{j\omega}) - D(\omega))e^{j\theta}\right\} \leq Y_n^p(\omega)sec(\frac{\pi}{2p})$$

When $p \to \infty$, the value of $sec(\frac{\pi}{2p}) \to 1$. This means that $Y^p(\omega)$ gives a good estimate of $P(e^{j\omega})$ for a sufficiently large integer p. In fact, for $p = 8$, $sec(\frac{\pi}{2p}) = 1.020$.

Therefore, instead of using magnitude constraints in passband in (3.22), the

following strengthened inequality constraints over discrete sets $\{\omega_l\}_{l=1}^{L}$ and $\{\theta_i\}_{i=1}^{2p}$ should be considered

$$\max_{1\leq i\leq 2p} \Re\left\{ \mathbf{h}^T\boldsymbol{\phi}(e^{j\omega_l})e^{j\theta_i}\right\} \leq \frac{\sigma_p}{sec(\frac{\pi}{2p})} + \Re\left\{D(\omega_l)e^{j\theta_i}\right\} \quad \omega\in\Omega_p \tag{3.26}$$

By using (3.7), the $\boldsymbol{\phi}(e^{j\omega_l})$ can be replaced with $e^{-j\omega_l k}$, then

$$\begin{aligned}
&\max_{1\leq i\leq 2p} \Re\left\{\mathbf{h}^T e^{-j\omega_l k}e^{j\theta_i}\right\} \leq \frac{\sigma_p}{sec(\frac{\pi}{2p})} + \Re\left\{D(\omega_l)e^{j\theta_i}\right\} \quad \omega\in\Omega_p\\
&\max_{1\leq i\leq 2p} \Re\left\{ \mathbf{h}^T e^{-j(\omega_l k-\theta_i)}\right\} \leq \frac{\sigma_p}{sec(\frac{\pi}{2p})} + \Re\left\{D(\omega_l)e^{j\theta_i}\right\} \quad \omega\in\Omega_p\\
&\max_{1\leq i\leq 2p} \mathbf{h}^T cos(\omega_l k-\theta_i) \leq \frac{\sigma_p}{sec(\frac{\pi}{2p})} + D(\omega_l)cos(\theta_i) \quad \omega\in\Omega_p
\end{aligned} \tag{3.27}$$

For the case of the magnitude contraint in the stopband (3.24), where it is often assumed that $D=0$, the new strengthened inequality contraint will be

$$Y_{s_n}^{p}(\omega) = \max_{1\leq i<2p} \Re\left\{(\mathbf{h}^T\boldsymbol{\phi}(e^{j\omega}))e^{j\theta_i}\right\} \quad \omega\in\Omega_s \tag{3.28}$$

which becomes

$$Y_{s_n}^{p}(\omega) \leq \max_{0\leq\theta<2\pi} \Re\left\{(\mathbf{h}^T\boldsymbol{\phi}(e^{j\omega}))e^{j\theta}\right\} \leq Y_{s_n}^{p}(\omega)sec(\frac{\pi}{2p}) \quad \omega\in\Omega_s$$

where the inequality contraints are discretised over discrete sets $\{\omega_l\}_{l=1}^{L}$ and $\{\theta_i\}_{i=1}^{2p}$

$$\max_{1\leq i\leq 2p} \Re\left\{ \mathbf{h}^T\boldsymbol{\phi}(e^{j\omega_l})e^{j\theta_i}\right\} \leq \frac{\sigma_s}{sec(\frac{\pi}{2p})} \quad \omega\in\Omega_s \tag{3.29}$$

If the $\boldsymbol{\phi}(e^{j\omega_l})$ is replaced with $e^{-j\omega_l k}$, it will be

$$\begin{aligned}
&\max_{1\leq i\leq 2p} \Re\left\{\mathbf{h}^T e^{-j\omega_l k}e^{j\theta_i}\right\} \leq \frac{\sigma_s}{sec(\frac{\pi}{2p})} \quad \omega\in\Omega_s\\
&\max_{1\leq i\leq 2p} \Re\left\{ \mathbf{h}^T e^{-j(\omega_l k-\theta_i)}\right\} \leq \frac{\sigma_s}{sec(\frac{\pi}{2p})} \quad \omega\in\Omega_s\\
&\max_{1\leq i\leq 2p} \mathbf{h}^T cos(\omega_l k-\theta_i) \leq \frac{\sigma_s}{sec(\frac{\pi}{2p})} \quad \omega\in\Omega_s
\end{aligned} \tag{3.30}$$

3.C Appendix: Linear Phase FIR Filter

The frequency response of an M coefficient filter:

$$P(e^{j\omega}) = \sum_{k=0}^{M-1} \alpha_k \phi_k(e^{j\omega}) = \boldsymbol{\alpha}^T \boldsymbol{\phi}(e^{j\omega}) \tag{3.31}$$

where

$$\boldsymbol{\alpha} = [\alpha_0, \alpha_1, \ldots \alpha_{(M-1)}]^T$$
$$\boldsymbol{\phi} = [\phi_0, \phi_1, \ldots, \phi_{(M-1)}]^T$$

and

$$\phi_k(e^{j\omega}) = e^{-j\omega k} \quad k = 0, 1, 2, \ldots \tag{3.32}$$

For a linear phase FIR filter, by choosing M as an even number, the coefficients α_k satisfy $\alpha_k = \alpha_{(M-k)}$ and $P(e^{j\omega})$ can be written as

$$P(e^{j\omega}) = A(\omega) e^{-jr\omega} \tag{3.33}$$

where $r = \frac{M}{2}$ and $A(\omega)$ is given by

$$A(\omega) = \sum_{k=0}^{r} h_k \cos(\omega) = \mathbf{h}^T \mathbf{e}(\omega) \tag{3.34}$$

with

$$\mathbf{h}_k = \begin{cases} \alpha_r, & k = 0 \\ 2\alpha_{(r-k)}, & k = 1, \ldots, r \end{cases}$$

$$\mathbf{h} = [h_0, h_1, \ldots h_{(r)}]^T$$
$$\mathbf{e}(\omega) = [1, cos(\omega), \ldots, cos(r)]^T$$

Problem (LP). Design a linear phase FIR filter $P(e^{j\omega})$ which solves the following constrained optimization problem

$$\min_{\mathbf{h}} \ \frac{1}{\pi}\int_{\Omega_s} |A(e^{j\omega})|^2 d\omega \tag{3.35}$$

subject to

$$|A(e^{j\omega}) - D(\omega)| \leq \sigma_p, \ \omega \in \Omega_p \tag{3.36}$$

$$|A(e^{j\omega}) - D(\omega)| \leq \sigma_s, \ \omega \in \Omega_s \tag{3.37}$$

where $D(\omega)$ is the desired (often non-causal) frequency response, Ω_p is the set of passband frequencies, Ω_s is the set of stopband frequencies, σ_p is a small strictly positive amplitude error upper bound for the passband, σ_s is a small strictly positive amplitude error upper bound for the stopband.

The objective function and the constraints are simplified and the nonlinear constraints (3.36) and (3.37) are linearised in order to solve the nonlinear optimisation problem (LP) effectively.

The objective function (3.35) is simplified to

$$\min_{\mathbf{h}} \ \left\{\frac{1}{2}\mathbf{h}^T Q\mathbf{h} + g^T\mathbf{h}\right\} \tag{3.38}$$

where

$$Q = \frac{2}{\pi}\int_{\Omega_s} \mathbf{e}(\omega)\mathbf{e}^T(\omega)d\omega$$
$$g = -\frac{2}{\pi}\int_{\Omega_s} \mathbf{e}(\omega)D(\omega)d\omega$$

By using the *real rotation* theorem (3.14), the inequality constraints can be linearised and the optimisation problem (**P**) can be written as :

$$\min_{\mathbf{h}} \left\{\frac{1}{2}\mathbf{h}^T Q\mathbf{h} + g^T\mathbf{h}\right\} \tag{3.39}$$

subject to

$$a_p^T(\omega,\theta)\mathbf{h} \leq b_p(\omega,\theta) \quad \omega \in \Omega_p, \theta \in [0,2\pi) \tag{3.40}$$

$$a_s^T(\omega,\theta)\mathbf{h} \leq b_s(\omega,\theta) \quad \omega \in \Omega_s, \theta \in [0,2\pi) \tag{3.41}$$

The optimisation problem is a semi-infinite quadratic programming problem and can be solved via discretization of ω and θ as the following:

Problem ($\mathbf{LP_b}$): *Given discrete sets of* $\{\theta_i\}_{i=1}^{2p}$ *and* $\{\omega_l\}_{l=1}^{L}$*, find* $\boldsymbol{h}$ *which solves the following quadratic programming problem.*

$$\min_{\mathbf{h}} \left\{ \frac{1}{2}\mathbf{h}^T Q\mathbf{h} + g^T\mathbf{h} \right\} \tag{3.42}$$

subject to

$$A_{lp}\mathbf{h} \leq b_{lp} \tag{3.43}$$

$$A_{ls}\mathbf{h} \leq b_{ls} \tag{3.44}$$

where in passband, for each l, A_{lp} is a 2p x r matrix with $a_p^T(\omega_l,\theta_i) = 2cos(\omega_l k - \theta_i)$ as its i^{th} row and b_{lp} a 2p-dimensional column vector with all its entries $b_{lp} = \frac{\sigma_p}{sec(\frac{\pi}{2p})} + D(\omega_l)cos(\theta_i)$. In stopband, for each l, A_{ls} is a 2p x r matrix with $a_s^T(\omega_l,\theta_i) = 2cos(\omega_l k - \theta_i)$ as its i^{th} row and b_{ls} a 2p-dimensional column vector with all its entries $b_{ls} = \frac{\sigma_s}{sec(\frac{\pi}{2p})}$.

Chapter 4

BER Performance of the OFDM System with Pulse Shaping over Multipath Fading Channels

It has been investigated in Chapter 3 that designing causal pulse shaping filters using an optimisation approach improves the PAPR reduction of the OFDM transmitted signal. In this chapter, the BER performance of the OFDM system with pulse shaping is investigated.

The rest of this chapter is organised as follows: Section 4.1 introduces different types of fading channels are presented. Section 4.2 presents the HIPERLAN/2 channel models which are used to simulate the multipath fading channels. The receiver OFDM system model with pulse shaping is introduced in Section 4.3. The BER performances for different channel models are presented in Section 4.4. Finally, the conclusion remarks are drawn in Section 4.5.

4.1 AWGN and Fading Channel Models

Multipath fading is caused by the constructive and destructive combination of randomly delayed, reflected, scattered, and diffracted signal components. Depending

on the nature of the propagation environment, such as the existence of a line-of-sight (LOS) path, there are different models that represent the statistical behavior of the multipath fading channels.

4.1.1 AWGN Channels

Since thermal noise is present in all communication systems, the thermal noise characteristics (additive, white and Gaussian) are most often used to model noise in communication systems [46]. Thus, additive white Gaussian noise (AWGN) channel is the most common communication channel. Since thermal noise is a Gaussian process and the samples are uncorrelated, the noise samples are also independent [45]. The signal in communication systems can be represented by random variables given by

$$y = x + z \tag{4.1}$$

where y represents the output , x represents the input and z represents the additive noise term. The values of the noise follows the Gaussian probability distribution function [46]

$$f(z) = \frac{1}{\sqrt{2\pi\sigma^2}} e^{\frac{-(z-\mu)^2}{2\sigma^2}} \tag{4.2}$$

where $\mu = 0$ and $\sigma^2 = E[z^2]$.

4.1.2 Rayleigh Fading Channels

Consider a Rayleigh distributed random variable of z where its probability density function can be defined by [60]

$$f(z) = \begin{cases} \frac{z}{\sigma^2}\exp(-\frac{z^2}{2\sigma^2}), & z \geq 0 \\ 0, & \text{otherwise} \end{cases} \tag{4.3}$$

where

$$\sigma^2 = E[|z|^2] \tag{4.4}$$

It is assumed that the random variable z consists of real and imaginary parts, x and y, respectively and can be written as

$$z = \sqrt{x^2 + y^2} \tag{4.5}$$

where x and y are two i.i.d. Gaussian random variables with zero mean and variance σ^2.

When a random signal is transmitted over a multipath fading channel, the real part and imaginary parts of the received signals are considered as the sum of many random variables. According to the central limit theorem, for sufficiently large number of paths, the real and imaginary parts of the signals can be modeled approximately as a Gaussian random process with zero mean. The envelope of this type of channel model will be Rayleigh distributed. Hence, a Rayleigh distribution is a good model to represent a non line-of-sight (NLOS) environment [58][59].

4.1.3 Rician Fading Channels

In the LOS environment, the fading is considered as Rician fading [58] because it is assumed that there is a dominant path in the multipath fading environments. The Rician distribution is related to the Gaussian distribution and its pdf can be expressed as [70]

$$f(z) = \frac{z}{\sigma^2}\exp\left(-\frac{z^2 + K^2}{2\sigma^2}\right) I_0\left(\frac{Kz}{\sigma^2}\right) \tag{4.6}$$

where $z = x + jy$, x has mean of μ_x and variance σ^2 and y has mean of μ_y and variance σ^2 with

$$K = \sqrt{\mu_x^2 + \mu_y^2} \tag{4.7}$$

$$I_0(x) = \frac{1}{2\pi}\int_0^{2\pi} e^{xcos(\phi)} d\phi \tag{4.8}$$

$I_0(x)$ is the modified Bessel function of the first kind of zero order [71].

4.2 HIPERLAN/2

High Performance Radio Local Area Network type 2 (HIPERLAN/2) is a standard defined by the ETSI/BRAN project [6]. HIPERLAN/2 networks supports high-speed communications between mobile terminals and various communication networks and the physical layer of HIPERLAN/2 is based on OFDM [69].

HIPERLAN/2 parameters for the indoor environment in [68] are used to simulate various multipath channel models. Channel A, B and C model Rayleigh channels and channel D models Rician channel. Table 4.1 summarises the HIPERLAN/2 channel models for indoor environments. The fading models use tapped delay lines where each tap suffers independent fading corresponding to an exponentially decaying average power delay profile.

Table 4.1: HIPERLAN/2 channel models for indoor environments.

Name	RMS delay	Max Delay	Characteristic
A	0.016T	0.122T	Rayleigh
B	0.032T	0.228T	Rayleigh
C	0.047T	0.328T	Rayleigh
D	0.044T	0.328T	Rician
E	0.078T	0.550T	Rayleigh

4.3 Receiver System Model

In Chapter 3, the transmitter part of the OFDM system with pulse shaping has been discussed. The modulated data symbol at the k^{th} subcarrier, Z_k is multiplied with the pulse shaping filter $P_k(e^{j\omega})$ and can be expressed as

$$d_k = P_k(e^{j\omega})Z_k \tag{4.9}$$

where Z_k are often assumed to be i.i.d random variables with zero mean and variance $\sigma^2 = E[|Z_k|^2]$ and N denotes the number of subcarriers. Then, the N-points IFFT is applied to d_k. The baseband equivalent of the OFDM signal with

pulse shaping is given by:

$$s(t) = \sum_{k=0}^{N-1} d_k e^{j2\pi kt/T}, \quad 0 \leq t < T \tag{4.10}$$

It is assumed that the OFDM signal is transmitted over multipath fading channels and experienced additive white Gaussian noise (AWGN). The block diagram for the receiver part of the OFDM system with pulse shaping is illustrated in Fig.4.1. The total bandwidth of the OFDM system is assumed to be larger than the coherence bandwidth of the fading channel. In this case, the fading can be considered as frequency-selective fading.

The complex baseband equivalent of the impulse response of the multipath

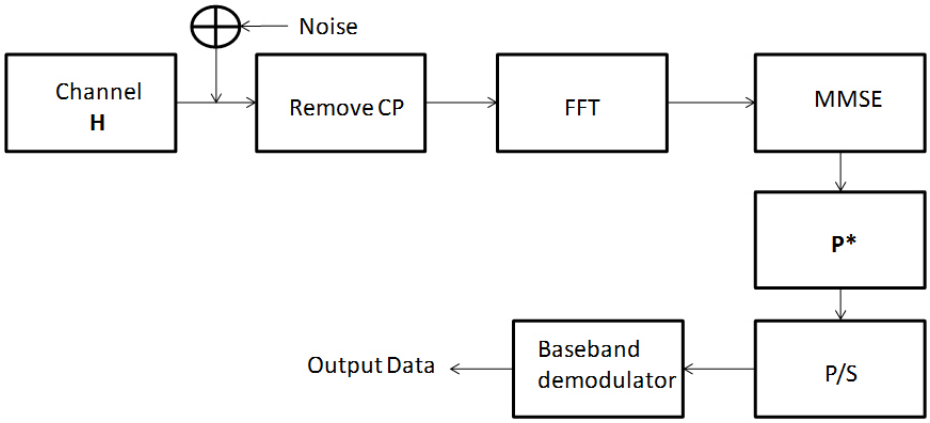

Figure 4.1: Receiver structure of precoded OFDM.

fading channel is represented by [35]

$$h(\tau) = \sum_{l=0}^{J-1} h_l \delta(\tau - \tau_l) \tag{4.11}$$

where h_l is the different complex tap weight with variance p_l, τ_l the time delay of the l-th path, and J the total number of multipaths. Each tap adopts a complex Gaussian distribution of zero-mean and the variance of the real part is equal to the variance of the imaginary part.

The received OFDM signal is given by

$$r(t) = \sum_{l=0}^{J-1} h_l s(t - \tau_l) + w(t) \ , -T_u \leq t < T \tag{4.12}$$

where $w(t)$ is a zero mean Gaussian white noise with its power spectral density N_0 and T_u is the time guard interval.

To maintain the orthogonality of the OFDM subcarriers, the guard interval is assumed to be larger than the maximum delay spread of the fading multipath channels. In the frequency domain, the demodulated data at the i^{th} subcarrier can be written as

$$\begin{aligned} Y_i &= \frac{1}{\sqrt{T}} \int_0^T r(t) e^{-j2\pi \frac{i}{T} t} dt \\ &= \sqrt{T} H_i d_i + W_i, \ i = 0, 1, ..., L-1 \end{aligned} \tag{4.13}$$

where d_i is obtained from (4.9), W_i is a zero mean Gaussian noise and variance N_0 and T is the duration of the OFDM signal. The frequency response of the channel, H_i at subcarrier k can be expressed as

$$H_i = \sum_{l=0}^{J-1} h_l e^{-j2\pi i \tau_l / T} \tag{4.14}$$

which is a complex Gaussian random variable with variance

$$2\delta^2 = \sum_{l=0}^{M-1} p_l \tag{4.15}$$

It is assumed that perfect CSI is known at the receiver of the OFDM system. When the HIPERLAN/2 system is used, two OFDM symbols preceding each burst of data transmitted are used for channel estimation [6]. Generally, the HIPERLAN/2 system is used for an indoor environment because it is assumed that the terminals only moves at a slow speed. By using (4.13), the CSI at the i^{th} subcarrier is given by

$$\hat{H}_i = \frac{Y_i}{\sqrt{T}\hat{d}_i} = H_i + \frac{W_i}{\sqrt{T}\hat{d}_i} \tag{4.16}$$

where

$$\hat{d}_i = \sum_{k=0}^{N-1} p_{i,k} C_k \ i = 0, 1, ..., L-1 \tag{4.17}$$

where $C_k = [C_0, C_1, ..., C_{N-1}]$ is the pilot symbol. This means that (4.17) is recognised at the receiver because it contains the predefined pulse shaping matrix

and the pilot symbol.

The received signal (4.13) can be expressed in matrix form as:

$$\mathbf{Y} = \sqrt{T}\mathbf{HPZ} + \mathbf{W} \tag{4.18}$$

where W is the noise vector, given as

$$W = [W_0, W_1, ..., W_{L-1}] \tag{4.19}$$

and matrix $\mathbf{H}$ is an $L \times L$ diagonal matrix denotes the channel coefficients of different subcarriers with

$$\mathbf{H} = \text{diag}(H_0, H_1, ..., H_{L-1}) \tag{4.20}$$

It is assumed that a one-tap equaliser minimum-mean-squared-error (MMSE) detector is utilised at the receiver. The optimal weighting parameter for every subcarrier is given by:

$$G_i = \frac{\hat{H}_i^*}{|\hat{H}_i|^2 + \frac{\delta_w^2}{\delta_s^2}}, \quad i = 0, 1, ..., L-1 \tag{4.21}$$

where $\frac{\delta_w^2}{\delta_s^2}$ is the ratio of the variance of the noise, $w(t)$ over the variance of the data transmitted symbol, $s(t)$. The weighting parameter G_k minimises the interference between OFDM modulated symbols and compensates the channel phase.

Fig.4.1 shows that the output of MMSE equaliser is multiplied by $\mathbf{P}^*$. Matrix $\mathbf{P}^*$ is the Hermitian transpose of $\mathbf{P}$. The demodulated data vector is given by

$$\mathbf{V} = \mathbf{P*\ G\ Y} \tag{4.22}$$

$$= \sqrt{T}\mathbf{P*\ G\ H\ P\ Z} + \mathbf{W'} \tag{4.23}$$

where **W'** is the complex Gaussian noise vector and

$$\mathbf{G} = \text{diag}(G_0, G_1, ..., G_{L-1}) \tag{4.24}$$

4.4 Numerical Simulations

In this section, numerical results are carried out to investigate the BER performance of the OFDM signal with the designed pulse shaping filter.

Fig. 4.2 illustrates the CCDF of the PAPR of the OFDM signal for $N = 64$, $\sigma_p = 10^{-5}$, $\sigma_s = 10^{-4}$, $M = 26$ and 10^4 QPSK data symbols are generated. The desired ideal filter ($D(\omega)$) is RC filter. The frequency reponse of the designed pulse shaping filter is illustrated in Fig. 4.3.

Fig. 4.4 and Fig. 4.5 illustrate the BER of the precoded OFDM using the designed linear phase FIR filter over AWGN and multipath fading channels. It is shown that the proposed precoded OFDM has better BER performance compared to the conventional OFDM. It is considered that the CSI is perfect and the precoded OFDM signal is transmitted over channel A and channel B of HIPERLAN/2 system. The precoding technique takes benefits from the frequency selectivity channel which leads to the improvement of the system performance and these results are consistent with [9][83][84].

Fig. 4.6 illustrates that for BER 10^{-4}, the proposed precoded OFDM only requires SNR around 18 dB whilst the conventional OFDM requires around 32 dB for channel A. Channel B has a smaller coherence bandwidth than channel A. As a result, it can be seen that the BER performance of the precoded OFDM is generally better in channel B than in channel A.

Fig.4.7 and Fig.4.8 show the OFDM signal is transmitted over channel D of HIPERLAN/2 where the fading channel is a Rician channel with $K = 10$. The BER performance is decreased for precoded OFDM by the fact that a Rician channel increases the line of sight to the precoding matrix.

4.5 Concluding Remarks

The BER performance of the OFDM system with designed pulse shaping filters over multipath fading channels has been investigated in this chapter. The HIPERLAN/2 standard channel models were used to simulate the multipath fading channels. The channel models included Rayleigh and Rician fading channels. In the receiver, it is assumed that the OFDM signal experienced AWGN, MMSE detec-

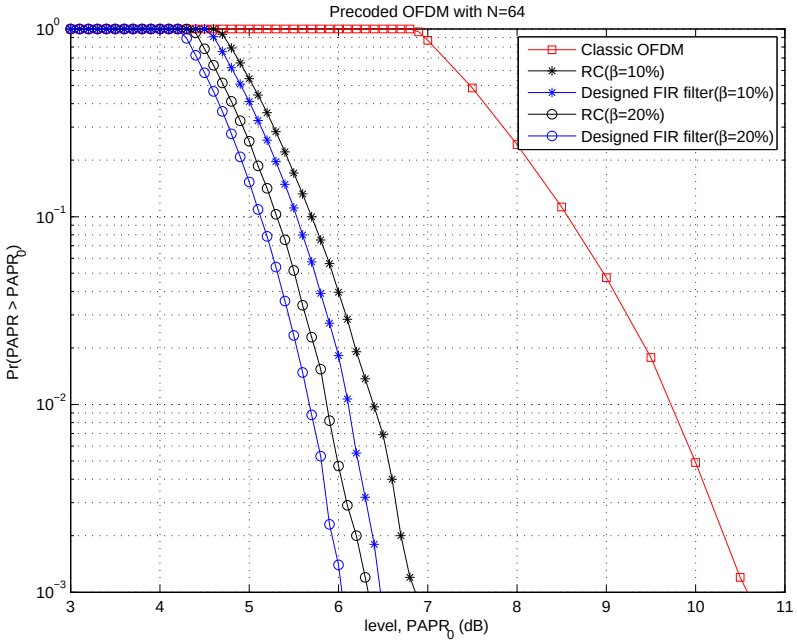

Figure 4.2: CCDF of PAPR of OFDM signal with the designed linear phase FIR filter.

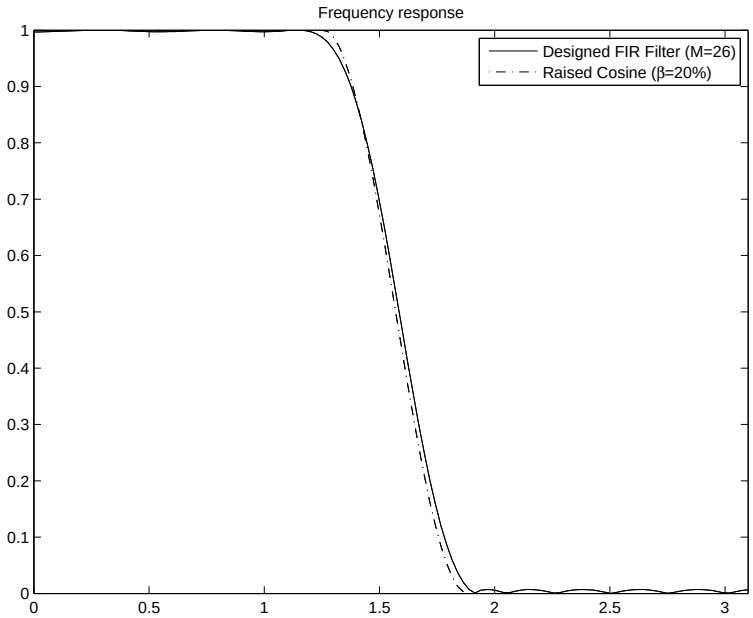

Figure 4.3: Frequency response of the designed FIR filter M=26.

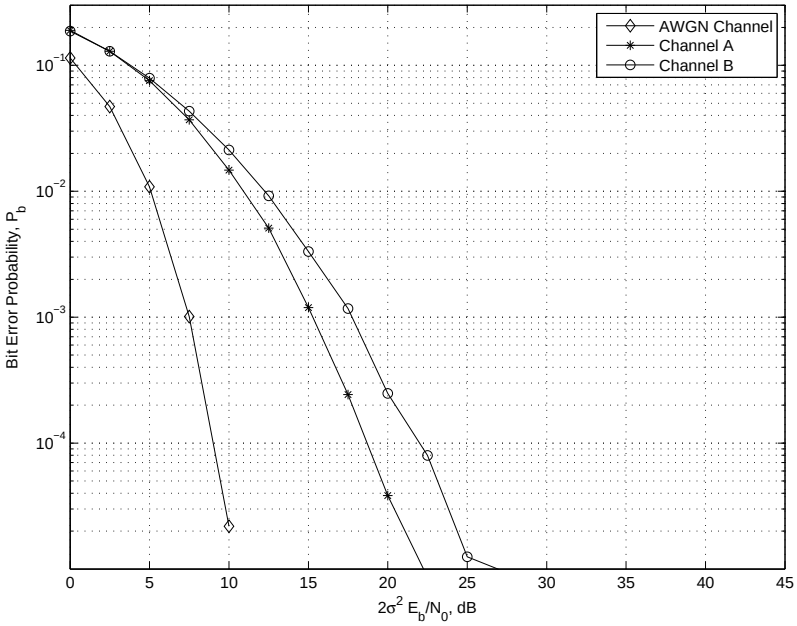

Figure 4.4: BER of OFDM signals over AWGN channel and multipath fading channels (channel A and channel B) for β=10 %.

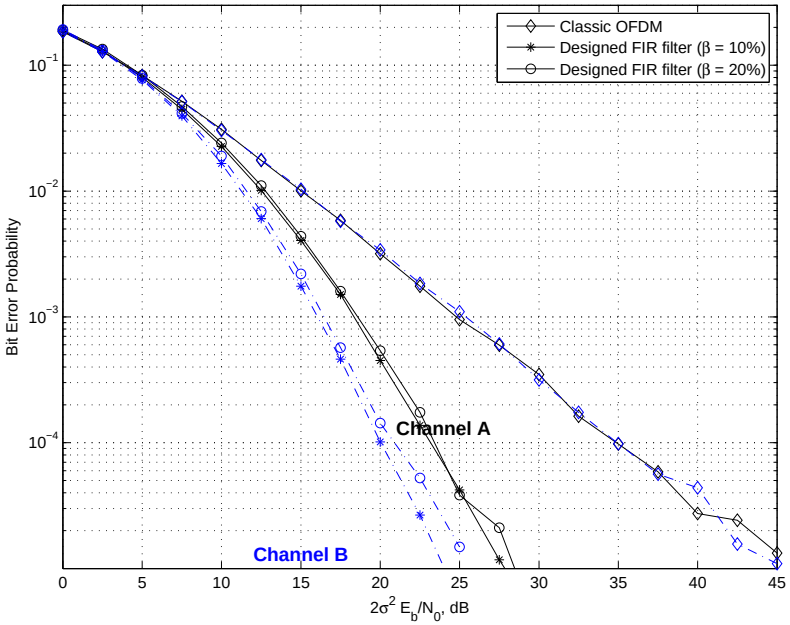

Figure 4.5: BER of OFDM signals over multipath fading channels (channel A and channel B).

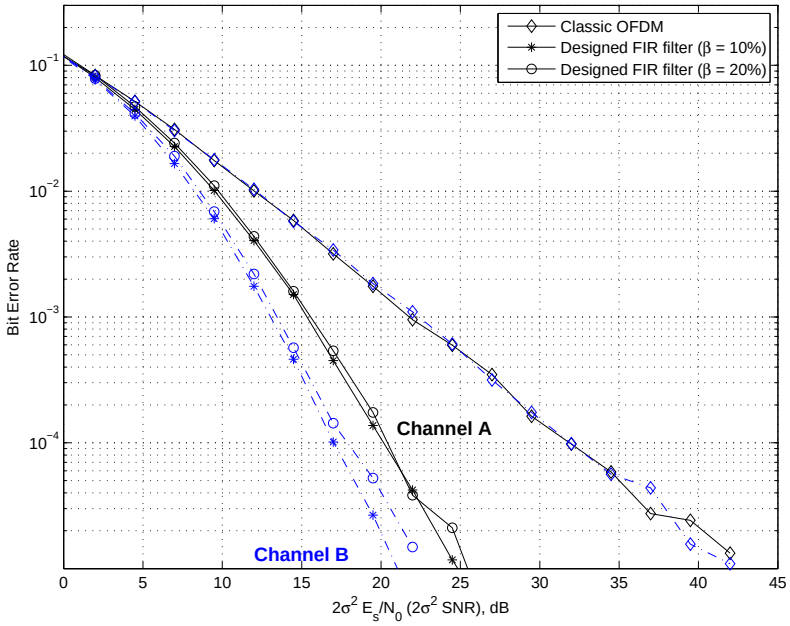

Figure 4.6: SNR of OFDM signals over multipath fading channels (channel A and channel B).

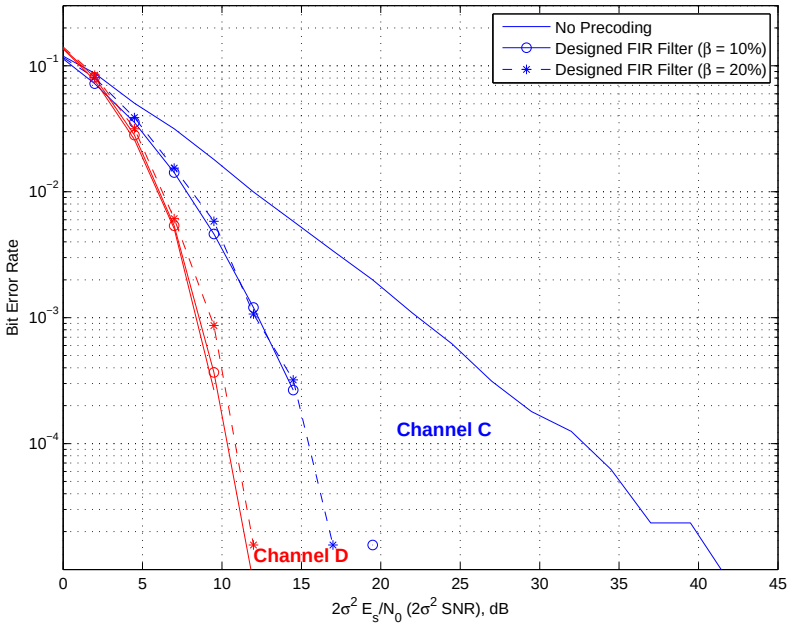

Figure 4.7: BER performance for channel C and channel D.

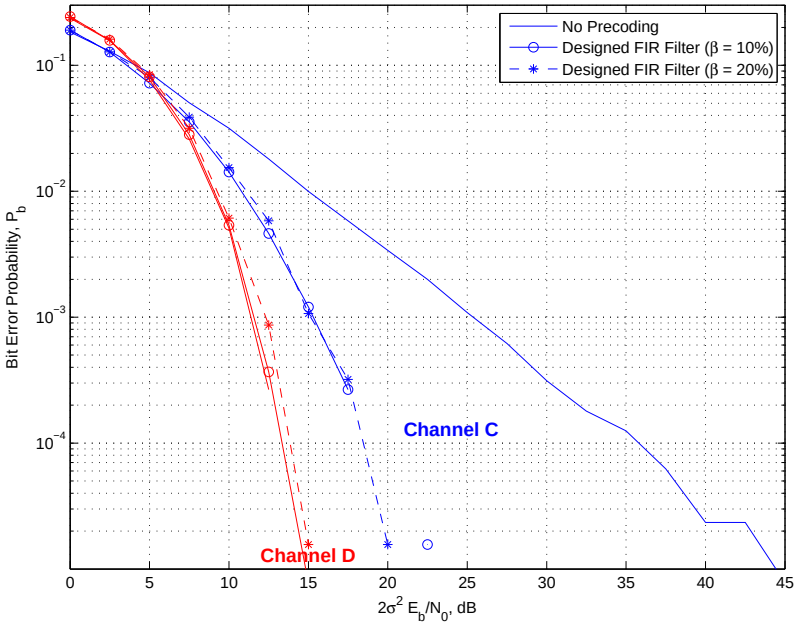

Figure 4.8: SNR performance for channel C and channel D.

tor is used and full CSI is known at the receiver. Numerical results demonstrated that OFDM signal with the designed pulse shaping filters not only reduces the PAPR of the OFDM signal but also improves the BER of the OFDM systems over multipath fading channels.

Chapter 5

PAPR Distribution Analysis of OFDM Signal with Pulse Shaping

In the existing literature, PAPR distribution analysis and quantification were carried out based on the assumption that the OFDM signals were stationary. When a standard OFDM signal is subjected to pulse shaping, the resulting signal is no longer stationary. It can be easily proven that the resulting signal is cyclostationary. In this chapter, PAPR distribution analysis and quantification will be carried out for OFDM signal with pulse shaping. A random phase can be introduced to stationarise the cyclostationary signal. After the stationarisation process, the complementary cumulative distribution function (CCDF) of the PAPR is analysed using the level crossing rate (LCR) theorem and an upper bound for the CCDF of the PAPR of the OFDM signal is derived.

The rest of this chapter is organised as follows: Section 5.1 introduces the LCR theorem, briefly summarises the upper bounds and approximation of the OFDM signals without pulse shaping and presents the definition of stationary and cyclostationary signals. Section 5.2 presents the analysis of the OFDM signal with pulse shaping. PAPR distribution analysis of the stationarised OFDM signal is presented in Section 5.3. Numerical results are presented in Section 5.4 and the conclusion remarks are given in Section 5.5.

5.1 Preliminaries

5.1.1 Level Crossing Rate Theorem

Given a random process $r(t)$ and a constant γ, let t_i denote the time instances when $r(t)$ crosses the line L_γ (which is parallel to the time axis) as illustrated in Fig.5.1 .

$$r(t_i) = \gamma \tag{5.1}$$

The level crossing rate problem is the determination of the statistical properties

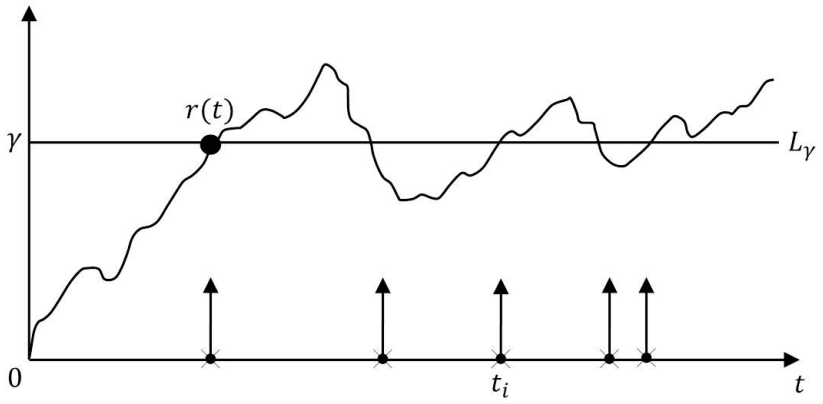

Figure 5.1: Level crossing of $r(t)$.

of a random process crosses a given threshold, γ at t_i [45]. It is assumed that $r(t)$ is stationary and let $N_r(\gamma, t)$ denote the number of points crossing the threshold γ at t_i. The following shows the mean of $N_r(\gamma, t)$ in terms of $f_r(r)$, the first order density of $r(t)$ and $f_{\dot{r}}(\dot{r})$, the first order density of its derivative $\dot{r}(t)$ [72].

$$E[N_r(\gamma, t)] = \int_{-\infty}^{\infty} |\dot{r}(t)|[f_{r\dot{r}}(r, \dot{r})]_{r=\gamma} d\dot{r} \tag{5.2}$$

where

$$f_{r\dot{r}}(r, \dot{r}) = f_r(r) f_{\dot{r}}(\dot{r}) \tag{5.3}$$

and $f_{r\dot{r}}(r, \dot{r})$ is the joint probability density of $r(t)$ and $\dot{r}(t)$.

The expected number of $r(t)$ crosses threshold, γ (for positive and negative

direction) for a period of T is given by

$$\begin{aligned} E[N_r(\gamma,T)] &= \int_0^T \int_{-\infty}^{\infty} |\dot{r}|[f_{r\dot{r}}(r,\dot{r})]_{r=\gamma} dr d\dot{r} dt \\ &= T\int_{-\infty}^{\infty} |\dot{r}|[f_r(r) f_{\dot{r}}(\dot{r})]_{r=\gamma} d\dot{r} \\ &= T\int_{-\infty}^{\infty} |\dot{r}| f_r(\gamma,\dot{r}) d\dot{r} \end{aligned} \tag{5.4}$$

According to [48], the upper bound of the CCDF of the PAPR of the OFDM signal can be expressed by

$$Pr\left\{\max_{0<t<T}|r(t)| > \gamma\right\} \leq E[N_r^+(\gamma,T)] \tag{5.5}$$

and

$$E[N_r^+(\gamma,T)] = T\int_0^{\infty} \dot{r} f_r(\gamma,\dot{r}) d\dot{r} \tag{5.6}$$

where $E[N_r^+(\gamma,T)]$ is the mean number of positive crossings at a given threshold γ in one OFDM symbol during period T.

5.1.2 PAPR Distribution Analysis of the OFDM Signal without Pulse Shaping

In the existing literature, PAPR distribution analyses were carried out based on the assumption that the OFDM signal was a stationary signal [73][79][80][48][50].

According to [50], the CDF of PAPR is given by

$$F(\gamma) = (1 - e^{-\gamma})^{\alpha N} \tag{5.7}$$

where γ is a specified PAPR threshold, α is a parameter determined from computer simulation. Hence, the empirical approximation of the CCDF of the PAPR can be expressed as

$$C_{PAPR_1}(\gamma) = 1 - (1 - e^{-\gamma})^{\alpha N} \tag{5.8}$$

In [44], the LCR theorem is used to derive the CCDF of the PAPR given by

$$C_{PAPR_2}(\gamma) = \begin{cases} 1 - (1 - \frac{\sqrt{\gamma}e^{-\gamma}}{\sqrt{\bar{\gamma}}e^{-\bar{\gamma}}})^{\sqrt{\frac{\pi}{3}}N\sqrt{\bar{\gamma}}e^{-\bar{\gamma}}} & \gamma > \bar{\gamma} \\ 1 & \gamma \leq \bar{\gamma} \end{cases} \tag{5.9}$$

where $\bar{\gamma}$ represents the prescribed PAPR reference level with the probability close to 0 and $\bar{\gamma} \geq \frac{\sqrt{2}}{2}$.

Another PAPR distribution analysis using LCR theorem is suggested by [48] where the upper bound of the CCDF can be expressed as

$$C_{PAPR_3}(\gamma) \leq \sqrt{\frac{\pi}{3}}N\sqrt{\gamma}e^{-\gamma} \tag{5.10}$$

Fig. 5.2 illustrates the comparison of (5.8), (5.9), (5.10) for $N = 64$ and $N = 256$. In the simulation, the OFDM symbols are QPSK modulated. Fig. 5.2 shows good results for the upper bound derived using the LCR theorem in (5.9). Therefore, LCR theorem based approach is effective in quantifying the PAPR of the OFDM signal. In the following, the LCR theorem will be used for the analysis of the PAPR of the OFDM signal with pulse shaping.

5.1.3 Cyclostationary Signal and Stationarisation Process

Cyclostationary random process. *A random process X(t) (complex or real) is called cyclostationary in strict sense with period T if, for every integer n, any collection of times $t_1, t_2, ..., t_n$ in Z or R, and Borel sets $A_1, A_2, ..., A_n$ of C or R* [63],

$$\begin{aligned} &Pr[X(t_1 + T) \in A_1, X(t_2 + T) \in A_2, ..., X(t_n + T) \in A_n] \\ &\quad = Pr[X(t_1) \in A_1, X(t_2) \in A_2, ..., X(t_n) \in A_n] \end{aligned} \tag{5.11}$$

where $T > 0$ is the fundamental period of this random process.

Wide sense cyclostationary random process. *A random process X(t) is*

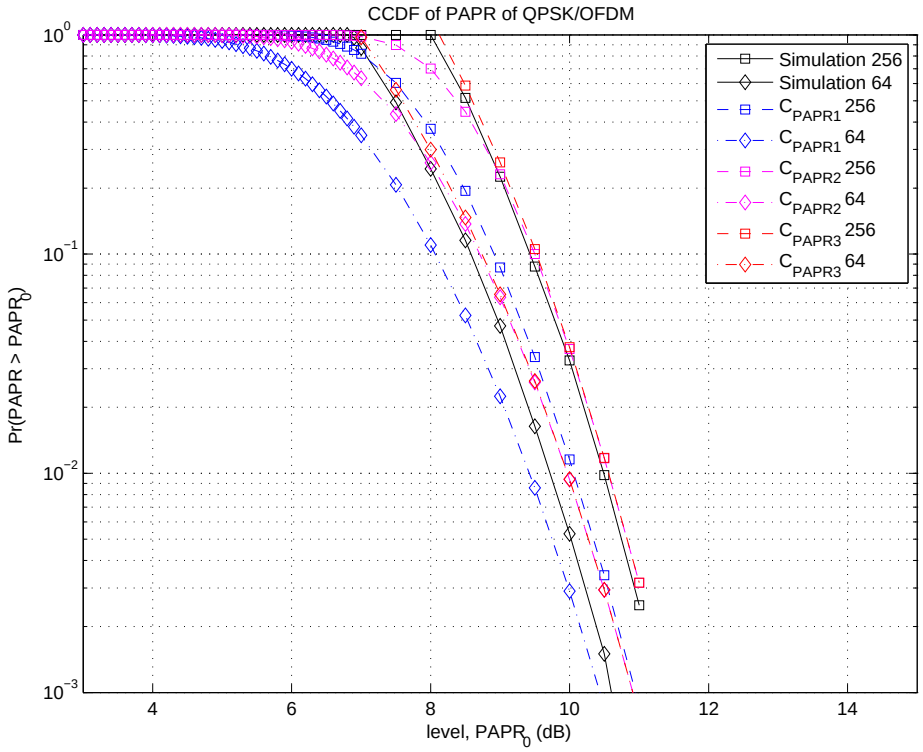

Figure 5.2: Comparison of bounds of PAPR distribution

called wide sense cyclostationary if

$$\begin{aligned} E[X(t+mT)] &= E[X(t)] \\ E[X(t_1+mT)X(t_2+mT)] &= E[X(t_1)X(t_2)] \end{aligned}$$

for any integer m [63].

Stationarisation of WSCS Signal. Assume that $x(t)$ is a WSCS signal with its mean and autocorrelation as follows

$$\begin{aligned} \eta_x(t+mT) &= \eta_x(t) \\ R_x(t_1+mT, t_2+mT) &= R_x(t_1, t_2) \end{aligned}$$

for every integer m. Let θ be a random phase, which is uniformly distributed over the interval between 0 and T and independent of $x(t)$. By introducing a random phase θ, the WSCS signal, $x(t)$, can be stationarised [64]. Such a process results

in the stationarised signal $y(t)$ as follows

$$y(t) = x(t + \theta) \tag{5.12}$$

which is stationary in wide sense with its mean and autocorrelation as follows [45]

$$\eta_y = \frac{1}{T}\int_0^T \eta_x(t)dt \tag{5.13}$$

$$R_y(\tau) = \frac{1}{T}\int_0^T R_x(t+\tau, t)dt \tag{5.14}$$

5.2 Analysis of OFDM Signal with Pulse Shaping

Let $s(t)$ denote the baseband equivalent of OFDM signal with pulse shaping

$$s(t) = \sum_{k=0}^{N-1} Z_k p_k(t) e^{j2\pi k \frac{t}{T}} \tag{5.15}$$

The continous OFDM signal with pulse shaping can be expressed as

$$q(t) = \sum_{i=-\infty}^{\infty} s(t - iT) \tag{5.16}$$

$$= \sum_{i=-\infty}^{\infty} \sum_{k=0}^{N-1} Z_{i,k} p_k(t - iT) e^{j2\pi k \frac{t-iT}{T}} \tag{5.17}$$

The mean value of $q(t)$ is given by

$$E[q(t)] = E\left[\sum_{i=-\infty}^{\infty} \sum_{k=0}^{N-1} Z_{i,k} p_k(t - iT) e^{j2\pi k \frac{t-iT}{T}}\right]$$

$$= \sum_{i=-\infty}^{\infty} \sum_{k=0}^{N-1} E[Z_{i,k}] p_k(t - iT) e^{j2\pi k \frac{t-iT}{T}} \tag{5.18}$$

$$= 0 \tag{5.19}$$

The autocorrelation of $q(t)$ is given by

$$\begin{aligned} R(t,t+\tau) &= E[q(t)q^*(t+\tau)] && (5.20)\\ &= E\left[\sum_{i=-\infty}^{\infty}\sum_{k_1=0}^{N-1} Z_{i,k_1}p_{k_1}(t-iT)e^{j2\pi k_1\frac{t-iT}{T}}\right. && (5.21)\\ &\qquad \left.\sum_{m=-\infty}^{\infty}\sum_{k_2=0}^{N-1} Z^*_{m,k_2}p^*_{k_2}(t+\tau-mT)e^{-j2\pi k_2\frac{t+\tau-mT}{T}}\right]\\ &= \sigma^2\sum_{i=-\infty}^{\infty}\sum_{k=0}^{N-1} p_k(t-iT)p^*_k(t+\tau-iT)e^{-j2\pi k\frac{\tau}{T}} && (5.22)\end{aligned}$$

where

$$E[Z_{i,k_1}Z_{m,k_2}] = \begin{cases}\sigma^2, & i=m \ \text{ and } \ k_1=k_2=k\\ 0, & \text{otherwise}\end{cases} \qquad (5.23)$$

The autocorrelation for the OFDM signal with pulse shaping, $R(t,t+\tau)$ is periodic within period T. This analysis shows that OFDM signal with pulse shaping is a WSCS signal.

Signal $q(t)$ in (5.16) is cyclostationary and can be stationarised as the following

$$\hat{q}(t) = q(t+\theta) \qquad (5.24)$$

where θ is a uniformly distributed random phase in the interval $[0\ T]$ with its pdf as follows

$$f_\theta(t) = \begin{cases}\frac{1}{T} & ,0\le t\le T\\ 0 & ,\text{otherwise}\end{cases} \qquad (5.25)$$

After shifting by a random phase as in (5.24), $\hat{q}(t)$ will have the same peak value of $q(t)$.

Consider that the mean power for the OFDM signal with pulse shaping in one

symbol duration, $E[|s(t)|^2]$, is given by

$$\begin{aligned} E[|s(t)|^2] &= E[s_k(t)s_m^*(t)] \\ &= E\left[\sum_{k=0}^{N-1} Z_k p_k(t) e^{jk2\pi t/T} \sum_{m=0}^{N-1} Z_m^* p_m^*(t) e^{-jm2\pi t/T}\right] \\ &= \sum_{k=0}^{N-1}\sum_{m=0}^{N-1} E[Z_k Z_m^*] p_k(t) p_m^*(t) e^{j2\pi(k-m)t/T} \\ &= \sigma^2 \sum_{k=0}^{N-1} p_k(t) p_k^*(t) \end{aligned} \tag{5.26}$$

where Z_k is assumed to be i.i.d with zero mean and have variance as follows

$$E[Z_k Z_m^*] = \begin{cases} \sigma^2, & k = m \\ 0, & k \neq m \end{cases}$$

Eq.(5.26) shows that the average power is not constant anymore due to pulse shaping. The average power can be defined as the average of the mean power of signal $s(t)$ in one symbol duration which can be expressed as

$$\begin{aligned} P_{avg} &= \frac{1}{T}\int_0^T E[|s(t)|^2]dt \\ &= \frac{\sigma^2}{T}\sum_{k=0}^{N-1}\int_0^T p_k(t)p_k^*(t)dt \end{aligned} \tag{5.27}$$

Continous signal, $q(t)$ will have the same average power as (5.27).

The average power of the stationarised signal ,$\hat{q}(t)$ can be expressed as

$$\begin{aligned} P'_{avg} &= E[|\hat{q}(t)|^2] \\ &= \lim_{i\to\infty}\frac{1}{2iT}\int_{-iT}^{iT} E\left[\sum_{k=-\infty}^{\infty} s(t+\theta-kT)s^*(t+\theta-kT)\right]dt \\ &= \lim_{i\to\infty}\frac{1}{2iT}\sum_{k=-i}^{i}\int_{-kT}^{(k+1)T} E\left[s(t+\theta-kT)s^*(t+\theta-kT)\right]dt \end{aligned} \tag{5.28}$$

where $R_s = E[s(t+\theta-kT)s^*(t+\theta-kT)]$ and can be expressed as

$$\begin{aligned} R_s &= E\left[\sum_{n=0}^{N-1} Z_{n,k}p_n(t+\theta-kT)e^{jn2\pi(t+\theta-kT)/T}Z_{n,k}^*p_n^*(t+\theta-kT)\right. \\ &\quad \left. e^{-jn2\pi(t+\theta-kT)/T}\right] \\ &= \sum_{n=0}^{N-1} E[|Z_{n,k}|^2 p_n(t+\theta-kT)p_n^*(t+\theta-kT)] \\ &= \sigma^2 \sum_{n=0}^{N-1} E[p_n(t+\theta-kT)p_n^*(t+\theta-kT)] \\ &= \sigma^2 \sum_{n=0}^{N-1} \int_{\theta=0}^{T} p_n(t+\theta-kT)p_n^*(t+\theta-kT)\frac{1}{T}d\theta \end{aligned} \tag{5.29}$$

Let $\gamma = t+\theta-kT$, (5.29) then can be expressed as

$$E[|\hat{q}(t)|^2] = \sigma^2 \sum_{n=0}^{N-1} \int_{\gamma=t-kT}^{t-(k-1)T} p_n(\gamma)p_n^*(\gamma)\frac{1}{T}d\gamma \tag{5.30}$$

The average of the power of stationarised signal $\hat{q}(t)$ in (5.30) can be written as

$$P'_{avg} = \frac{\sigma^2}{T} \sum_{n=0}^{N-1} \int_{\delta=0}^{T} p_n(\delta)p_n^*(\delta)d\delta \tag{5.31}$$

Eq.(5.31) shows that the average power is the same as in Eq. (5.27).

Then, the PAPR distribution for both $q(t)$ and $\hat{q}(t)$ can be written as follows

$$\begin{aligned} P_r\{PAPR_q \le \gamma\} &= P_r\{PAPR_{\hat{q}} \le \gamma\} \\ P_r\{\frac{\max\limits_{-\infty\le t<\infty}|q(t)|^2}{P_{avg}} \le \gamma\} &= P_r\{\frac{\max\limits_{-\infty\le t<\infty}|\hat{q}(t)|^2}{P'_{avg}} \le \gamma\} \end{aligned} \tag{5.32}$$

5.3 PAPR Distribution Analysis of Stationarised OFDM Signal

5.3.1 Derivation of Joint pdf of OFDM Signal with Pulse Shaping

For any time instant t, the OFDM signal, $s(t)$, can be expressed as

$$s(t) = x(t) + jy(t)$$

where $x(t)$ is the real part of $s(t)$ and $y(t)$ the imaginary parts of $s(t)$. According to the central limit theorem, in the case where the number of subcarriers is very large, both $x(t)$ and $y(t)$ can be approximated as two independent Gaussian random processes [22]. Hence the envelope of $s(t)$ can be approximated as a Rayleigh random process.

For mathematical convenience, a square-root of the PAPR, represented by the crest factor (CR) is given by

$$CR = \sqrt{PAPR} = \frac{\max\limits_{0\leq t<T} |s(t)|}{\sqrt{P_{av}}} \tag{5.33}$$

$$= \max_{0\leq t<T} r(t) \tag{5.34}$$

where

$$r(t) = \frac{|s(t)|}{\sqrt{P_{av}}} = \sqrt{\frac{x^2(t) + y^2(t)}{P_{av}}} \tag{5.35}$$

is the envelope of the complex baseband OFDM signal with pulse shaping that is normalised by average power.

The real and imaginary parts of $s(t)$ are given by:

$$x(t) = \sum_{k=0}^{N-1} |Z_k||p_k(t)| \cos(\varphi_t) \tag{5.36}$$

$$y(t) = \sum_{k=0}^{N-1} |Z_k||p_k(t)| \sin(\varphi_t) \tag{5.37}$$

where $\varphi_t = \psi_t + \psi_z + \psi_p$ and $\psi_t = \frac{2\pi kt}{T}$, $\psi_z = \arg(Z_k)$ and $\psi_p = \arg(p_k(t))$.

The first derivative of $x(t)$ and $y(t)$ can be written as

$$\dot{x}(t) = \frac{dx(t)}{dt} \tag{5.38}$$

$$= \sum_{k=0}^{N-1} |Z_k||\dot{p_k}(t)| \cos(\dot{\varphi_t}) + |Z_k||p_k(t)| \frac{2\pi k}{T} \cos(\varphi_t + \frac{\pi}{2}) \tag{5.39}$$

$$\dot{y}(t) = \frac{dy(t)}{dt} \tag{5.40}$$

$$= \sum_{k=0}^{N-1} |Z_k||\dot{p_k}(t)| \sin(\dot{\varphi_t}) + |Z_k||p_k(t)| \frac{2\pi k}{T} \sin(\varphi_t + \frac{\pi}{2}) \tag{5.41}$$

where $\dot{\varphi}_t = \psi_t + \psi_z + \dot{\psi}_p$ and $\psi_p = \arg(\dot{p}_k(t))$

Let $x, \dot{x}, y, \dot{y}$ denote the samples of Gaussian processes $x(t), \dot{x}(t), y(t), \dot{y}(t)$, respectively, at the same time instant. In order to derive the level crosing rate, the joint pdf of $x, \dot{x}, y, \dot{y}$ is required. The joint pdf of $x, \dot{x}, y, \dot{y}$ is given by [45]

$$f_{x,y}(\mathbf{X}) = \frac{1}{\sqrt{(2\pi)^n |\mathbf{R}|}} \exp[-\frac{1}{2}\mathbf{X}\mathbf{R}^{-1}\mathbf{X}^t] \tag{5.42}$$

where $\mathbf{X} = [x, \dot{x}, y, \dot{y}]$, $n = 4$, $\mathbf{R}$ is the covariance matrix and $|\mathbf{R}| = det(\mathbf{R})$. The covariance values of $x, \dot{x}, y, \dot{y}$ to form matrix $\mathbf{R}$ are derived in Appendix 5.A. The covariance matrix can be expressed as

$$\mathbf{R} = \begin{bmatrix} \sigma_{xx} & \sigma_{x\dot{x}} & 0 & 0 \\ \sigma_{x\dot{x}} & \sigma_{\dot{x}\dot{x}} & 0 & 0 \\ 0 & 0 & \sigma_{xx} & \sigma_{x\dot{x}} \\ 0 & 0 & \sigma_{x\dot{x}} & \sigma_{\dot{x}\dot{x}} \end{bmatrix} \tag{5.43}$$

where the determinant of $\mathbf{R}$ is as follows

$$det(\mathbf{R}) = |\mathbf{R}| = (\sigma_{xx}\sigma_{\dot{x}\dot{x}} - \sigma_{x\dot{x}}^2)^2 \tag{5.44}$$

The inverse matrix of $\mathbf{R}$ is given by

$$\mathbf{R}^{-1} = \frac{1}{K} \begin{bmatrix} \sigma_{\dot{x}\dot{x}} & -\sigma_{x\dot{x}} & 0 & 0 \\ -\sigma_{x\dot{x}} & \sigma_{xx} & 0 & 0 \\ 0 & 0 & \sigma_{\dot{x}\dot{x}} & -\sigma_{x\dot{x}} \\ 0 & 0 & -\sigma_{x\dot{x}} & \sigma_{xx} \end{bmatrix} \tag{5.45}$$

where $K = (\sigma_{xx}\sigma_{\dot{x}\dot{x}} - \sigma_{x\dot{x}}^2)$.

From substituting (5.43) into (5.42), the joint pdf of $x, \dot{x}, y, \dot{y}$ can be obtained as

$$f_{x,\dot{x},y,\dot{y}}(x, \dot{x}, y, \dot{y}) = \frac{1}{4\pi^2 K} \exp[-\frac{1}{2}(\frac{x^2\sigma_{\dot{x}\dot{x}}}{K} - 2\frac{x\dot{x}\sigma_{x\dot{x}}}{K} + \frac{\dot{x}^2\sigma_{xx}}{K} + \frac{y^2\sigma_{\dot{x}\dot{x}}}{K} - 2\frac{y\dot{x}\sigma_{x\dot{x}}}{K} + \frac{\dot{y}^2\sigma_{xx}}{K})] \tag{5.46}$$

After converting the variables to to polar coordinates, the joint pdf for $r, \dot{r}, \theta, \dot{\theta}$ is derived in Appendix 5.B and can be expressed as

$$f_{r,\dot{r},\theta,\dot{\theta}}(r,\dot{r},\theta,\dot{\theta}) = \frac{r^2\sigma^4}{4\pi^2 K}\exp[-\frac{\sigma^2}{2}(\frac{r^2}{\sigma_{\dot{x}\dot{x}}^{-1}K} - 2\frac{r\dot{r}}{\sigma_{x\dot{x}}^{-1}K} + \frac{(\dot{r}^2 + r^2\dot{\theta}^2)}{\sigma_{xx}^{-1}K})] \tag{5.47}$$

Next is to integrate (5.47) with respect to variable θ from 0 to 2π to obtain the joint pdf of r,$\dot{r}, \dot{\theta}$ as follows

$$\begin{aligned} f_{r,\dot{r},\dot{\theta}}(r,\dot{r},\dot{\theta}) &= \int_0^{2\pi} \frac{r^2\sigma^4}{4\pi^2 K}\exp[-\frac{\sigma^2}{2}(\frac{r^2}{\sigma_{\dot{x}\dot{x}}^{-1}K} - 2\frac{r\dot{r}}{\sigma_{x\dot{x}}^{-1}K} + \frac{(\dot{r}^2 + r^2\dot{\theta}^2)}{\sigma_{xx}^{-1}K})]d\theta \\ &= \frac{r^2\sigma^4}{2\pi K}\exp[-\frac{\sigma^2}{2}(\frac{r^2}{\sigma_{\dot{x}\dot{x}}^{-1}K} - 2\frac{r\dot{r}}{\sigma_{x\dot{x}}^{-1}K} + \frac{(\dot{r}^2 + r^2\dot{\theta}^2)}{\sigma_{xx}^{-1}K})] \end{aligned} \tag{5.48}$$

Then, by integrating (5.48) with respect to variable $\dot{\theta}$ from $-\infty$ to ∞, the joint pdf of r and $\dot{r}$, denotes by $f_{r,\dot{r}}(r,\dot{r})$ can be written as

$$\begin{aligned} f_{r,\dot{r}}(r,\dot{r}) &= \int_{-\infty}^{\infty} \frac{r^2\sigma^4}{2\pi K}\exp[-\frac{\sigma^2}{2}(\frac{r^2}{\sigma_{\dot{x}\dot{x}}^{-1}K} - 2\frac{r\dot{r}}{\sigma_{x\dot{x}}^{-1}K} + \frac{(\dot{r}^2 + r^2\dot{\theta}^2)}{\sigma_{xx}^{-1}K})]d\dot{\theta} \\ &= \int_{-\infty}^{\infty} \frac{r^2\sigma^4}{2\pi K}\exp[-\frac{\sigma^2}{2}(\frac{r^2}{\sigma_{\dot{x}\dot{x}}^{-1}K} - 2\frac{r\dot{r}}{\sigma_{x\dot{x}}^{-1}K} + \frac{(\dot{r}^2 + r^2\dot{\theta}^2)}{\sigma_{xx}^{-1}K})]d\dot{\theta} \end{aligned}$$

$$f_{r,\dot{r}}(r,\dot{r}) = \frac{r^2\sigma^4}{2\pi K}\exp[-\frac{\sigma^2}{2}(\frac{r^2}{\sigma_{\dot{x}\dot{x}}^{-1}K} - 2\frac{r\dot{r}}{\sigma_{x\dot{x}}^{-1}K} + \frac{\dot{r}^2}{\sigma_{xx}^{-1}K})]\int_{-\infty}^{\infty}\exp[-\frac{\sigma^2}{2}\frac{r^2\dot{\theta}^2}{\sigma_{xx}^{-1}K}]d\dot{\theta} \tag{5.49}$$

Note: $\int \exp(-ax^2)dx = \frac{\sqrt{\pi}erf(\sqrt{a}x)}{2\sqrt{a}}$ *and* $erf(\infty) = 1$ *and* $erf(-\infty) = -1$

$$f_{r,\dot{r}}(r,\dot{r}) = \frac{r^2\sigma^4}{2\pi K}\exp[-\frac{\sigma^2}{2}(\frac{r^2}{\sigma_{\dot{x}\dot{x}}^{-1}K} - 2\frac{r\dot{r}}{\sigma_{x\dot{x}}^{-1}K} + \frac{\dot{r}^2}{\sigma_{xx}^{-1}K})](\frac{\sqrt{2\pi K}}{\sqrt{\sigma^2 r^2\sigma_{xx}}})$$

$$f_{r,\dot{r}}(r,\dot{r}) = \frac{r\sigma^3}{\sqrt{\sigma_{xx}2\pi K}}\exp[-\frac{\sigma^2}{2}(\frac{r^2}{\sigma_{\dot{x}\dot{x}}^{-1}K} - 2\frac{r\dot{r}}{\sigma_{x\dot{x}}^{-1}K} + \frac{\dot{r}^2}{\sigma_{xx}^{-1}K})] \tag{5.50}$$

5.3.2 Derivation of the Upper Bound for the Stationarised OFDM Signal with Pulse Shaping

According to [44], (5.6) can be expressed by

$$E[N_r^+(z,T)] = Tv_r^+(z) \tag{5.51}$$

where

$$v_r^+(z) = \int_0^\infty \dot{r} f_r(z,\dot{r}) d\dot{r} \tag{5.52}$$

The LCR in (5.52) can be obtained by substituting $f_r(z,\dot{r})$ into (5.50). The (5.52) can be expressed as

$$v_r^+(z) = \int_0^\infty \dot{r} \frac{z\sigma^3}{\sqrt{\sigma_{xx} 2\pi K}} \exp[-\frac{\sigma^2}{2}(\frac{z^2}{\sigma_{\dot{x}\dot{x}}^{-1} K} - 2\frac{z\dot{r}}{\sigma_{x\dot{x}}^{-1} K} + \frac{\dot{r}^2}{\sigma_{xx}^{-1} K})] d\dot{r} \tag{5.53}$$

The probability that the stationarised OFDM signal, $\hat{r}(t)$ will cross a given threshold z during period T can be expressed as

$$Pr\left\{\max_{0<t<T} |\hat{r}(t)| > z\right\} = Pr[N_{\hat{r}}^+(z,T) \geq 1] \tag{5.54}$$

where $N_{\hat{r}}^+(z,T)$ denotes the number of times when $\hat{r}(t)$ crosses the level γ during period T. By using Markov inequality, (5.54) can be converted into

$$Pr\left\{\max_{0<t<T} |\hat{r}(t)| > z\right\} \leq E[N_{\hat{r}}^+(z,T)] \tag{5.55}$$

where $E[N_{\hat{r}}(z,T)]$, the upper bound of the CCDF is given by

$$E[N_{\hat{r}}^+(z,T)] = Tv_{\hat{r}}^+(z) \tag{5.56}$$

and

$$v_{\hat{r}}^+(z) = \frac{1}{T}\int_0^T v_r^+(z) dt \tag{5.57}$$

In Appendix 5.C, the LCR of the stationarised OFDM signal, $\hat{r}(t)$, is derived and

can be expressed as

$$v_{\hat{r}}^{+}(z) = \frac{1}{T}\int_0^T \frac{z\sigma^3}{\sqrt{\sigma_{xx}2\pi(\sigma_{xx}\sigma_{\dot{x}\dot{x}} - \sigma_{x\dot{x}}^2)}} \exp[-\frac{\sigma^2 z^2}{2\sigma_{xx}}] \left\{ \frac{(\sigma_{xx}\sigma_{\dot{x}\dot{x}} - \sigma_{x\dot{x}}^2)}{\sigma^2\sigma_{xx}} \exp[\frac{2z^2\sigma^2}{(\sigma_{xx}\sigma_{\dot{x}\dot{x}} - \sigma_{x\dot{x}}^2)} \frac{\sigma_{x\dot{x}}^2}{\sigma_{xx}}] + 2z\frac{\sigma_{x\dot{x}}}{\sigma_{xx}} \right. \left. (1 + \sqrt{\frac{2\pi(\sigma_{xx}\sigma_{\dot{x}\dot{x}} - \sigma_{x\dot{x}}^2)}{\sigma_{xx}\sigma^2}} erf(2z\frac{\sigma_{x\dot{x}}}{\sigma_{xx}})) \right\} dt \tag{5.58}$$

The upper bound of the CCDF of the PAPR distribution of the stationarised OFDM signal can be expressed as

$$C_{PAPR}(z) \leq \int_0^T \frac{\sqrt{z}\sigma^3}{\sqrt{\sigma_{xx}2\pi(\sigma_{xx}\sigma_{\dot{x}\dot{x}} - \sigma_{x\dot{x}}^2)}} \exp[-\frac{\sigma^2 z}{2\sigma_{xx}}] \left\{ \frac{(\sigma_{xx}\sigma_{\dot{x}\dot{x}} - \sigma_{x\dot{x}}^2)}{\sigma^2\sigma_{xx}} \exp[\frac{2z\sigma^2}{(\sigma_{xx}\sigma_{\dot{x}\dot{x}} - \sigma_{x\dot{x}}^2)} \frac{\sigma_{x\dot{x}}^2}{\sigma_{xx}}] + 2\sqrt{z}\frac{\sigma_{x\dot{x}}}{\sigma_{xx}} \right. \left. (1 + \sqrt{\frac{2\pi(\sigma_{xx}\sigma_{\dot{x}\dot{x}} - \sigma_{x\dot{x}}^2)}{\sigma_{xx}\sigma^2}} erf(2\sqrt{z}\frac{\sigma_{x\dot{x}}}{\sigma_{xx}})) \right\} dt \tag{5.59}$$

5.4 Numerical Results

In this section, numerical results are presented to demonstrate the effectiveness of the derived upper bound. In the simulation, 10^4 QPSK OFDM symbols are generated and the *Raised Cosine* (RC) filter [35] is used as the shaping pulse.

Fig.5.3. illustrates the comparison of the derived upper bound and the simulation results for $N = 64$, $\beta = 10\%$ and $\beta = 20\%$ where the derived upper bound is very close to the simulation results. Fig.5.4 demonstrates the comparison of the derived upper bound and the simulation results for larger number of subcarriers $N = 128$. Numerical results show that the proposed upper bound is tight.

Fig.5.5. illustrates the results for the designed FIR filter with $N = 64$, $\beta = 10\%$ and $\beta = 20\%$. Numerical results consistently show that the proposed upper bound is tight.

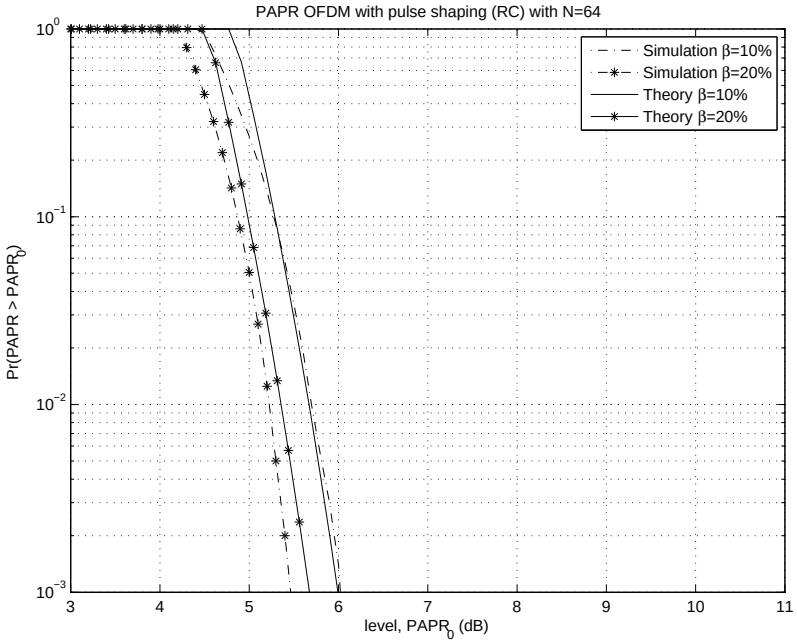

Figure 5.3: Comparison of the proposed upper bound with the simulation results for N=64.

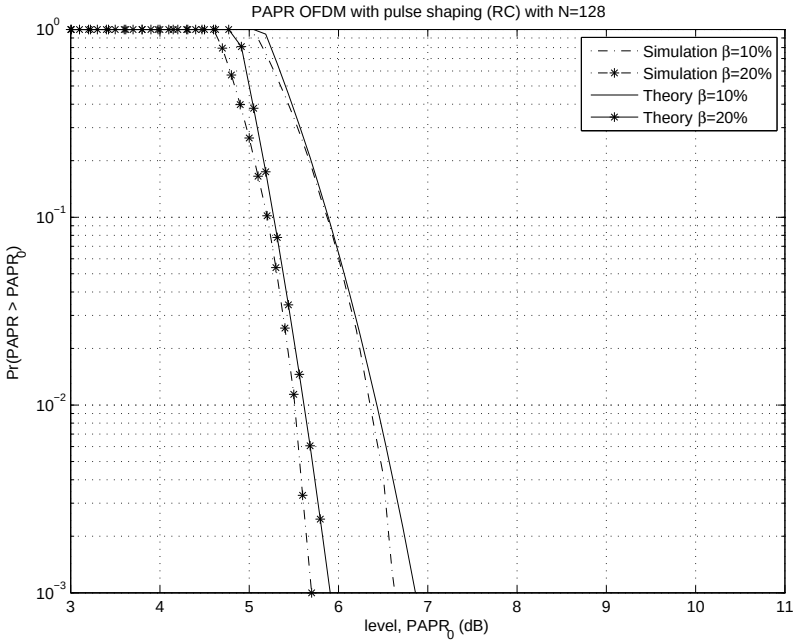

Figure 5.4: Comparison of the proposed upper bound with the simulation results for N=128.

5.5 Concluding Remarks

In this chapter, theoretical analysis of the PAPR distribution of the OFDM signal with pulse shaping has been investigated. Without pulse shaping, OFDM signal is stationary. However, with pulse shaping, the OFDM signal is a WSCS signal. Direct analysis of the PAPR distribution of a cyclostationary signal can be very complex. By introducing a random phase, the WSCS signal was then transformed to a WSS signal. After the stationarisation process, the joint pdf of the stationarised signal was derived to obtain the level crossing rate. Then, the CCDF of PAPR was analysed using the LCR theorem and an upper bound for the CCDF of PAPR was derived. Numerical results demonstrated that the proposed upper bound was tight.

5.A Appendix: Covariances and Expected Value

In this section, the covariances and expected values of $x, \dot{x}, y, \dot{y}$ for matrix $\mathbf{R}$ are presented.

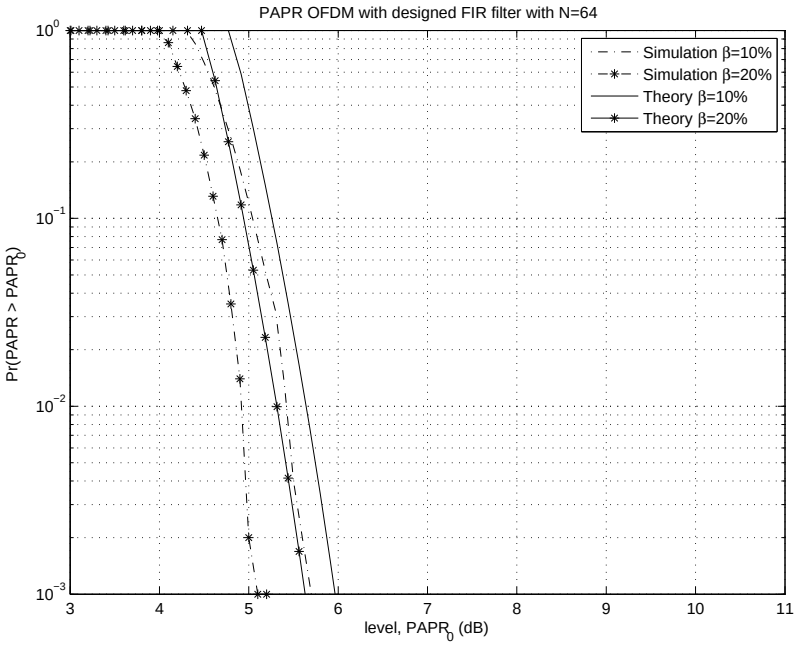

Figure 5.5: Comparison of the proposed upper bound with the simulation results for the designed FIR filter (N=64).

It is assumed that Z_k is assumed i.i.d random variables with

$$E[Z_k] = 0 \tag{5.60}$$

and

$$E[Z_k Z_i^*] = \begin{cases} \sigma^2, k = i \\ 0, k \neq i \end{cases} \tag{5.61}$$

Z_k can be written in a form of $a_k + jb_k$ where a_k and b_k are uniformly distributed and i.i.d random variables where

$$E[a] = E[b] = E[ab] = 0 \tag{5.62}$$

$$E[a^2] = E[b^2] = \sigma^2/2 \tag{5.63}$$

$$\cos(\arg Z_k) = \frac{a}{\sqrt{a^2 + b^2}} \tag{5.64}$$

$$\sin(\arg Z_k) = \frac{b}{\sqrt{a^2 + b^2}} \tag{5.65}$$

Then, the expected value of real and imaginary part of the signal can be expressed as

$$E[x(t)] = E\left[\sum_{k=0}^{N-1} Z_k p_k(t) \cos(\varphi_t)\right] \tag{5.66}$$

$$= \sum_{k=0}^{N-1} E[Z_k] p_k(t) \cos(\varphi_t) = 0 \tag{5.67}$$

$$E[y(t)] = E\left[\sum_{k=0}^{N-1} Z_k p_k(t) \sin(\varphi_t)\right] \tag{5.68}$$

$$= \sum_{k=0}^{N-1} E[Z_k] p_k(t) \sin(\varphi_t) = 0 \tag{5.69}$$

The expected value of the first derivation of x can be expressed as

$$\begin{aligned} E[\dot{x}(t)] &= E\left[\sum_{k=0}^{N-1} |Z_k||\dot{p_k}(t)|\cos(\dot{\varphi}_t) + |Z_k||p_k(t)|\tfrac{2\pi kt}{T}\cos(\varphi_t + \tfrac{\pi}{2})\right] \\ &= \sum_{k=0}^{N-1} E[|Z_k|]|\dot{p_k}(t)|\cos(\dot{\varphi}_t) + E[|Z_k|]|p_k(t)|\tfrac{2\pi kt}{T}\cos(\varphi_t + \tfrac{\pi}{2}) \\ &= 0 \end{aligned} \tag{5.70}$$

The expected value of the first derivation of y is given by

$$\begin{aligned} E[\dot{y}(t)] &= E\left[\sum_{k=0}^{N-1} |Z_k||\dot{p_k}(t)|\sin(\dot{\varphi}_t) + |Z_k||p_k(t)|\tfrac{2\pi kt}{T}\sin(\varphi_t + \tfrac{\pi}{2})\right] \\ &= \sum_{k=0}^{N-1} E[|Z_k|]|\dot{p_k}(t)|\sin(\dot{\varphi}_t)] + E[|Z_k|]|p_k(t)|\tfrac{2\pi kt}{T}\sin(\varphi_t + \tfrac{\pi}{2})] \\ &= 0 \end{aligned} \tag{5.71}$$

It can be seen that the mean value of $x, \dot{x}, y, \dot{y}$ can be written as

$$E[x(t)] = E[y(t)] = E[\dot{x}(t)] = E[\dot{y}(t)] = 0 \tag{5.72}$$

In order to build the covariance matrix $\mathbf{R}$, the covariances for $x, \dot{x}, y, \dot{y}$ are required. These covariances are as follows:

$$C_{xx} = E[(x - E[x])(x - E[x])] = E[x^2] = \sigma_{xx} \tag{5.73}$$

$$\begin{aligned} \sigma_{xx} &= E[x^2(t)] && (5.74) \\ &= E\left[\sum_{k=0}^{N-1} Z_k p_k(t)\cos(\varphi_t) Z_k p_k(t)\cos(\varphi_t)\right] \\ &= \sum_{k=0}^{N-1} E\left[Z_k Z_k\right] E[p_k(t)p_k(t)] E[\cos(\varphi_t)\cos(\varphi_t)] \\ &= \sigma^2 \sum_{k=0}^{N-1} p_k(t)p_k(t) && (5.75) \end{aligned}$$

$$C_{yy} = E[(y - E[y])(y - E[y])] = E[y^2] = \sigma_{yy} \tag{5.76}$$

$$\begin{aligned}\sigma_{yy} &= E[y^2(t)] \quad (5.77)\\ &= E\left[\sum_{k=0}^{N-1} Z_k p_k(t)\sin(\varphi_t) Z_k p_k(t)\sin(\varphi_t)\right]\\ &= \sum_{k=0}^{N-1} E\left[Z_k Z_k p_k(t)p_k(t)\sin(\varphi_t)\sin(\varphi_t)\right]\\ &= \sigma^2 \sum_{k=0}^{N-1} p_k(t)p_k(t) \quad (5.78)\end{aligned}$$

Hence, $\sigma_{xx} = \sigma_{yy}$

$$C_{x\dot{x}} = E[(x - E[x])(\dot{x} - E[\dot{x}])] = E[x\dot{x}] = \sigma_{x\dot{x}} \quad (5.79)$$

$$\begin{aligned}\sigma_{x\dot{x}} &= \frac{dE[x^2(t)]}{2dt} = \frac{\sigma^2}{2}\sum_{k=0}^{N-1}\frac{d}{dt}E[p_k(t)p_k(t)]\\ &= \frac{\sigma^2}{2}\sum_{k=0}^{N-1}\frac{d}{dt}p_k^2(t) \quad (5.80)\end{aligned}$$

$$C_{y\dot{y}} = E[(y - E[y])(\dot{y} - E[\dot{y}])] = E[y\dot{y}] = \sigma_{y\dot{y}} \quad (5.81)$$

$$\begin{aligned}\sigma_{y\dot{y}} &= \frac{dE[y^2(t)]}{2dt} = \frac{\sigma^2}{2}\sum_{k=0}^{N-1}\frac{d}{dt}E[p_k(t)p_k(t)]\\ &= \frac{\sigma^2}{2}\sum_{k=0}^{N-1}\frac{d}{dt}p_k^2(t) \quad (5.82)\end{aligned}$$

Hence, $\sigma_{x\dot{x}} = \sigma_{y\dot{y}}$

$$C_{\dot{x}\dot{x}} = E[(\dot{x} - E[\dot{x}])(\dot{x} - E[\dot{x}])] = E[\dot{x}^2] = \sigma_{\dot{x}\dot{x}} \quad (5.83)$$

$$\begin{aligned}
\sigma_{\dot{x}\dot{x}} &= E\left[\sum_{k=0}^{N-1}(|Z_k||\dot{p_k}(t)|cos(\dot{\varphi}_t)+|Z_k||p_k(t)|\frac{2\pi kt}{T}cos(\varphi_t+\frac{\pi}{2}))^2\right] \\
&= \sum_{k=0}^{N-1}E[(|Z_k||\dot{p_k}(t)|cos(\dot{\varphi}_t))^2+2|Z_k||\dot{p_k}(t)|cos(\dot{\varphi}_t)|Z_k||p_k(t)|\frac{2\pi kt}{T}cos(\varphi_t+\frac{\pi}{2}) \\
&+ (|Z_k||p_k(t)|\frac{2\pi kt}{T}cos(\varphi_t+\frac{\pi}{2}))^2 \\
&= \sum_{k=0}^{N-1}E[|Z_k|]^2\left\{|\dot{p_k}(t)|^2E[cos(\dot{\varphi}_t)]^2+2|\dot{p_k}(t)||p_k(t)|\frac{2\pi kt}{T}cos(\dot{\varphi}_t)cos(\varphi_t+\frac{\pi}{2})\right. \\
&+ \left.|p_k(t)|^2\frac{4(\pi kt)^2}{T^2}E[cos(\varphi_t+\frac{\pi}{2})]^2\right\} \\
&= \sigma^2\sum_{k=0}^{N-1}[\frac{1}{2}|\dot{p_k}(t)|^2+2|\dot{p_k}(t)||p_k(t)|\frac{2\pi kt}{T}cos(\dot{\varphi}_t)cos(\varphi_t+\frac{\pi}{2}) \\
&+ \frac{1}{2}|p_k(t)|^2\frac{4(\pi kt)^2}{T^2}] \qquad (5.84)
\end{aligned}$$

$$C_{\dot{y}\dot{y}} = E[(\dot{y}-E[\dot{y}])(\dot{y}-E[\dot{y}])] = E[\dot{y}^2] = \sigma_{\dot{y}\dot{y}} \qquad (5.85)$$

$$\begin{aligned}
\sigma_{\dot{y}\dot{y}} &= E\left[\sum_{k=0}^{N-1}(|Z_k||\dot{p_k}(t)|sin(\dot{\varphi}_t)+|Z_k||p_k(t)|\frac{2\pi kt}{T}sin(\varphi_t+\frac{\pi}{2}))^2\right] \\
&= \sum_{k=0}^{N-1}E[(|Z_k||\dot{p_k}(t)|sin(\dot{\varphi}_t))^2+2|Z_k||\dot{p_k}(t)|sin(\dot{\varphi}_t)|Z_k||p_k(t)|\frac{2\pi kt}{T}sin(\varphi_t+\frac{\pi}{2}) \\
&+ (|Z_k||p_k(t)|\frac{2\pi kt}{T}sin(\varphi_t+\frac{\pi}{2}))^2 \\
&= \sum_{k=0}^{N-1}E[|Z_k|]^2\left\{|\dot{p_k}(t)|^2E[sin(\dot{\varphi}_t)]^2+2|\dot{p_k}(t)||p_k(t)|\frac{2\pi kt}{T}sin(\dot{\varphi}_t)sin(\varphi_t+\frac{\pi}{2})\right. \\
&+ \left.|p_k(t)|^2\frac{4(\pi kt)^2}{T^2}E[sin(\varphi_t+\frac{\pi}{2})]^2\right\} \\
&= \sigma^2\sum_{k=0}^{N-1}\frac{1}{2}|\dot{p_k}(t)|^2+2|\dot{p_k}(t)||p_k(t)|\frac{2\pi kt}{T}sin(\dot{\varphi}_t)cos(\varphi_t+\frac{\pi}{2}) \\
&+ \frac{1}{2}|p_k(t)|^2\frac{4(\pi kt)^2}{T^2} \qquad (5.86)
\end{aligned}$$

Hence, $\sigma_{\dot{x}\dot{x}} = \sigma_{\dot{y}\dot{y}}$.

The covariances between $x(t)$ and $y(t)$ can be expressed as

$$C_{xy} = E[(x - E[x])(y - E[y])] = E[xy] = \sigma_{xy} \tag{5.87}$$

$$C_{yx} = E[(y - E[y])(x - E[x])] = E[yx] = \sigma_{yx} \tag{5.88}$$

Then, σ_{xy} and σ_{yx} can be expressed as follows

$$\begin{aligned} \sigma_{xy} &= E[x(t)y(t)] \\ &= E\left[\sum_{k=0}^{N-1} Z_k p_k(t)\cos(\varphi_t) Z_k p_k(t)\sin(\varphi_t)\right] \\ &= \sum_{k=0}^{N-1} E\left[Z_k Z_k p_k(t) p_k(t) cos(\varphi_t)\sin(\varphi_t)\right] \end{aligned} \tag{5.89}$$

As φ_t can be rewritten as $\varphi_t = \arg Z_k + \psi_b$ where $\psi_b = \frac{2\pi kt}{T} + \arg(p_k(t))$,

$$\sigma_{xy} = \sum_{k=0}^{N-1} E\left[Z_k Z_k p_k(t) p_k(t)\cos(arg Z_k + \psi_b)\sin(\arg Z_k + \psi_b)\right] \tag{5.90}$$

After algebraic manipulation and using (5.64) and (5.65), the following can be expressed

$$\begin{aligned} \sigma_{xy} &= \sigma^2 \sum_{k=0}^{N-1} p_k(t)^2 E\left[ab\cos^2(\psi_b) - ab\sin^2(\psi_b) + a^2\cos(\psi_b)\sin(\psi_b) - b^2\cos(\psi_b)\sin(\psi_b)\right] \\ &= 0 \end{aligned} \tag{5.91}$$

The derivatives of $x(t)$ and $y(t)$ are independent of each other and the covariance values can be expressed as

$$C_{\dot{x}\dot{y}} = E[(\dot{x} - E[\dot{y}])(\dot{y} - E[\dot{x}])] = C_{\dot{y}\dot{x}} = 0$$

$$C_{\dot{x}y} = E[(\dot{x} - E[\dot{x}])(y - E[\dot{y}])] = C_{y\dot{x}} = 0$$

$$C_{x\dot{y}} = E[(x - E[x])(\dot{y} - E[\dot{y}])] = C_{\dot{y}x} = 0$$

Therefore, the covariance matrix can now be written as

$$R = \begin{bmatrix} \sigma_{xx} & \sigma_{x\dot{x}} & 0 & 0 \\ \sigma_{x\dot{x}} & \sigma_{\dot{x}\dot{x}} & 0 & 0 \\ 0 & 0 & \sigma_{xx} & \sigma_{x\dot{x}} \\ 0 & 0 & \sigma_{x\dot{x}} & \sigma_{\dot{x}\dot{x}} \end{bmatrix} \tag{5.92}$$

5.B Appendix: Derivation of the Joint pdf

In this section, the joint pdf for $r, \dot{r}, \theta, \dot{\theta}$ is derived.

The joint pdf of $x, \dot{x}, y, \dot{y}$ is defined by [45]

$$f_{x,y}(\mathbf{X}) = \frac{1}{4\pi^2\sqrt{|\mathbf{R}|}} \exp[-\frac{1}{2}\mathbf{X}\mathbf{R}^{-1}\mathbf{X}^t]$$

$$f_{x,y}(\mathbf{X}) = \frac{1}{4\pi^2\sqrt{|(\sigma_{xx}\sigma_{\dot{x}\dot{x}} - \sigma_{x\dot{x}}^2)^2|}} \exp[-\frac{1}{2}\mathbf{X}\mathbf{R}^{-1}\mathbf{X}^t]$$

where

$$R^{-1} = \frac{1}{K}\begin{bmatrix} \sigma_{\dot{x}\dot{x}} & -\sigma_{x\dot{x}} & 0 & 0 \\ -\sigma_{x\dot{x}} & \sigma_{xx} & 0 & 0 \\ 0 & 0 & \sigma_{\dot{x}\dot{x}} & -\sigma_{x\dot{x}} \\ 0 & 0 & -\sigma_{x\dot{x}} & \sigma_{xx} \end{bmatrix} \tag{5.93}$$

where $K = (\sigma_{xx}\sigma_{\dot{x}\dot{x}} - \sigma_{x\dot{x}}^2)$

$$f_{x,y}(x, \dot{x}, y, \dot{y}) = \frac{1}{4\pi^2\sqrt{|(\sigma_{xx}\sigma_{\dot{x}\dot{x}} - \sigma_{x\dot{x}}^2)^2|}} exp[-\frac{1}{2}\mathbf{X}\mathbf{R}^{-1}\mathbf{X}^t]$$

By using the value of K and covariances , the joint PDF can be written as

$$f_{x,\dot{x},y,\dot{y}}(x, \dot{x}, y, \dot{y}) = \frac{1}{4\pi^2 K} \exp[-\frac{1}{2}(\frac{x^2\sigma_{\dot{x}\dot{x}}}{K} - 2\frac{x\dot{x}\sigma_{x\dot{x}}}{K} + \frac{\dot{x}^2\sigma_{xx}}{K} + \frac{y^2\sigma_{\dot{x}\dot{x}}}{K} - 2\frac{y\dot{y}\sigma_{x\dot{x}}}{K} + \frac{\dot{y}^2\sigma_{xx}}{K})] \tag{5.94}$$

The transformation of the Cartesian coordinates (x, y) into the polar coordinate system (r, θ) leads to the following transformation formulae

$$x = \sigma r \cos(\theta) \tag{5.95}$$

$$y = \sigma r \sin(\theta) \tag{5.96}$$

$$\dot{x} = \sigma(\dot{r}\cos(\theta) - r\dot{\theta}\sin(\theta)) \tag{5.97}$$

$$\dot{y} = \sigma(\dot{r}\sin(\theta) + r\dot{\theta}\cos(\theta)) \tag{5.98}$$

where $\sigma = \sqrt{P_{av}}$, $r = \sqrt{x^2 + y^2}$ and $\theta = arctan(y/x)$.

After converting the variables into polar coordinates, the joint PDF can be written as

$$f_{r,\dot{r},\theta,\dot{\theta}}(r, \dot{r}, \theta, \dot{\theta}) = f_{x,\dot{x},y,\dot{y}}(x, \dot{x}, y, \dot{y})|J| \tag{5.99}$$

where J is the Jacobi matrix as follows

$$J = \begin{bmatrix} \frac{\partial x}{\partial r} & \frac{\partial x}{\partial \dot{r}} & \frac{\partial x}{\partial \theta} & \frac{\partial x}{\partial \dot{\theta}} \\ \frac{\partial \dot{x}}{\partial r} & \frac{\partial \dot{x}}{\partial \dot{r}} & \frac{\partial \dot{x}}{\partial \theta} & \frac{\partial \dot{x}}{\partial \dot{\theta}} \\ \frac{\partial y}{\partial r} & \frac{\partial y}{\partial \dot{r}} & \frac{\partial y}{\partial \theta} & \frac{\partial y}{\partial \dot{\theta}} \\ \frac{\partial \dot{y}}{\partial r} & \frac{\partial \dot{y}}{\partial \dot{r}} & \frac{\partial \dot{y}}{\partial \theta} & \frac{\partial \dot{y}}{\partial \dot{\theta}} \end{bmatrix} \tag{5.100}$$

$$J = \begin{bmatrix} \sigma\cos(\theta) & 0 & r\sigma\sin(\theta) & 0 \\ -\sigma\dot{\theta}\sin\theta & \sigma\cos(\theta) & -\sigma(\dot{r}\sin(\theta) + r\dot{\theta}\cos(\theta)) & -\sigma r\sin(\theta) \\ \sigma\sin(\theta) & 0 & \sigma r\cos(\theta) & 0 \\ -\sigma\dot{\theta}\cos(\theta) & \sigma\sin(\theta) & \sigma(\dot{r}\cos(\theta) - r\dot{\theta}\sin(\theta)) & \sigma r\cos(\theta) \end{bmatrix} \tag{5.101}$$

The determination of the Jacobian matrix is as follows

$$|J| = r^2\sigma^4 \tag{5.102}$$

After the transformation to polar coordinates, the joint pdf for $r, \dot{r}, \theta, \dot{\theta}$ can be

written as

$$\begin{aligned} f_{r,\dot{r},\theta,\dot{\theta}}(r,\dot{r},\theta,\dot{\theta}) &= \frac{r^2\sigma^4}{4\pi^2K}\exp[-\frac{1}{2}(\frac{(\sigma r\cos(\theta))^2\sigma_{\dot{x}\dot{x}}}{K} - 2\frac{\sigma r\cos(\theta)\sigma(\dot{r}\cos(\theta)-r\dot{\theta}\sin(\theta))\sigma_{x\dot{x}}}{K} \\ &+ \frac{(\sigma(\dot{r}\cos(\theta)-r\dot{\theta}\sin(\theta)))^2\sigma_{xx}}{K} + \frac{(r\sin(\theta))^2\sigma_{\dot{x}\dot{x}}}{K} \\ &- 2\frac{r\sin(\theta)\sigma(\dot{r}\sin(\theta)+r\dot{\theta}\cos(\theta))\sigma_{x\dot{x}}}{K} + \frac{(\sigma(\dot{r}\sin(\theta)+r\dot{\theta}\cos(\theta)))^2\sigma_{xx}}{K})] \\ &= \frac{r^2\sigma^4}{4\pi^2K}exp[-\frac{1}{2}(\frac{\sigma^2r^2\sigma_{\dot{x}\dot{x}}}{K} - 2\frac{\sigma^2r\dot{r}\sigma_{x\dot{x}}}{K} + \frac{\sigma^2(\dot{r}^2+r^2\dot{\theta}^2)\sigma_{xx}}{K})] \\ &= \frac{r^2\sigma^4}{4\pi^2K}exp[-\frac{\sigma^2}{2}(\frac{r^2\sigma_{\dot{x}\dot{x}}}{K} - 2\frac{r\dot{r}\sigma_{x\dot{x}}}{K} + \frac{(\dot{r}^2+r^2\dot{\theta}^2)\sigma_{xx}}{K})] \\ &= \frac{r^2\sigma^4}{4\pi^2K}exp[-\frac{\sigma^2}{2}(\frac{r^2}{\sigma^{-1}_{\dot{x}\dot{x}}K} - 2\frac{r\dot{r}}{\sigma^{-1}_{x\dot{x}}K} + \frac{(\dot{r}^2+r^2\dot{\theta}^2)}{\sigma^{-1}_{xx}K})] \end{aligned} \tag{5.103}$$

5.C Appendix: LCR of the Stationarised OFDM Signal

In this section, the LCR of the stationarised OFDM signal, $\hat{r}(t)$ is derived. Before the stationarisation process, the LCR of $r(t)$ is given by

$$v_r^+(z) = \int_0^\infty \dot{r}\frac{z\sigma^3}{\sqrt{\sigma_{xx}2\pi K}}\exp[-\frac{\sigma^2}{2}(\frac{z^2}{\sigma^{-1}_{\dot{x}\dot{x}}K} - 2\frac{z\dot{r}}{\sigma^{-1}_{x\dot{x}}K} + \frac{\dot{r}^2}{\sigma^{-1}_{xx}K})]d\dot{r} \tag{5.104}$$

$$v_r^+(z) = \frac{z\sigma^3}{\sqrt{\sigma_{xx}2\pi K}}\int_0^\infty \left\{\exp[-\frac{\sigma^2}{2}(c+b\dot{r}+a\dot{r}^2)]\right\}\dot{r}d\dot{r} \tag{5.105}$$

where

$$a = \frac{\sigma_{xx}}{K} \tag{5.106}$$

$$b = -\frac{2z\sigma_{x\dot{x}}}{K} \tag{5.107}$$

$$c = \frac{z^2\sigma_{\dot{x}\dot{x}}}{K} \tag{5.108}$$

To simplify the quadratic formula, consider that $\dot{r} = x$

$$f(x) = ax^2 + bx + c = a(x-h)^2 + k \tag{5.109}$$

where $h = -b/2a$ and $k = ah^2 + bh + c$. Therefore, the exponent can be written in form of

$$e^{a(x-h)^2+k} = e^{a(x-h)^2}e^k \tag{5.110}$$

where

$$h = 2z\frac{\sigma_{x\dot{x}}}{\sigma_{xx}} \tag{5.111}$$

and

$$\begin{aligned} k &= ah^2 + bh + c \\ &= \frac{\sigma_{xx}}{K}(z\frac{\sigma_{x\dot{x}}}{\sigma_{xx}})^2 - \frac{2z\sigma_{x\dot{x}}}{K}(z\frac{\sigma_{x\dot{x}}}{\sigma_{xx}}) + \frac{z^2\sigma_{\dot{x}\dot{x}}}{K} \\ &= \frac{z^2}{K}\left\{-\frac{\sigma_{x\dot{x}^2}}{\sigma_{xx}} + \sigma_{\dot{x}\dot{x}}\right\} \\ &= \frac{z^2}{K}\frac{K}{\sigma_{xx}} = \frac{z^2}{\sigma_{xx}} \end{aligned} \tag{5.112}$$

Using (5.110), the level crossing in (5.105) can be simplified to

$$v_r^+(z) = \frac{z\sigma^3}{\sqrt{\sigma_{xx}2\pi K}}\int_0^\infty \left\{exp[-\frac{\sigma^2}{2}(a(\dot{r}-h)^2 + k]\right\}\dot{r}d\dot{r} \tag{5.113}$$

Next, the integration process can be done by using the following substitution:

$$y = \dot{r} - h \tag{5.114}$$

$$dy = d\dot{r} \tag{5.115}$$

By using (5.114), (5.113) can be expressed as

$$\begin{aligned} v_r^+(z) &= \frac{z\sigma^3}{\sqrt{\sigma_{xx}2\pi K}}\exp[-\frac{\sigma^2}{2}k]\int_{-h}^\infty \left\{exp[-\frac{\sigma^2}{2}(ay^2 + k)]\right\}(y+h)dy \\ &= \frac{z\sigma^3}{\sqrt{\sigma_{xx}2\pi K}}\exp[-\frac{\sigma^2}{2}k]\int_{-h}^\infty exp[-\frac{\sigma^2}{2}ay^2](y+h)dy \end{aligned}$$

$$v_r^+(z) = \frac{z\sigma^3}{\sqrt{\sigma_{xx}2\pi K}}\exp[-\frac{\sigma^2}{2}k]\left\{\int_{-h}^\infty yexp[-\frac{\sigma^2}{2}ay^2]dy + h\int_{-h}^\infty \exp[-\frac{\sigma^2}{2}ay^2]dy\right\} \tag{5.116}$$

Part 1 of integration[1]

$$\int_{-h}^{\infty} y \exp[-\frac{\sigma^2}{2} a y^2] dy \tag{5.119}$$

$$u = y^2$$

$$du = 2ydy$$

$$\int_{h^2}^{\infty} \exp[-\frac{\sigma^2}{2} au] \frac{du}{2} = \frac{1}{\sigma^2 a} \exp[-\frac{\sigma^2}{2} a h^2]$$

Part 2 of integration [1]

$$h \int_{-h}^{\infty} \exp[-\frac{\sigma^2}{2} a y^2] dy = h(1 + \frac{1}{2}\sqrt{\frac{2\pi}{\sigma^2 a}} erf(h))$$

where $erf(x)$ is an error function

$$erf(x) = \frac{2}{\sqrt{\pi}} \int_0^x e^{-y^2} dy$$

Then, (5.116) can be expressed as

$$v_r^+(z) = \frac{z\sigma^3}{\sqrt{\sigma_{xx} 2\pi K}} \exp[-\frac{\sigma^2}{2} k] \left\{ \frac{1}{2\sigma^2 a} \exp[-\frac{\sigma^2}{2} a h^2]] + h(1 + \frac{1}{2}\sqrt{\frac{2\pi}{\sigma^2 a}} erf(h)) \right\} \tag{5.120}$$

Next is to replace parameter h and a in (5.120), this results in

$$\begin{aligned} v_r^+(z) &= \frac{z\sigma^3}{\sqrt{\sigma_{xx} 2\pi K}} \exp[-\frac{\sigma^2 k}{2}] \left\{ \frac{K}{\sigma^2 \sigma_{xx}} exp[-\frac{\sigma^2}{2} \frac{\sigma_{xx}}{K} (2z \frac{\sigma_{x\dot{x}}}{\sigma_{xx}})^2] + 2z \frac{\sigma_{x\dot{x}}}{\sigma_{xx}} \right. \\ &\left. (1 + \sqrt{\frac{2\pi K}{\sigma_{xx}\sigma^2}} erf(2z \frac{\sigma_{x\dot{x}}}{\sigma_{xx}})) \right\} \end{aligned} \tag{5.121}$$

[1]Note that in Gaussian integral that

$$\int_0^{\infty} x e^{-tx^2} dx = \frac{1}{2t} \tag{5.117}$$

$$\int_0^{\infty} e^{-tx^2} dx = \frac{1}{2}\sqrt{\frac{\pi}{t}} \tag{5.118}$$

which can be simplified into

$$v_r^+(z) = \frac{z\sigma^3}{\sqrt{\sigma_{xx}2\pi K}}\exp[-\frac{\sigma^2 k}{2}]\left\{\frac{K}{\sigma^2\sigma_{xx}}exp[-\frac{2z^2\sigma^2}{K}\frac{\sigma_{x\dot{x}}^2}{\sigma_{xx}}]+2z\frac{\sigma_{x\dot{x}}}{\sigma_{xx}}\right.$$
$$\left.(1+\sqrt{\frac{2\pi K}{\sigma_{xx}\sigma^2}}erf(2z\frac{\sigma_{x\dot{x}}}{\sigma_{xx}}))\right\} \quad (5.122)$$

By substituting k in (5.122), it results in

$$v_r^+(z) = \frac{z\sigma^3}{\sqrt{\sigma_{xx}2\pi K}}\exp[-\frac{\sigma^2 z^2}{2\sigma_{xx}}]\left\{\frac{K}{\sigma^2\sigma_{xx}}exp[-\frac{2z^2\sigma^2}{K}\frac{\sigma_{x\dot{x}}^2}{\sigma_{xx}}]+z\frac{\sigma_{x\dot{x}}}{\sigma_{xx}}\right.$$
$$\left.(1+\sqrt{\frac{2\pi K}{\sigma_{xx}\sigma^2}}erf(2z\frac{\sigma_{x\dot{x}}}{\sigma_{xx}}))\right\} \quad (5.123)$$

By substituting K to the above equation, (5.123) can be written as

$$v_r^+(z) = \frac{z\sigma^3}{\sqrt{\sigma_{xx}2\pi(\sigma_{xx}\sigma_{\dot{x}\dot{x}}-\sigma_{x\dot{x}}^2)}}\exp[-\frac{\sigma^2 z^2}{2\sigma_{xx}}]$$
$$\left\{\frac{(\sigma_{xx}\sigma_{\dot{x}\dot{x}}-\sigma_{x\dot{x}}^2)}{\sigma^2\sigma_{xx}}exp[-\frac{2z^2\sigma^2}{(\sigma_{xx}\sigma_{\dot{x}\dot{x}}-\sigma_{x\dot{x}}^2)}\frac{\sigma_{x\dot{x}}^2}{\sigma_{xx}}]+2z\frac{\sigma_{x\dot{x}}}{\sigma_{xx}}\right. \quad (5.124)$$
$$\left.(1+\sqrt{\frac{2\pi(\sigma_{xx}\sigma_{\dot{x}\dot{x}}-\sigma_{x\dot{x}}^2)}{\sigma_{xx}\sigma^2}}erf(2z\frac{\sigma_{x\dot{x}}}{\sigma_{xx}}))\right\}$$

By using (5.57), the LCR for the stationarised signal can be expressed as

$$v_{\hat{r}}^+(z) = \frac{1}{T}\int_0^T \frac{z\sigma^3}{\sqrt{\sigma_{xx}2\pi(\sigma_{xx}\sigma_{\dot{x}\dot{x}}-\sigma_{x\dot{x}}^2)}}\exp[-\frac{\sigma^2 z^2}{2\sigma_{xx}}]$$
$$\left\{\frac{(\sigma_{xx}\sigma_{\dot{x}\dot{x}}-\sigma_{x\dot{x}}^2)}{\sigma^2\sigma_{xx}}\exp[-\frac{2z^2\sigma^2}{(\sigma_{xx}\sigma_{\dot{x}\dot{x}}-\sigma_{x\dot{x}}^2)}\frac{\sigma_{x\dot{x}}^2}{\sigma_{xx}}]+2z\frac{\sigma_{x\dot{x}}}{\sigma_{xx}}\right. \quad (5.125)$$
$$\left.(1+\sqrt{\frac{2\pi(\sigma_{xx}\sigma_{\dot{x}\dot{x}}-\sigma_{x\dot{x}}^2)}{\sigma_{xx}\sigma^2}}erf(2z\frac{\sigma_{x\dot{x}}}{\sigma_{xx}}))\right\}dt$$

Chapter 6

Pulse Shaping Approach to PAPR Reduction for Multiuser OFDM Systems

Pulse shaping approach was used in Chapter 3 and Chapter 4 to reduce the PAPR of the single user OFDM transmitted signal in order to improve the overall OFDM communication system performance in terms of PAPR reduction and BER performance improvement. In this chapter, the effectiveness of pulse shaping approach to PAPR reduction for multiuser OFDM (MU-OFDM) system is investigated.

Multiuser OFDM is a promising technique for high downlink capacities in mobile communication systems. In multiuser communication systems, the OFDM bandwidth is shared among multiple users. It is critical to design the OFDM subcarriers in such a way that users do not interfere with each other [89]. Previous work in [85] proposed to design different precoder for different user for MU-OFDM. However, the proposed design [85] does not consider PAPR reduction of the OFDM signal. Recently [86], a method is proposed to establish user independence and to reduce the PAPR of the MU-OFDM signal but the results only show marginal PAPR reduction.

In this chapter, computationally efficient optimisation approach is proposed to design a set of pulse shaping waveforms to reduce the PAPR of the MU-OFDM signal. Designing of a set of pulse shaping waveforms is fundamentally different from

designing a shaping pulse for a single user OFDM system because cross-correlations between the different pulse shaping waveforms have to be taken into consideration. Therefore, the filter design technique in Chapter 3 cannot be applied to solve the problem of designing a set of pulse shaping waveforms. The trade-off among users are considered and formulated as mathematical problem which can be solved efficiently and implemented effectively in practical application. The implementation issue, such as minimising interference among users is mathematically formulated as cross correlation and autocorrelation constraints.

The rest of the chapter is organised as follows: Section 6.1 presents the OFDM system model for multiuser communication. Section 6.2 introduces the pulse shaping filter design for MU-OFDM signal and computationally efficient method is presented to solve the pulse shaping waveform set design problem. Numerical results are presented in Section 6.3 to demonstrate the effectiveness of the designed set of pulse shaping waveforms in reducing the PAPR of the MU-OFDM signal. Finally, concluding remarks are drawn in Section 6.4.

6.1 System Model

6.1.1 MU-OFDM System Model without Pulse Shaping

Consider that U users utilise the OFDM system with N subcarriers. The number of subcarriers allocated for each user is $N_u = \frac{N}{U}$. It is assumed that each user has N_u number of data streams mapped to the allocated subcarriers as illustrated in Fig.6.1. The baseband equivalent of the OFDM transmitted signal for the u^{th} user is given by

$$\hat{s}^u(t) = \sum_{k=0}^{N'_u} Z_k^u e^{j2\pi kt/T}, \quad 0 \leq t < T \tag{6.1}$$

where $N'_u = (u-1)N_u + m$ and $m = 0, 1, 2, ...N_u - 1$. The subcarrier allocation can be on a fixed basis or on a dynamic basis [87][88]. It is assumed that the subcarriers allocation method is fixed.

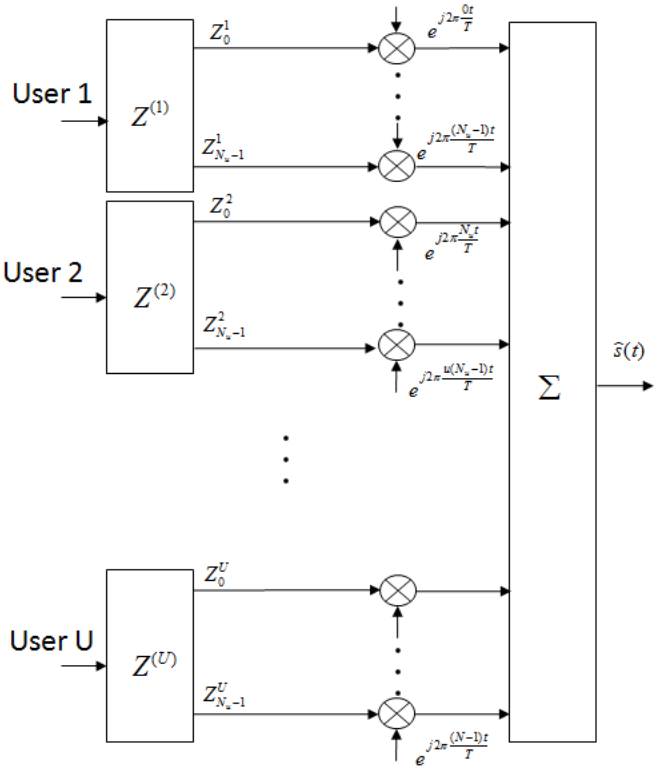

Figure 6.1: Block diagram of multiuser OFDM system.

6.1.2 MU-OFDM System Model with Pulse Shaping

When a single user OFDM signal is subjected to pulse shaping, the baseband equivalent of the OFDM transmitted signal is given by

$$\hat{s}(t) = \sum_{k=0}^{N-1} Z_k p_k(t) e^{j2\pi kt/T}, 0 \leq t \leq T \tag{6.2}$$

where $p_k(t)$ is the shaping pulse at the k^{th} subcarrier with a duration of T.

For multiuser communication systems, U users share the N subcarriers OFDM system. The number of subcarriers allocated for each user is $N_u = \frac{N}{U}$ and the baseband equivalent MU-OFDM signal with pulse shaping can be expressed as

$$s(t) = \sum_{u=1}^{U} s^u(t), 0 \leq t \leq T \tag{6.3}$$

where

$$s^u(t) = \sum_{k=0}^{N'_u} Z_k^u p_k^u(t) e^{j2\pi kt/T} \tag{6.4}$$

where $N'_u = (u-1)N_u + m,\ m = 0, 1, 2, ...N_u - 1$ and $p^u_k(t)$ is a pulse shaping waveform at the k^{th} subcarrier for the u^{th} user.

Pulse shaping in the frequency domain can be regarded as a precoding process. The block diagram of the precoded multiuser OFDM (PMU-OFDM) is illustrated in Fig.6.2. The baseband equivalent of the PMU-OFDM transmitted signal at the u^{th} user can be expressed as

$$s^u(t) = \sum_{k=0}^{N'_u-1} d^u e^{j2\pi kt/T}, \quad 0 \leq t<T \tag{6.5}$$

where $N'_u = (u-1)N_u + m,\ m = 0, 1, 2, ...N_u - 1$ and

$$d^u_k = P^u_k(e^{j\omega})Z^u_k \tag{6.6}$$

To reduce the PAPR of the MU-OFDM transmitted signal, the proposed approach is to design one principle pulse for each individual user and the different shaping pulses for all the subcarriers belonging to this particular user can be generated by cyclic shifting of this principle pulse. Let $P^u_0(e^{j\omega})$ denotes the frequency response of the principle pulse for u^{th} user, then

$$P^u_k(e^{j\omega}) = P_0(e^{j\omega})e^{-j\omega k}, k = 1, ..., N'_u - 1 \tag{6.7}$$

where $N'_u = (u-1)N_u + m,\ m = 0, 1, 2, ...N_u - 1$.

In practical implementations, (6.7) is often discretised and the discretised pulse can be expressed as

$$P^u_k = P^u_0 e^{-j2\pi \frac{ik}{N_u}} \tag{6.8}$$

where $i = 0, 1, ..., L-1,\ L = (1+\beta)N_u$ and $k = 1, ..., N'_u - 1$.

6.2 Pulse Shaping Waveform Set Design for MU-OFDM System

The design of a set of pulse shaping waveforms can be generalised as the design of a set of filters with specified constraints in time and frequency domain [42][85].

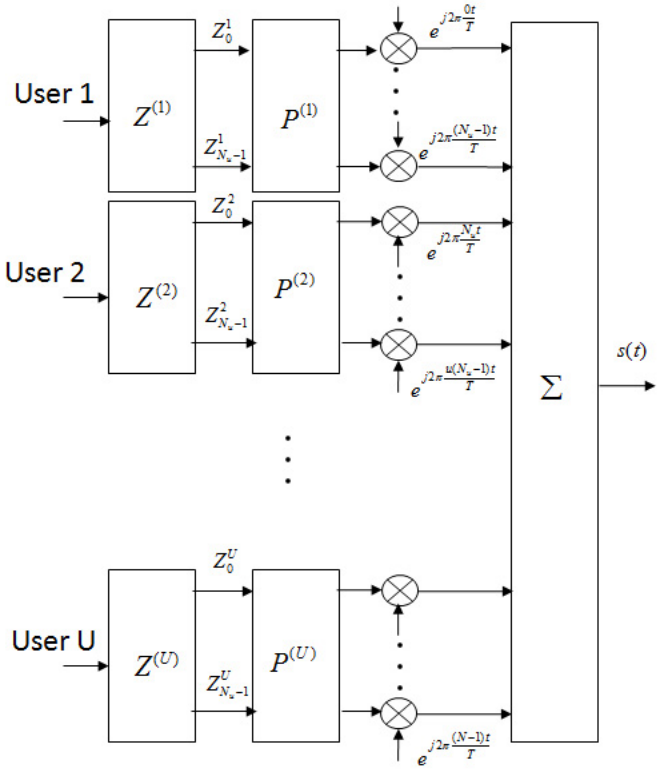

Figure 6.2: Block diagram of PMU-OFDM.

The objective of the design problem is to minimise the stopband energy of the designed pulse shaping waveforms and to maintain the spectral shaping efficiency. Constraints are introduced in the problem formulation in order to minimise ISI and CCI. All of the pulse shaping waveforms in the set are specified to have low autocorrelation value at nonzero lags and low cross-correlation value at all lags for low ISI and CCI, respectively.

6.2.1 Problem Formulation

For any given u, consider the following FIR filter $P_u(e^{j\omega})$

$$P_u(e^{j\omega}) = \sum_{k=0}^{M-1} h_u(k)\phi_k(e^{j\omega}) = \boldsymbol{h_u}^T \boldsymbol{\phi}(e^{j\omega}) \tag{6.9}$$

where

$$\boldsymbol{h_u} = [h_u(0), h_u(1), \ldots h_u(M-1)]^T$$
$$\boldsymbol{\phi} = [\phi_0, \phi_1, \ldots, \phi_{M-1}]^T$$

where

$$\phi_k(e^{j\omega}) = e^{-j\omega k} \quad k = 0, 1, 2, \ldots \tag{6.10}$$

The pulse shaping waveform set design problem, denoted as Problem (PU), can be stated as follows.

Problem(PU). Design a set of U filters $P_U = \{P_1(e^{j\omega}), P_2(e^{j\omega}), ..., P_U(e^{j\omega})\}$ which solves the following constrained optimisation problem

$$\min_{h_u} \max_{U} \max_{\omega_p \in \Omega_p} \left\{ ||P_u(e^{j\omega_p})|^2 - |D(\omega_p)|^2| + \frac{\gamma}{\pi} \int_{\Omega_s} |P_u(e^{j\omega})|^2 d\omega \right\} \tag{6.11}$$

for $u = 1, 2, \ldots, U$ and subject to the following autocorrelation constraint

$$|R_{ac}(m)| = |\sum_{i=0}^{M-1} h_u(i) h_u(i - mD)| \leq \eta_1 \tag{6.12}$$

where $m = 1, 2, ...$ and also the cross-correlation constraint

$$|R_{cc}(m)| = |\sum_{i=0}^{M-1} h_n(i) h_u(i - mD)| \leq \eta_2 \tag{6.13}$$

for $n \neq u$, $n = 1, 2, \ldots, U$, $u = 1, 2, \ldots, U$ and $m = 0, \pm 1, \pm 2, \ldots$, where $D(\omega)$ is a prescribed desired frequency response (usually the frequency response of an ideal filter), Ω_p the passband frequency set, Ω_s the stopband frequency set, D a positive integer representing the number of samples per symbol interval and γ a weighting parameter chosen by the designer.

Remarks: (a) The first part of the objective function is to shape every filter to a desired spectral shape (as prescribed by $D(\omega)$). The second part of the objective function is to minimise the stopband energy leakage. The parameter γ in the objective function is chosen by the designer to reflect the designer's preference for better fitting (small γ) or lower stopband energy leakage (larger γ) of the designed set of pulse shaping waveforms. $D(\omega)$ is often selected to be the frequency response of a Nyquist pulse. One of the main reasons to use a Nyquist pulse is to allow the implementation of the matched filter at the receiver. (b) In constraint (6.12) and (6.13), η_1 and η_2 are small positive value in order to maintain a low ISI and low ICI, respectively.

6.2.2 Problem Conversion

After some algebraic manipulations (see Appendix 6.A), the optimisation problem (PU) can be converted to the following simplified optimisation problem (PUb) in which both the objective function and the contraints are quadratic of the parameters to be optimised

Problem(PUb). Find $h_u(u = 1, 2, ..., U)$ which solve the following optimisation problem

$$\min_{h_u} \max_{u} \max_{\omega_p \in \Omega_p} \left\{ ||h_u^T Q(\omega) h_u| - |D(\omega_p)|^2| + \frac{\gamma}{\pi} \int_{\Omega_s} Q_s(\omega) d\omega \right\} \tag{6.14}$$

for $u = 1, 2, ..., U$ subject to

$$|h_u^T Q_m h_u| \leq \eta_1 \tag{6.15}$$

for $2 \leq u \leq U$ and $m = 1, 2, ...$ and

$$|h_n^T G_m h_u| \leq \eta_2 \tag{6.16}$$

where $n \neq u$, $n = 1, 2, \ldots, U$, $u = 1, 2, \ldots, U$, $m = 0, \pm 1, \pm 2, \ldots$, $G_m = Q_m$ for $m > 0$ and $G_m = Q_m^T$ for $m \leq 0$.

Remarks: Instead of solving problem (PUb) to obtain $P_1(e^{j\omega})$, $P_2(e^{j\omega})$, ..., $P_U(e^{j\omega})$ simultaneously, in our numerical computation, iterative technique is used to design $P_u(e^{j\omega})$ in a sequential manner. First, problem (PUb) is solved for $P_1(e^{j\omega})$ subject to autocorrelation constraint (6.15). Then, by using $P_1(e^{j\omega})$, the optimisation problem (PUb) is solved for $P_2(e^{j\omega})$, $P_3(e^{j\omega})$, $P_4(e^{j\omega})$, etc one by one in an iterative fashion with both autocorrelation constraint (6.15) and crosscorrelation constraint (6.16).

6.3 Numerical Results

In this section, numerical results are presented to demonstrate the effectiveness of the designed set of pulse shaping waveforms in reducing the PAPR of the MU-OFDM signal. The ideal frequency response $D(\omega)$ is the non-causal raised cosine filter with $\beta = 0.2$ as illustrated in Fig.6.3. Fig.6.4 and 6.5 illustrate the spectra

and the impulse responses of a set of four designed pulse shape waveforms. Other design parameters are $D = 4$, $M = 48$, $\eta_1 = 0.001$, $\eta_2 = 0.001$ and $N = 64$. The autocorrelation is set at low value at $m \neq 0$ ($|R_{ac}(m)| \leq 0.001$) and the cross-correlation is set at low value at $m = 0, \pm 1, \pm 2, \ldots$ ($|R_{cc}(m)| \leq 0.001$) to minimise ISI and ICI.

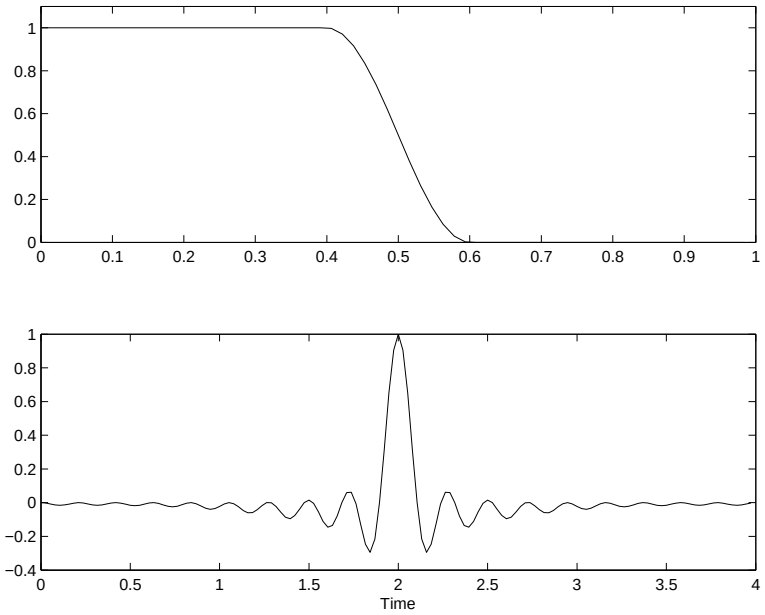

Figure 6.3: Time domain and frequency domain responses of raised cosine.

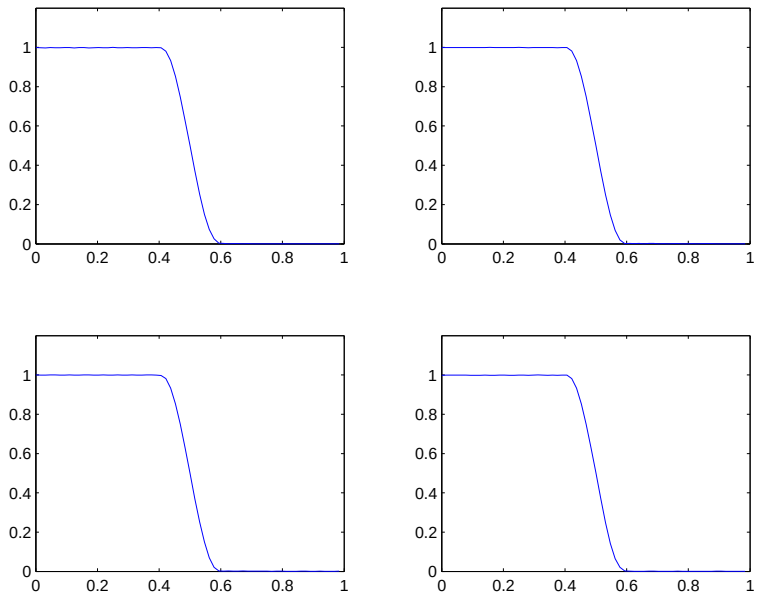

Figure 6.4: Frequency spectrum of the four designed set of filters.

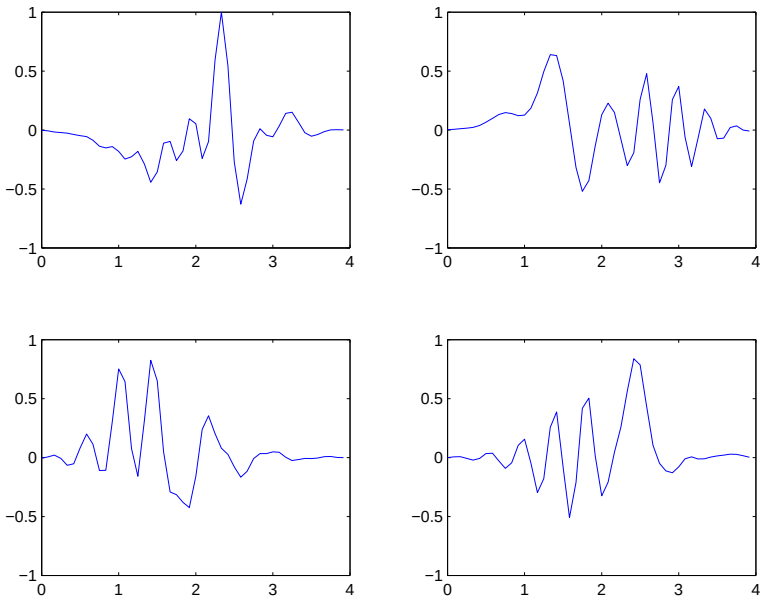

Figure 6.5: Impulse response of the four designed set of pulse shaping filters.

Fig.6.6 illustrates the CCDF of the PAPR of the PMU-OFDM for $U = 2$. It shows that the designed set of pulse shaping waveforms reduces the PAPR by approximately 2 dB for $N = 64$, $N = 128$ and $N = 256$.

Fig.6.7 illustrates that the designed set of pulse shaping waveforms reduces

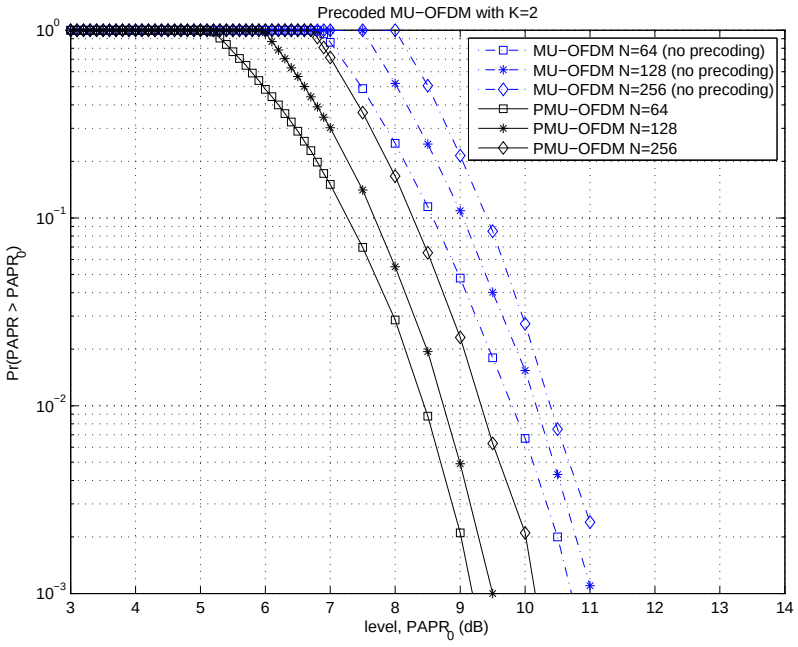

Figure 6.6: PAPR for PMU-OFDM with U=2.

the PAPR for different numbers of subcarriers. For $N = 128$, the PAPR can be reduced by approximately 2 dB for $U = 2$ and 3 dB for $U = 4$. For $U = 4$ and $N = 256$, the PAPR can be reduced by approximately 2 dB.

For further investigation, Fig.6.8 compares the CCDF of the PAPR of MU-

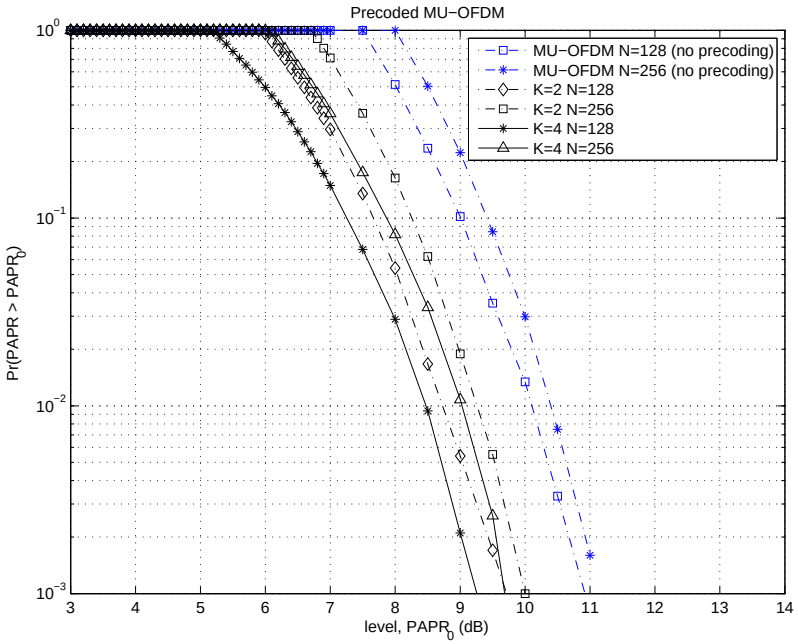

Figure 6.7: PAPR for PMU-OFDM with U=2 and U=4.

OFDM for $U = 2$, $U = 4$ and $U = 8$ for $N = 256$. For $U = 8$ the PAPR of the OFDM signal can be reduced by approximately 2 dB.

6.4 Concluding Remarks

In this chapter, PAPR reduction of the OFDM signal using pulse shaping approach for multiuser communication systems has been investigated. In multiuser communications, users' independence needs to be established to prevent ISI and CCI. Designing a set of pulse shaping waveforms using an optimisation approach for MU-OFDM communication systems was proposed. The pulse shaping waveform set design problem was formulated as a constrained minimax optimisation problem with both autocorrelation and cross-correlation constraints. The optimisation design problem was solved effectively by iterative technique. Numerical results demonstrated the effectiveness of the designed pulse shaping waveform set

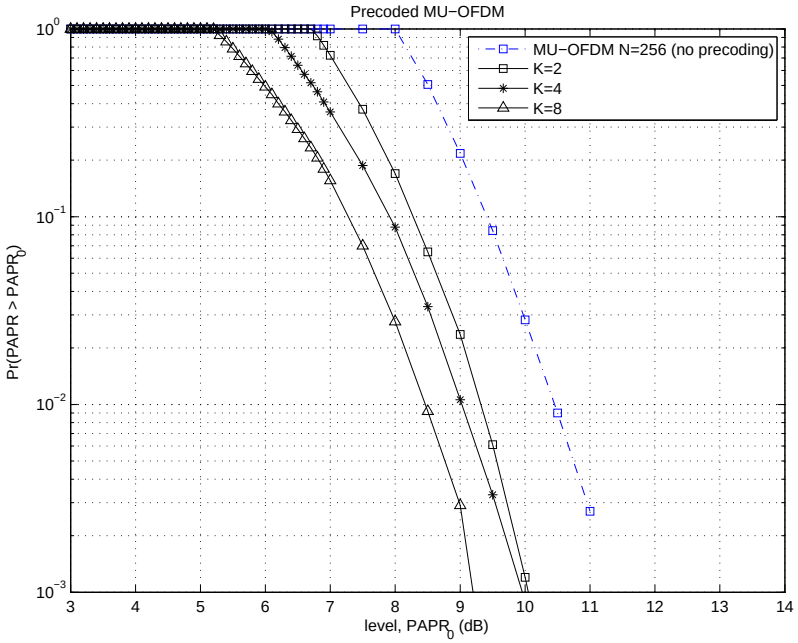

Figure 6.8: PAPR for PMU-OFDM for N=256.

in reducing the PAPR of the OFDM signal in multiuser communication systems.

6.A Appendix: Problem Simplification

In this section, the objective function and the constraint of Problem (PU) are simplified.

It is assumed that the matched filter is used and the channel is considered flat, the magnitude of the overall transfer function can be expressed as

$$|P_u(e^{j\omega})|^2 = h_u^T Q(\omega) h_u \tag{6.17}$$

where $h_u = [h_u(0), h_u(1), ..., h_u(M-1))$ and

$$Q(\omega) = e(\omega)e(\omega)^T \tag{6.18}$$

The magnitude error in the passband can be expressed as

$$\xi_p = ||h_u^T Q(\omega) h_u| - |D(\omega_p)|^2| \quad \omega_p \in \Omega_p \tag{6.19}$$

The energy error in the stopband can be written as

$$\xi_s = h_u^T Q_s(\omega) h_u \tag{6.20}$$

where Q_s is a matrix of NxN defined by

$$Q_s = \frac{1}{\pi} \int_{\Omega_s} Q(\omega) d\omega \tag{6.21}$$

In order to simplify constraints (6.12) and (6.13), the following matrix is defined as

$$Q_m = \begin{bmatrix} 0_{NU} & 0_m \\ I_m & 0_{NU}^T \end{bmatrix} \tag{6.22}$$

where I_m represents an $(N - mD) \times (N - mD)$ identity matrix, 0_m represents a $(mD) \times (mD)$ zero matrix, 0_{NU} represents an $(mD) \times (N - mD)$ zero matrix. The autocorrelation constraints in (6.12) can be expressed as

$$|R_{ac}(m)| = |h_u^T Q_m h_u| \leq \eta \tag{6.23}$$

and the crosscorrelation constraints in (6.13) can be expressed as

$$|R_{cc}(m)| = |h_n^T G_m h_u| \leq \eta \tag{6.24}$$

where $G_m = Q_m$ for $m > 0$ and $G_m = Q_m^T$ for $m \leq 0$.

Chapter 7

Conclusions and Future Research

In recent years, OFDM modulation technique has been adopted and implemented by many wireless communication standards due to its high bandwidth efficiency and robustness against multipath fading. One of the main drawbacks of the OFDM systems is that the transmitted signal often exhibits a high PAPR. The PAPR of the OFDM transmitted signal determines the power efficiency of the HPA. Therefore, reducing the PAPR of the OFDM signal is essential as power efficiency in wireless communication relates to coverage range, power consumption and the size of the terminals. This thesis has investigated the pulse shaping approach to reducing the PAPR of the OFDM signal for both single user and multiuser communication systems. Both theoretical analysis and extensive numerical studies have been carried out to justify the effectiveness and efficiency of the proposed approach.

7.1 Summary

In Chapter 2, some of the currently available PAPR reduction techniques and their pros and cons were briefly summarised. Pulse shaping approach is effective in reducing the PAPR of the OFDM signal with only minimal increase of implementation complexity. Numerical results demonstrated that the selected non-causal Nyquist pulses can reduce the PAPR of the OFDM signal.

Instead of using the existing non-causal Nyquist pulses (which need to be truncated and shifted before implementation), in Chapter 3, causal pulse shaping filters were designed using computationally efficient optimisation approach for PAPR reduction of the OFDM signal. The pulse shaping filter design problem was formulated as a nonlinear constrained optimisation problem. In order to solve this design problem efficiently, the nonlinear constraint was linearised. Then, the design problem was converted to a semi-infinite quadratic programming problem and was solved via discretisation. Numerical results demonstrated that the shaping pulse generated by the designed causal filter performed better than the non-causal Nyquist pulses in terms of PAPR reduction of the OFDM signal and implementation simplicity.

In Chapter 4, the BER performance of the OFDM systems with pulse shaping over multipath fading channels was investigated. The HIPERLAN/2 channel models for indoor environment were used to simulate the multipath fading channels. In the OFDM receiver, the matched filters and the MMSE detector were used. Numerical results demonstrated that the OFDM with the designed pulse shaping not only reduces the PAPR but also improved the BER performance of the OFDM signal over the multipath fading channels.

In Chapter 5, theoretical analysis of the PAPR distribution of the OFDM signal with pulse shaping had been investigated. Without pulse shaping, OFDM signal is stationary. However, with pulse shaping, the resulted OFDM signal becomes a WSCS signal. By introducing a random phase, the WSCS signal was converted to a WSS signal. The joint pdf of the stationarised signal was derived to obtain the LCR of the OFDM signal. The CCDF of PAPR was analysed using the LCR theorem and an upper bound for the CCDF of PAPR was derived. Numerical results demonstrated that the proposed upper bound is tight.

Finally, Chapter 6 was devoted to the PAPR reduction of the OFDM signal using pulse shaping approach for multiuser communication systems. In multiuser communications, users' independence needs to be established to prevent ISI and CCI. It was proposed to design a set of pulse shaping waveforms (each waveform for a different user) to reduce the PAPR of the OFDM signal. The design of a set of pulse shaping waveforms is fundamentally different from the design of a single

filter as in Chapter 3 because cross-correlations between the different pulse shaping waveforms have to be taken into consideration. The pulse shaping waveform set design problem was formulated as a non-convex optimisation problem. The design problem was then simplified and solved effectively by iterative techniques. Numerical results demonstrated the effectiveness of the designed pulse shaping waveform set in reducing the PAPR of the OFDM signal in multiuser communication systems.

7.2 Future Research

There are various possibilities to extend this research work:

- The Filter Bank Multi-Carrier (FBMC) based systems combined with Offset Quadrature Amplitude Modulation (OQAM) are considered as a promising candidate to be the front runner to become the radio waveform in the forthcoming 5G Radio Access Technology (RAT) [8]. The FBMC system has a very similar structure to OFDM with pulse shaping. One of the disadvantages of FBMC is also the high PAPR in the transmitted signal. In the future, the proposed filter design can be modified and developed for FBMC systems.

- The pulse shaping approach has been shown effective for multiuser communication systems. Multiuser communication systems increase the efficiency of system capacity. Multiple antennas can increase the system capacity and multi-input-multi-output (MIMO) can be incorporated in the OFDM system. In the future, the proposed pulse shaping waveform set design can be extended for multiuser MIMO OFDM systems.

- Finally, transmission over underwater acoustic (UWA) channel is popular for some related industries such as oil and gas exploration. Modeling UWA channel is complex because of large time-delay spread, wide Doppler spread and limited bandwidth. In recent years, UWA communications have taken advantage of the OFDM modulation technique. In the future, an optimisation problem for OFDM with pulse shaping can be developed in order to

reduce the PAPR and to improve the BER in the UWA environment.

Bibliography

[1] R. Prasad and R. van Nee, *OFDM for wireless multimedia communications.*, Boston, Artech House Publishers, 2000.

[2] J.S. Chow, J.C. Tu, and J.M. Cio, "Discrete Multitone Transceiver System for HDSL Applications," *IEEE J. Select. Areas Commun.*, vol. 9, pp. 895-908,Aug. 1991.

[3] A. Batra, J. Balakrishnan, G. R. Aiello, J. R. Foerster and A. Dabak, "Design of a multiband OFDM system for realistic UWB channel environments," *IEEE Trans. on Microwave Theory and Techniques*, vol. 52, issue 9, pp. 2123-2138, 2004.

[4] J. Chuang and N. Sollenberger, "Beyond 3G: Wideband Wireless Data Access Based on OFDM and Dynamic Packet Assignment," *IEEE Commun. Mag.*, pp. 78-87, July 2000.

[5] R. B. Marks emphet al., "IEEE standard for local and metropolitan area networks. Part 16: Air interface for fixed and mobile broadband wireless access systems. Amendment 2: Physical and medium access control layers for combined fixed and mobile operation in licensed bands and corrigendum 1," IEEE 802.16e-2005, Feb. 2006.

[6] ETSI BRAN, HIPERLAN *Type 2 Functional Specification Part 1 - Physical (PHY) Layer*, Apr. 2000. DTS/BRAN-0023003.

[7] J. A. C. Bingham, "Multicarrier modulation for data transmission: an idea whose time has come, " *IEEE Comm. Magazine*, vol. 28, pp. 5-14, May 1990.

[8] B. Farhang-Boroujeny, "OFDM versus filter bank multicarrier",*IEEE Signal Proc. Magazine*, pp.92-112, May 2011.

[9] S.B. Slimane, "Reducing the peak-to-average power ratio of OFDM signals through precoding," *IEEE Trans. Veh. Technol.* , vol. 56, no.2, pp. 686-695, Mar. 2007.

[10] S.B. Slimane, "Peak-To-Average Power Ratio Reduction of OFDM Signals using Pulse Shaping," *IEEE Globecom*, vol.3, p.1412-1416, 2000.

[11] D.Falconer, "Linear precoding of OFDMA signals to minimize their instantaneous power variance," *IEEE Trans. on Commun.*, vol. 59 ,no. 4 ,pp. 1154-1162 , Apr. 2011.

[12] C. H. (George) Yuen and B.Farhang-Boroujeny, "Analysis of the optimum precoder in SC-FDMA", *IEEE Trans. on Wireless Commun.*, vol. 11, no. 11, pp. 4096-4107, Nov. 2012.

[13] R. Reine and Z. Zang, "Analysis and comparison of a set of ISI waveforms for PAPR reduction in OFDM systems." *IEEE TENCON Conf.*, pp. 246-250, Nov. 2011.

[14] J. Amstrong, "Peak-to-average power reduction for OFDM by repeated clipping and frequency domain filtering", *IEEE Electronics Lett.*, vol. 38, issue. 5, pp. 246-247, 2002.

[15] S. Kimura, T. Nakamura, M. Saito and M. Okada, PAR reduction for OFDM signals based on deep Clipping, *3rd International Symposium on Communications, Control and Signal Processing*, pp. 911 - 916, March 2008.

[16] F. Roesler, "Riemann's hypothesis as an eigenvalue problem", *Linear Algebra Appl.*, vol. 81, pp. 153-198, 1986.

[17] A. W. Kim, J. K. Kim, H. Ryu, "A computational complexity reduction scheme using Walsh Hadamard sequence in SLM method", *IEEE proc. conf. commun., circuits, and syst.*, pp. 762-766, 2006.

[18] H. Nikookar and K. S. Lidsheim, "Random phase updating algorithm for OFDM transmission with low PAPR", *IEEE Trans. Broadcasting*, vol. 48, no. 2, pp. 123-128, Jun. 2002.

[19] P. Fan and X. G. Xia, "Block coded modulation for the reduction of the peak to average power ratio in OFDM systems," *IEEE Trans. Consum. Electron.*, vol. 45, no. 4, pp. 1025-1029, Nov. 1999.

[20] S. Nordebo, Z. Zang and I.Claesson, "A semi-infinite quadratic programming algorithm with applications to array pattern synthesis," *IEEE Transactions on Circuit and Systems*, II,vol.48, issue 3, p.225-232, March, 2001.

[21] R.L. Streit and A.H. Nuttall, "A Note on the Semi-Infinite Programming Approach to Complex Approximation", *Mathematics of Computation*,40,162,599-605,1983.

[22] T.W. Parks and C.S. Burrus, *Digital Filter Design*, New York, Wiley, 1987.

[23] D. Falconer, S. L. Ariyavisitakul, A. Benyamin-Seeyar, and B. Eidson, "Frequency domain equalization for single-carrier broadband wireless systems, " *IEEE Commun. Mag.*, vol. 40, no. 4, pp. 58-66, Apr. 2002.

[24] O. Mauritz and B.M. Popovič, "Optimum family of spectrum-shaping functions for PAPR reduction of DFT-Spread OFDM Signals," *IEEE Vehicular Technology Conf.*, pp.1-5, 25-28 Sept. 2006.

[25] S.B. Slimane, "Peak-To-Average Power Ratio Reduction of OFDM Signals using Broadband Pulse Shaping," *Proc. IEEE Vehicular Tech. Conf.*, vol.2, p.889-893, 2002.

[26] L.Wang, C. Tellambura, "Clipping Noise Guided Sign-Selection for PAR Reduction in OFDM Systems." *IEEE Trans. on Signal Processing*, vol. 56, pp. 5644-5653, 2008.

[27] X. Li and L.J.Cimini, "Effects of Clipping and Filtering on the Performance of OFDM," *IEEE Commun. Lett.*, Vol.2, Issue.5, pp.131-133, 1998.

[28] M. Wang, D.E. Quevedo, G.C. Goodwin, B.S. Krongold, "OFDMA Uplink PAR Reduction via Tone Reservation," *IEEE Globecom*, pp.3802-3806, 2007.

[29] L.Wang, C. Tellambura, "Clipping Noise Guided Sign-Selection for PAR Reduction in OFDM Systems." *IEEE Trans. on Signal Processing*, Vol.56, Issue.3, pp.1675-1694, 2008.

[30] J. Tellado, Peak to average power reduction for multicarrier modulation, Ph.D. dissertation, Stanford University, Sept. 1999.

[31] P. Tan, N. C. Beaulieu, "A novel Pulse-Shaping for Reduced ICI in OFDM Systems," *IEEE Vehicular Tech. Conf.*, Vol.1, p.1090-3038, 2004.

[32] P. Tan and N.Beaulieu, "Reduced ICI in OFDM systems using the "better than" raised-cosine pulse," *IEEE Comm. Lett.*, March 2004.

[33] A. Assalini and A.M. Tonello, "Improved Nyquist Pulses," *IEEE Trans. Lett.*, Vol. 8, Issue.2, pp.87-89, 2004.

[34] B. Farhang-Boroujeny, "A Square-Root Nyquist (M) Filter Design for Digital Communication Systems," *IEEE Trans. in Signal Processing*, Vol.56, Issue.5, p.2127-2132, May 2008.

[35] J. Proakis and M. Salehi, *Contemporary Communication Systems using MATLAB,* Canada, Brookse/Cole, 2000, p.250.

[36] J. W. Adams, "FIR digital filters with least-squares stopbands subject to peak-gain constraints", *IEEE Trans. on Circuits and Syst.*, vol. 38, issue 4, pp. 378-388, 1991.

[37] S. Nordebo, I. Claesson, and Z. Zang, "Optimum Window Design by Semi-Infinite Quadratic Programming." *IEEE Signal Processing Letters*, Vol.6, No.10, pp.262-265, 1999.

[38] S. Nordebo, and Z. Zang, "Semi-Infinite Linear Programming: A Unified Approach to Digital Filter Design with Time and Frequency-Domain Specifications." *IEEE Trans. on circuits and systems*, Vol.46, No.6, pp.765-775, 1999.

[39] H. Dai and H. V. Poor, "Advanced Signal Processing for Power Line Communications," *IEEE Commun. Mag.*, vol. 41, no. 5, pp. 100-107, May 2003.

[40] N.C. Beaulieu, Edmonton, C. Tan, M.O. Damen, "A "better than" Nyquist pulse", *IEEE Comm. Letters*, vol.5, issue 9, pp. 367-368, Sept 2001.

[41] M.A. Yusoff and Z. Zang, "Waveform set Design using Hermite-Rodriguez Functions for CDMA Communications", *IEEE 2009 International Conf. Signal Acquisition and Proc."*,pp.26 - 29, Apr. 2009.

[42] Z. Zang and S. Nordholm, "Design of OFDMA digital waveforms using non-convex optimization methods," *Annals of Operations Research*, vol.133, pp.319-330, 2005.

[43] K. W. Richard, "UMTS Overview", *IEE Electronics and Communication Engineering Journal*", Vol. 12, No.3, June 2000, pp.93-100.

[44] H. Ochai and H. Imai, "On the Distribution of the Peak-to-Average Power Ratio in OFDM Signals", *IEEE Trans. Commun.*, vol.49, No.2, Feb. 2001.

[45] A. Papoulis and S. U. Pillai, "Probability, random variables, and stochastic processes", *McGraw-Hill, Inc. U.S.A*, 2002.

[46] B. Sklar, "Digital Communications: Fundamentals and Applications", *Prentice Hall*, 1988.

[47] A. Abdi, K. Wills, H.A. Barger, M.S. Alouini and M. Kaveh, "Comparison of the level crossing rate and average fade duration of Rayleigh, Rice and Nakagami fading models with mobile channel data", *IEEE Vehicular Tech. Conf. 2000,* 52^{th}, vol.4, pp. 1850-1857, Sept. 2000.

[48] X. Zhou and J. Caffery, "A new distribution bound and reduction scheme for OFDM PAPR", *Wireless Personal Multi. Commun. 2002, the* 5^{th} *International Symposium*, vol.1, pp. 27-30, Oct 2002.

[49] S. Wei, D.L Geockel and P.E. Kelly, "A modern extreme value theory approach to calculating the distribution of the peak-to-average power ratio in OFDM systems", *IEEE International Conf. Commun.*, vol.3, pp. 1686-1690, 2002.

[50] R. van Nee and A. de Wild, "Reducing the peak-to-average power ratio of OFDM", *IEEE Vehicular Tech. Conf.*, vol. 3, pp. 2072-2076, 1998

[51] M. Bellanger, "On computational complexity in digital filters," in *Proc. Eur. Conf. Circuit Theory Design*, Aug 1981, pp.58-63.

[52] K. Ichige, M. Iwaki, and R. Ishii, "Accurate estimation of minimum filter length for optimum FIR digital filters, " *IEEE Trans. Circuits Syst. II*, vol. 47, no. 10, pp. 1008-1016, Oct. 2000.

[53] R. Hettich and K. O. Kortanek,"Semi-infinite programming: Theory, methods, and applications," SIAM Rev. , vol. 35, no.3, pp. 380-429, Sept. 1993.

[54] Tri T. Ha, *Theory and design of digital communication systems*, Cambridge university press, Nov. 2010, pp.86.

[55] M. A. Masnadi-Shirazi and M. Ghasemi, "Laguerre digital filter design," *in Proc. ICASSP'95*, vol.2, pp. 1284-1287.

[56] M. Al-Attraqchi, S. Boussakta and S. Le Goff ,"An enhanced OFDM/OQAM system exploiting Walsh-Hadamard Transform," *IEEE 73rd Vehicular Technology Conf.*, pp.1-5, May 2011.

[57] H.A. Leftah, S. Boussakta, "Precoded DCT-OFDM system for baseband and wireless transmission: Performance analysis and evaluation", *IEEE 5th Wireless Telecommun. Symposium*, pp.1-6, Apr. 2012.

[58] T. S. Rappaport, "Characterization of UHF multipath radio channels in factory buildings," *IEEE Trans. on Antennas and Propagation,* vol. 37, no. 8, pp. 1058-1069, Aug. 1989.

[59] D. C. Cox, "Universal digital portable radio communications," *IEEE Proc.*, vol. 75, no. 4, pp. 436-477, Apr. 1987.

[60] T. S. Rappaport, *Wireless communications: principles and practice*, Prentice Hall, New Jersey, 1996.

[61] J. C. I. Chuang, "The effects of time delay spread on portable radio communications channels with digital modulation," *IEEE Journal on Selected Areas in Commun.*, vol.5, no. 5, pp. 879-889, June 1987.

[62] W. A. Gardner, Napolitano, L. Paura, "Cyclostationary: Half of a century research", *Journal Signal Processing*, vol. 86, no. 4, pp. 639-697, Apr. 2006.

[63] W.A. Gardner, *Introduction to Random Processes with Applications to Signals and Systems*, Macmillan, New York, 1985 (Chapter 12).

[64] W. A. Gardner, L. E. Franks, " Characterization of cyclostationary random signal processes", *IEEE Trans. on Inf. Theory*, vol. 21, no. 1, pp. 4-14, Jan. 1975.

[65] H. L. Hurd, "A Brief introduction to Periodically Correlated (Cyclostationary) Random Sequences", *http://www.stat.unc.edu/faculty/hurd/papers/intro.ps.*

[66] H. L. Hurd, A. Miamee, *Periodically correlated random sequences: spectral theory and practice*, Wiley, 2007.

[67] S. D. Assimonis, M. Matthaiou, G. K. Karagiannidis, and J. A. Nossek, " Optimized "Better Than" Raised- Cosine Pulse for Reduced ICI in OFDM Systems", *IEEE International Conf. on Telecommun. (ICI)*, pp. 249-252, Apr. 2010.

[68] J. Medbo, H. Andersson, P. Schramm, H. Asplund, and J.E.Berg, "Channel models for HIPERLAN/2 in different indoor scenarios," EURO-COST, Bradford, U.K., COST 259 TD(98)70, Apr. 1998.

[69] D.I. Axiotis, F.I. Lazarakis, and C. Vlahodimitropoulos, "Mobility and traffic parameters for simulating interoperating UMTS and HIPERLAN/2 MTMR enabled networks," *IEEE 57th Vehicular Technology Conf.*, pp.2745-2749, Apr. 2003.

[70] S. Haykin, *Communication Systems*, 4th ed., pp.70-71, John Wiley and Sons, Inc., 2001.

[71] S. Haykin, *Communication Systems*, 4th ed., pp.735-739, John Wiley and Sons, Inc., 2001.

[72] S. O. Rice, "Mathematical analysis of random noise", in *Selected papers on noise and stochastic processes*, N. Wax, Dover publications, Inc., New York, pp. 133-294, 1954.

[73] J. R. Rice and F. P. Beer, "First occurence time of high level crossings in a continous random process", *Journal of the Acoustical Society of America*, 39, 1966, pp.323-335.

[74] S. Ariyavisitakul and T.-P. Liu,"Characterizing the effects of nonlinear amplifiers on linear modulation for digital portable radio communications", *IEEE Trans. Veh. Technol.*, vol. 39, no. 4, pp. 383-389, Nov. 1990.

[75] A. J. Paulraj, D. A. Gore, R. U. Nabar, and H. Bolcskei, "An overview of MIMO communications - a key to gigabit wireless", *Proc. IEEE*, vol. 92, no. 2, pp. 198-218, Feb. 2004.

[76] Alamouti, "A simple transmit diversity technique for wireless communications," *IEEE J. Sel. Areas Commun.*, vol. 16, no. 8, pp. 1451-1458, Oct. 1998.

[77] P. P. Vaidyanathan, *Multirate systems and filter banks*, Englewood Cliffs, NJ: Prentice-Hall, 1993.

[78] C. Kirjner-Neto and E. Polak, On the conversion of optimization problems with maxmin constraints to standard optimization problems, *SIAM J. Optim.*, vol. 8, no. 4, pp. 887-915, 1998.

[79] H. Ochiai and H. Imai, "On the distribution of the peak-to-average power ratio in OFDM signals," *IEEE. Trans. on Commun.* , vol. 49, no. 2, Feb. 2001.

[80] B. Yan, J. Yang, H. Zhang and Y. Zhu, "Distribution bound of PAPR in OFDM signals," in *IEEE Conf. on Commun., Circuits and Systems Proc.*, vol. 2, pp. 1398-1401, June 2006.

[81] X. Zhou, G. Y. Li, and G. Sun, "Multiuser spectral precoding for OFDM-based cognitive radios", *IEEE Globecom*, pp. 1-5, 2011, Texas, USA.

[82] W. C. Jakes, *Microwave mobile communications"*, IEEE Press, 1974.

[83] D. L. Goeckel and G. Ananthaswamy, On the design of multidimensional signal sets for OFDM systems, *IEEE Trans. Commun.*, vol. 50, no. 3, pp. 442452, Mar. 2002.

[84] A. O. Hero and T. L.Marzetta, Cutoff rate and signal design for the quasistatic Rayleigh fading space-time channel, *IEEE Trans. Inf. Theory*, vol. 47, no. 6, pp. 24002416, Sep. 2001.

[85] X. Zhou, G. Y. Li, and G. Sun, "Multiuser spectral precoding for OFDM-based cognitive radio systems", *IEEE Journal on Selected Areas in Commun.*, vol.31, no. 3, pp. 345-352, March 2013.

[86] J. Fang and I. Lu, "Efficient multiuser spectral precoding for reducing out-of-band emission for OFDM-based cognitive radios", *IEEE Conf. Syst., Applications and Techno.*, pp. 1-5, Long Island, May, 2013.

[87] C. Y. Wong, R. S. Cheng, K. B. Lataief and R. D. Murch, "Multiuser OFDM with adaptive subcarrier, bit, and power allocation", *IEEE Journal on Sel. Areas in Commun.*, pp. 1747-1758, Oct., 1999.

[88] P. H. Huang, Y. Gai, B. Krishnamachari and A. Sridharan, "Subcarrier allocation in multiuser OFDM systems: complexity and approximability", *IEEE Wireless Commun. and Networking Conf.*, pp. 1-6, Apr., 2010.

[89] G. Chandran and J. S. Jaffe, "Signal set design with constrained amplitude spectrum and specified time-bandwidth product", *IEEE Trans. on Commun.*, vol. 44, no. 6, pp.725-732, 1996.

[90] Z. Zang and S. Nordholm, "Orthogonal digital waveform set for multidimensional signaling and multiuser communications with matched filter receivers", *10th Asia Pacific Conf. Commun. and 5th Int. Symposium on Multi-Dimensional Mobile Commun.* , China, 2004.

Every reasonable effort has been made to trace and acknowledge the authors of copyright material. The author would be pleased to hear from any copyright owner who has been omitted or incorrectly acknowledged.